PVMD
Photovoltaic Materials and Devices

Master of Science Thesis

Understanding μc-Si:H solar cell performance and its optimization using modeling

Chimdindu U. Nebo
1386093

Supervisors:
Prof. Miro Zeman (PVMD group, EWI-faculty, TU Delft)
Ir. Solomon Agbo (PVMD group, EWI-faculty, TU Delft)

Thesis Committee:

Prof. Miro Zeman	(PVMD group, EWI-faculty, TU Delft)
Dr. René van Swaaij	(PVMD group, EWI-faculty, TU Delft)
Dr. ir. M. Bartek	(ECTM group, EWI-faculty, TU Delft)
Ir. Solomon Agbo	(PVMD group, EWI-faculty, TU Delft)

September
2009

TU Delft

Abstract

In recent times, thin-film solar cells have gained a lot of attention. This can be attributed to the low material cost as well as its low energy consumption. The micromorph solar cell configuration consisting of a top amorphous silicon cell and a bottom microcrystalline silicon cell has proved to be one of the promising approaches in thin-film silicon solar cells. The importance of the microcrystalline silicon cell lies in its higher performance in absorption of photons in the long wavelength region of the spectrum.

In this thesis we made use of the ASA simulator to study microcrystalline silicon solar cells. We started by carrying out the calibration process of a model microcrystalline solar cell to be used for the simulations. A sensitivity study was carried out for both optical and electrical parameters of the solar cell. The study showed that the RMS roughness of the interfaces of the solar cell especially the TCO-p interface significantly affect the solar cell performance. It is shown in this work that parasitic absorption in the front TCO and the p-layer can be enormous and reduce the overall absorption in the absorber layer. The electrical properties of the solar cell were also studied, showing the sensitivity of the solar cells external parameters (short circuit current density, open circuit voltage, fill factor) as well as the solar cell efficiency to properties such as the mobility gap, layer thickness, activation energy, etc. The effect of a buffer layer between the p-i interface and graded absorber layer on the open circuit voltage was investigated. The result shows that the external parameters of the solar cell are improve upon by implementing the i-layer grading. The Voc also increases with aSi:C buffer layer inserted between p- and i-layer. The Jsc and the fill factor and not affected much.

The use of modeling and simulation is a very useful tool in the study of solar cells. This work shows that the feature is bright with regards to what can be achieved in the optimization of microcrystalline silicon solar cells.

Contents

1 Solar cells

1.1 Introduction

In recent times, thin-film silicon solar cells have generally received a lot of attention and have been considered the most widespread alternative to bulk crystalline solar cells. This is based on the low material consumption and large area deposition at low substrate temperature, which allows for the use of cost-effective substrate materials such as glass, stainless steel and plastic. Thin-film silicon technology is one of the largest in terms of production capacity among the thin-film technologies. The so-called micromorph solar cell configuration has gained a lot of attention recently due to its potential of achieving a high stabilized efficiency. In this tandem configuration, a microcrystalline silicon (μc-Si:H) bottom cell is combined with an amorphous silicon (a-Si:H) top cell. The μc-Si:H is used due to the fact that it has extended response in the infrared wavelength region when compared to the amorphous cell.

1.2 Renewable Energy

1.2.1 What is renewable energy?

Renewable energy can be seen simply as energy that is tapped freely from nature. , It could be in form of solar energy, wind energy, rain, tides (hydro power), geothermal heat, and energy from biomasses [1, 2]. These renewable sources of energy are naturally replaceable and are in constant supply on earth.

1.2.2 Why renewable energy?

The world is gradually getting more conscious about sustainability, which is living today in a way that guarantees generations to come will still be able to live the same way. The effects of global warming, CO_2 emissions, emission of green house gases hence climate changes, etc on our environment, all caused by the way humans have lived, are issues of great concern today. Our unsustainable methods of energy production, the harmful consequences of those methods and the depletion of the earth’s natural resources are all facts that make scientists and world governments to seek renewable, non harmful ways of satisfying the enormous energy and power needs of the world today. Renewable energy sources seem to be a part of the answer to the sustainable solution we seek, since we don't threaten the existence of life using renewable methods. We also don't deplete the earth crust of its resources and create risky situations like in the case of making use of nuclear techniques to produce energy.

1.2.3 Sources of renewable energy

- Solar Energy, this comes from the sun and can be turned into electricity and heat. The sun has produced energy for billions of years, solar energy is the sun's rays (radiation) that reach the earth
- Wind: wind is simply air in motion, caused by the uneven heating of the earth's surface by the sun. Because of the various constituents of the earth's surface, the heat from the sun is absorbed at different rates. In the day time, the air above land gets heated up faster than that above water, the air above the land therefore expands faster and rises, this gives rise to the cooler heavier air rushing in to take its place creating winds. At night, the reverse happens due to the faster cooling of the air above land to that over water. Wind energy is employed mostly in the generation of electricity using wind mills.
- Geothermal energy, this source is from inside the earth
- Biomass: This is organic material made from plants and animals. Biomass contain stored energy from the sun, energy is absorbed from the sun by photosynthesis, which is also passed on to animals as chemical energy when they eat plants. When burned, the chemical energy in biomass is released as heat. Hence fire wood is a biomass form of fuel.
- Hydropower and ocean energy, from water,

1.3 Solar cells

A solar cell or photovoltaic cell is a device that converts light energy into electrical energy by the photovoltaic effect. The photovoltaic effect stands for the process by which electrical energy is generated by incident radiant energy at the junction of two dissimilar materials such as a pn-diode, p-i-n or n-i-p diodes. This electrical energy can be generated by creating a potential difference at the junction of two dissimilar materials when a photon strikes a photovoltaic material. If the energy of the photon is higher than the energy band gap of the material, electron hole pairs are generated, and electrons move from the valence band into the conduction band. In the conduction band, electrons move around and hence generate current; this movement is caused by the presence of an electric field which causes drift and differences in concentration which causes diffusion. The generation and recombination of these electron hole pairs can be seen in Figure 1 below. This diagram illustrates pictorially the different possible ways of generation e.g. from (1) band –to- band, (2) R-G centre generation (from traps) and photo emission from (3) band gap centers. The recombination process is the reverse of the generation process and can be imagined also by looking at figure 1.

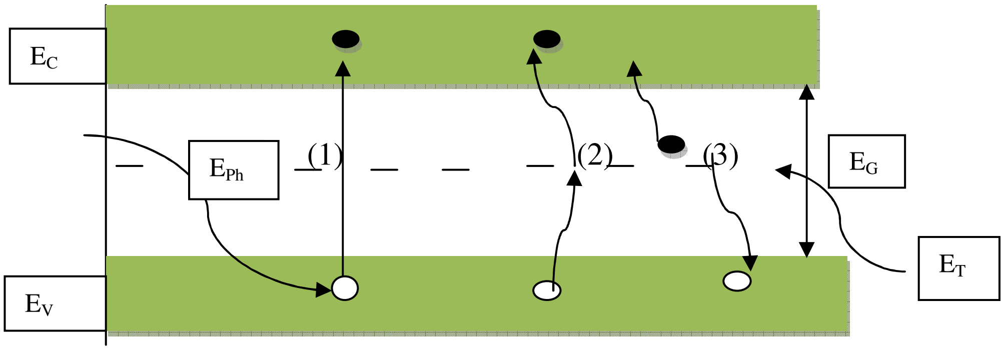

Figure1-1: Generation of Electron hole pairs, showing (1) band -to- band, (2) R-G centre generation (from traps) and photo emission from (3) band gap centers

In general, photocells are responsible for photogeneration of charge carriers (electrons and holes) in a light absorbing material and the separation of the charge carriers to a conductive contact that will transmit the electricity. The p-n junction is shown in figure 1-2 below.

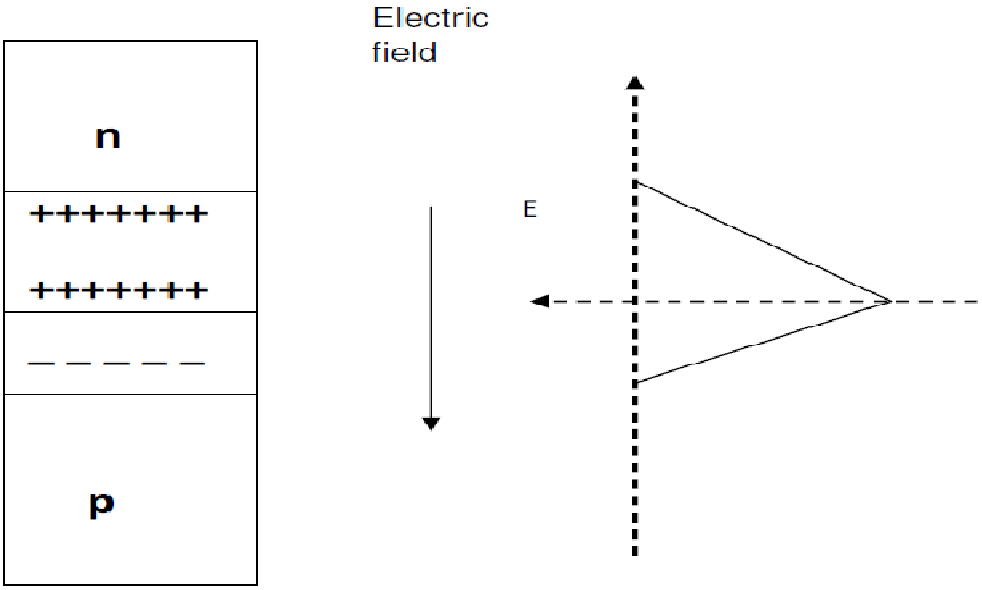

Figure 1-2: p-n junction showing space charge and depletion region

The p-n junction is formed by putting the two types of material (p type and n type) together; the junction is formed at the place where the two type materials meet. The p type material consists of holes as majority carriers, this can be formed by introducing trivalent (acceptor) atoms such as phosphorous into the silicon material, and the n type material, in the same way has electrons as majority carriers, formed by introducing pentavalent (donor) atoms into the semiconductor. At the junction where the p and n type materials meet, holes start to diffuse into the n type material, and electrons diffuse into the p type material leaving behind donor and acceptor ions respectively, a space charge builds up, creating a depletion region which inhibits any further electron transfer, unless a forward bias is applied. The free carrier pairs created by incident light energy are separated by the p-n junction and contribute to current.

The photovoltaic effect was first observed by A. E. Becquerel in 1839 and the first solar cell was built in 1883 by Charles Fritts, who used selenium and gold to form the junction [3]. The modern day solar cells were found accidentally in 1954 by Bell laboratories when they noticed that silicon doped with certain impurities was very sensitive to light, figure 1-3 below shows the schematic of a c-Si solar cell showing the p-n junction.

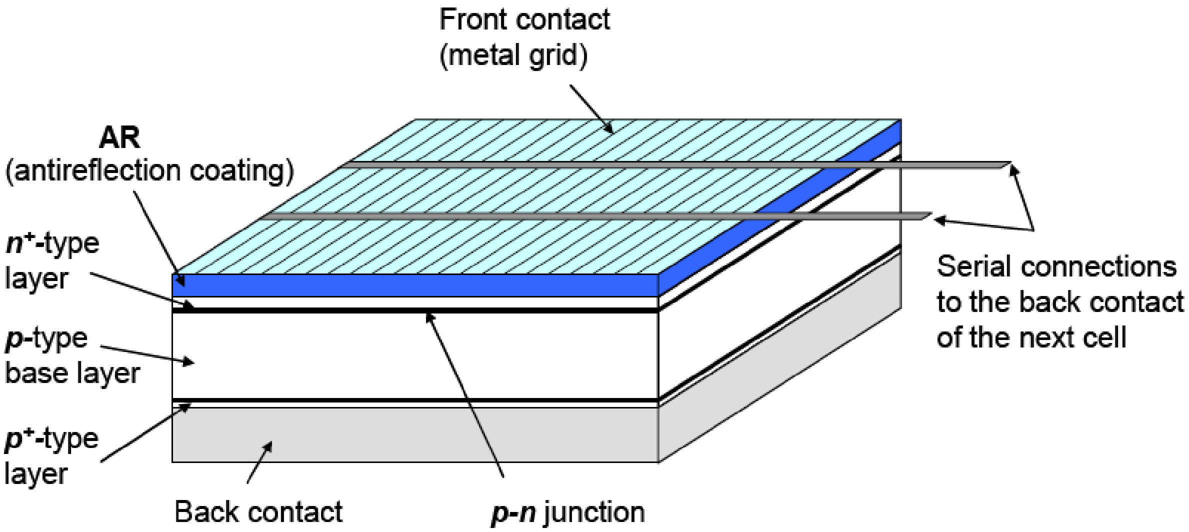

Figure 1-3: Structure of a c-Si solar cell [1]

The structure of the c-Si solar cell shown above consists of a front contact (metal grid) for collection of charged carriers. This front contact is made to cover as little area as possible in order to leave enough space on the cell for light passage. Below the front contacts is the anti reflective coating (AR) which channels the photons into the cell and as the name implies, prevents reflection of light away from the cell. Once the photons have passed the AR, they come in contact with the semi conductor material, in this case the heavily doped n-type layer, then a p-n junction is formed in the middle of this n-type layer and the p-type layer below it. This p-type layer acts as the absorber layer. Below is a heavily doped p-type layer then the back contact for collection of charged carriers. Solar cells are semiconductors. The movements of carriers generate the electric current in solar cells. When light photons are incident on a solar cell, a certain amount of them are absorbed transferring the energy of the photons to the semiconductor. If the energy of the photons is greater than the energy band gap of the material, an electron hole pair is generated. In the diagram above, this absorption will take place in the absorber p-layer, at the p-n junctions exist electric fields which depending on their bias, will allow the passage of one carrier type only. At the n-type layer electrons will be swept across to the front contact while at the p-type layer, holes will be swept across to the back contact. If an external conductive path is created or the circuit closed by connecting the front and the back contacts, the electrons will flow through this path to their original p-type material to recombine with the holes they created.

1.3.1 Current and voltage in a solar cell

To characterize a solar cell, two important quantities are taken into consideration. They are

- Short circuit current (J_{sc}): The current that flows when the terminals are connected to each other (zero load resistance).
- Open circuit voltage (V_{oc}): The voltage between the terminals of the solar cell when no current is drawn (infinite load resistance).

The short circuit current increase with light intensity, as higher intensity means more photons, which in turn means more electrons. Since the short circuit current is roughly proportional to the area of the solar cell, the short circuit current density, $J_{sc} = I_{sc} / A$, is often used to compare solar cells [4].

The connection of a load to a solar cell decreases the current, and a voltage develops as charge builds up at the terminals. The resulting current can be seen as a superposition of the short circuit current, caused by the absorption of photons and a dark current, which is caused by a potential built up over the load and flows in the opposite diode. The dark current density is given by

$$J_{dark}(V) = J_0(e^{qv/k_BT} - 1) \tag{1.1}$$

In the equation, J_0 stands for a constant, q is the electron charge and V is the voltage between the terminals. The resulting current can be calculated / approximated as a superposition of the short circuit current and the dark current:

$$J = J_{sc} - J_0(e^{qv/k_BT} - 1) \tag{1.2}$$

To find the expression for the open circuit voltage, we set $J = 0$. This means the two currents cancel out and hence no current flows, which is exactly the case in open circuit conditions. The resulting expression is

$$V_{oc} = \frac{K_B T}{q} \ln(\frac{J_{sc}}{J_0} + 1) \tag{1.3}$$

Generally, the power delivered from a source is P = IV, in the case of solar cells we use current density J and hence get power density:

$$P_d = JV \tag{1.4}$$

The maximum power density occurs somewhere between V = 0 (short circuit condition) and $V = V_{oc}$ (open circuit voltage condition) at a voltage V_m.

The corresponding current density is called J_m, and thus the maximum power density is

$$P_{d,m} = J_m V_m \tag{1.5}$$

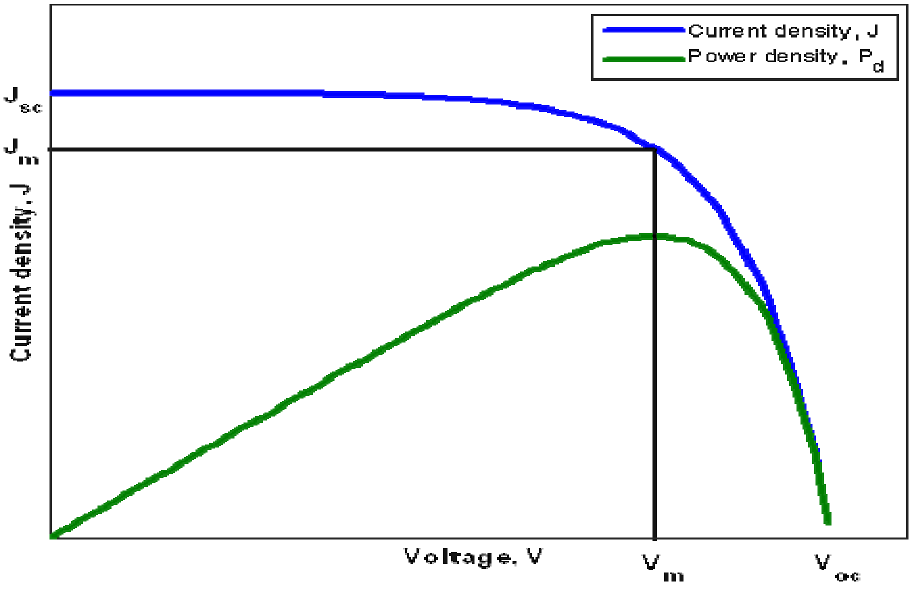

Figure 1-4: maximum power [4]

The efficiency of a solar cell is defined by:

$$\eta = \frac{J_m V_m}{P_s} \tag{1.6}$$

Another important quantity of the solar cell is its fill factor, and is defined by

$$FF = \frac{J_m V_m}{J_{sc} V_{oc}} \tag{1.7}$$

The fill factor gives a measure of how much of the open circuit voltage and short circuit current is used or utilized at maximum power. Using the fill factor FF, we can express the efficiency as

$$\eta = \frac{J_{sc} V_{oc} FF}{P_s} \tag{1.8}$$

These four quantities discussed above, Voc, Jsc, FF and η are used in characterizing the performance of a solar cell. They are measured under standard lighting conditions, known as the Air Mass 1.5 spectrum, light flux of 1000W/m^2 and temperature of 25^{0}C.

1.3.2 Solar radiation

One of the basic processes behind the photovoltaic effect, on which the operation of solar cells is based, is generation of electron hole pairs due to absorption of visible or other electromagnetic radiation by a semiconductor material [1]. Electromagnetic radiation can be described in terms of photons, which are characterized by energy (hv) expressed in electron volts, or in terms of wavelength (λ) and frequency (v). The relationship between these quantities can be seen below:

$$v = c / \lambda \tag{1.9}$$

$$hv = \frac{1}{q}\frac{hc}{\lambda} \tag{1.10}$$

where c is the speed of light in vacuum (2.998*10^8 m/s), h the Planck's constant, and q the elementary charge. The sun to a good approximation could be seen as a perfect emitter of radiation at a temperature of 5800 K, and thus considered as a black body. The sun emits electromagnetic light in different wavelengths or regions of the solar spectrum. Figure 3 below shows the solar irradiance outside the earth's atmosphere, denoted by AM), and at sea level denoted by AM1.5, this is the standard at which solar cells are measured.

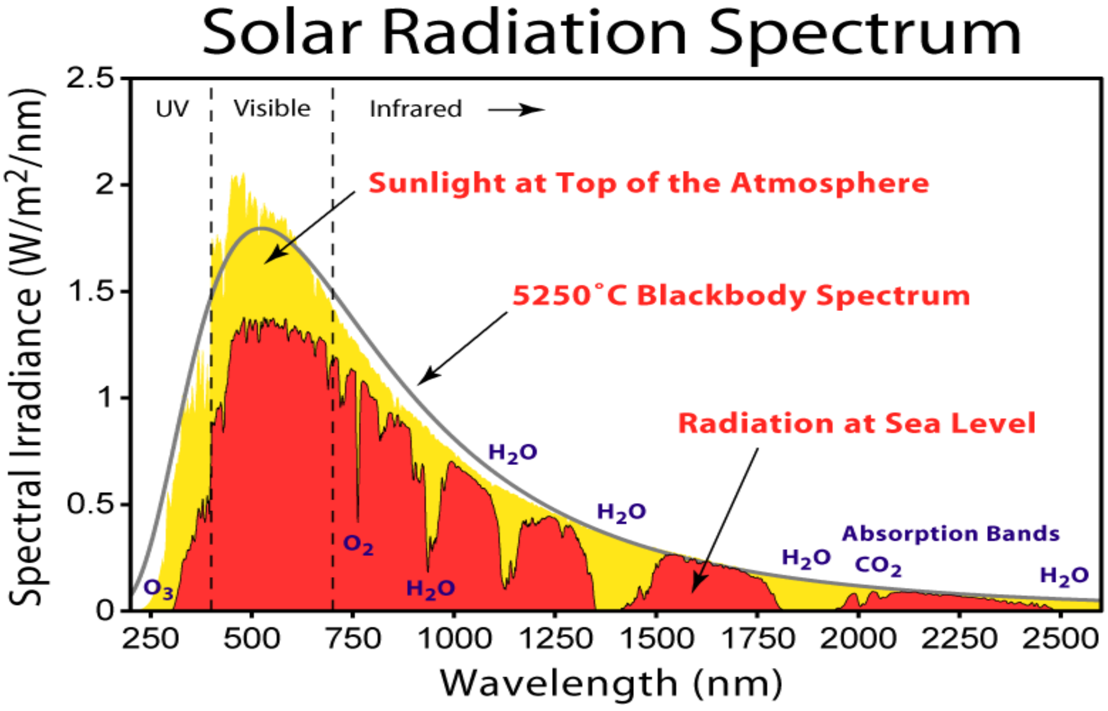

Figure 1-5: The solar irradiance spectrum AM0 and AM 1.5 [6]

As the sun irradiates the earth, and the solar radiation passes the atmosphere, part of the incident energy is removed by scattering, absorption or by molecules, clouds, and aerosols [6]. Wavelengths less than 300nm are filtered out by molecules like Ozone, nitrogen and oxygen.

Dips in the infrared area of the spectrum as seen in the diagram are caused by water and CO_2. Only photons of appropriate energy can be absorbed and generate the electron-hole pairs needed for electricity in solar cells, hence the importance of studying the spectral distribution of the solar radiation [5]. Two quantities used to describe the solar radiation spectrum, are the spectral power density, and the photon flux density, $P(\lambda)$ and $\Phi(\lambda)$ respectively. The spectral power density is the incident power of solar radiation per unit area per unit wavelength, and is related to the photon flux by:

$$\varphi(\lambda) = p(\lambda)\frac{\lambda}{hc} \tag{1.11}$$

At the suns surface, its power density is 62 MW/m^2, and at a point just outside the atmosphere, the power density is reduced to 1353 W/m^2 because of the suns reduced angular range.

1.4 Thin-film silicon solar cells

Thin-film silicon solar cells also seen as second generation solar cells for terrestrial applications have been receiving a lot of attention in recent times, and are considered to be the most widespread alternative to bulk crystalline solar cells. This is thought because of the relatively low material requirements for its production as well as large area deposition at low substrate temperature, which allows for use of cost effective materials such as glass, stainless steel and plastic. The thin-film silicon technology is the largest in terms of production capacity among the thin-film technologies. Thin film silicon solar cells, at around 1μm can be deposited at low temperatures (200ºC) on various substrate materials. These thin film silicon solar cells require a lot less material than regular wafer-based crystalline silicon solar cell, making them cheaper. Also the quantity of energy used to manufacture thin film solar cells is about a factor of 2 lower than that of crystalline silicon solar cells, hence faster energy payback time. At this moment, the stabilized efficiency is still limited [7]. Thin film silicon layers can be grown by various deposition methods such as plasma-enhanced chemical vapor deposition (PECVD), hot wire chemical vapor deposition, glow discharge deposition technique, the expanding thermal plasma CVD [1].

There are two forms of thin film silicon solar cell, materials: hydrogenated amorphous silicon (a-Si:H) and hydrogenated microcrystalline silicon (μc-Si:H).

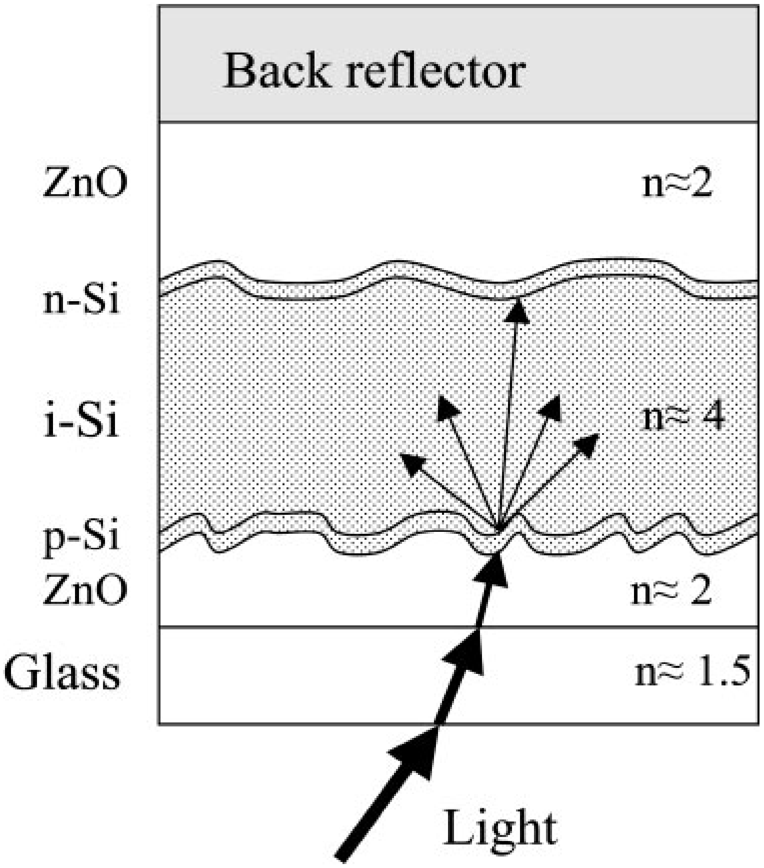

Figure 1-6: Schematic of a typical p-i-n thin film solar cell [7]

1.4.1 Hydrogenated amorphous silicon (a-Si:H)

a-Si:H layers are non crystalline layers that were first deposited accidentally by R. Chittick when he was experimenting with silane plasma. Chitticks results were further investigated at Dundee University by W. E. Spear and his colleagues who studied the first systematic study on plasma enhanced chemical vapor deposition with silane plus doping gases [7]. a-Si:H has very high absorption coefficient in the visible part of the solar spectrum hence a one micrometer thick layer is sufficient to absorb 90% of usable solar light energy [1], this high absorption coefficient is due to the disorderly atomic structure of the amorphous silicon, making it behave like a direct band gap semiconductor. It is not advisable for a-Si:H to use p-n type diodes as solar cell structure because the doping capability is poor. Doping destroys the a-Si:H layer quality, owing to the fact that it creates additional silicon dangling bonds. These dangling bonds are the main recombination centers. Carrier collection in p-n type solar cells are obtained by minority carrier diffusion within the p and n layers. Given that diffusion lengths in crystalline solar cells are sufficiently high to ensure pretty good carrier collection. However, in a-Si:H, minority carrier diffusion lengths are extremely small, making it not possible to base minority carrier collection of photogenerated carriers on diffusion alone [7]. As a result of the afore listed, p-i-n diodes are always used for a-Si:H solar cells. The structure is shown in figure 1-6 above. In this p-i-n structure, the main part of the absorption takes place in the intrinsic (i) layer, also called absorber layer.

Amorphous silicon solar cell has proven to be an attractive pv device for both the present and the future; however it suffers from the light induced degradation effect known as the staebler-wronski effect and stabilizes only at lower efficiency values from the original efficiency value after being exposed for a certain length of time.

1.4.2 Hydrogenated microcrystalline silicon (μc-si:H)

Plasma deposited hydrogenated micro crystalline silicon (μc-si:H) layers were first deposited in 1968 by Veprek and Maracek [1], however it wasn’t until the early 1990’s that actual microcrystalline solar cells were fabricated. Pioneering work done at IMT Neuchatel resulted in the fabrication of pin/nip-type hydrogenated microcrystalline silicon solar cells with fully stable AM 1.5 conversion efficiencies [1]. Unlike other forms of silicon (Amorphous, monocrystalline), microcrystalline silicon is a highly complex material which depending on deposition techniques, can take on very different micro-structural forms of which only certain forms are suitable for solar cells. Just like the a-Si:H discussed above, μc-si:H can be produced at relatively low temperatures (typically 200-300^{o}C) by glow discharge and other plasma assisted deposition methods, as well as hot wire deposition. Compared to polycrystalline silicon, and other high temperature deposition and growth techniques, microcrystalline silicon shows smaller grain sizes, its grain boundaries are hydrogenated, and there could be a significant amount of amorphous tissue in the layer [8]. Note that the type of μc-Si:H layer grown depends on the underlying layer and or on the substrate materials used, for instance, μc-Si:H layers deposited on glass or on amorphous silicon tend to have larger amorphous volume fraction than those deposited on underlying crystalline material. It is important to note that the initial growth phase is very delicate and important and is also under study [1].

In the production of μc-si:H solar layers, silane (SiH_4) is used as an original source gas and is strongly diluted with hydrogen [9], when introduced into the plasma, so as to induce formation of a microcrystalline, rather than an amorphous lattice structure. In initial experiments, very low deposition rates were recorded with values well below 1 Å/s. These layers had a strong n-type character, and could be easily doped with e.g. phosphine, in order to push the Fermi level upwards towards the conduction band edge and to obtain layers with an even more pronounced n-type characteristic, or with diborane, to push the Fermi level downwards to the valence band edge to obtain p-type layers. These n/p-type layers are still used today both by production lines and research laboratories [9], to produce pin-type thin film silicon solar cells where the photovoltaic active layers consist of hydrogenated amorphous silicon. Because of the facts earlier mentioned that hydrogenated microcrystalline silicon is a material with an indirect bandgap. Hence its absorption coefficient in the visible part of the solar spectrum is relatively low. This implies that thick layers are necessary to obtain sufficient absorption and photgeneration. The fact that the many grain boundaries present can cause obstruction of electronic transport in microcrystalline silicon layers if the grain boundaries are not well passivated by hydrogen, make the use of hydrogenated microcrystalline silicon as the PV active layer within a thin-film solar cell not straight forward. Hence it took many years before microcrystalline intrinsic layers were attempted in thin-film silicon solar cells. Fully microcrystalline silicon solar cells can be advantageous when combined in a hybrid form with amorphous silicon solar cells in tandem known as micromorph structure. This configuration greatly increases the efficiency when compared to the single microcrystalline structure, yielding stable efficiency results.

1.4.3 Deposition of microcrystalline silicon

The most widely used method for the growth or deposition of microcrystalline silicon for use in solar cells is the plasma enhanced chemical vapor deposition (PECVD). This method is based on electrically excited capacitively coupled plasma reactors. The plasma is usually excited with an AC signal whose frequency is generally equal to a standard value of 13.56 MHz, This value is reserved for industrial applications within the radio frequency range. The deposition rate of device quality amorphous silicon layers can be increased significantly by increasing the plasma excitation frequency from 13.56 to around 70 MHz, this has been proven to be true also for microcrystalline silicon, although the effect has not been studied at great length [9]. This increment in the excitation frequency can increase deposition rate by a factor of 5, the maximum power level above which a significant amount of powder is formed in the reactor is also pushed up. According to [9], these effects are linked to a reduction in sheath width and to a change in ion bombardment with increasing plasma excitation frequency. The maximum energy of ions impinging on the growth surface is reduced, as the frequency increases, at the same time, the ion flux is augmented. In microcrystalline silicon, it was observed by the group at IMT Neuchatel that crystallite sizes increase as the plasma excitation frequency increases. The trade-off for increasing frequencies is that at these frequencies, it is difficult to obtain uniform layer deposition over large areas, thus large area thin film silicon solar modules production by VHF PECVD remains a major technical challenge.

Hydrogenation and Crystallization

When pure silane is used in deposition in a glow discharge reactor, the resulting layers are usually amorphous. When hydrogen is added to the plasma, the layer quality is marginally altered; the layer remains amorphous though until a certain threshold concentration is reached [9]. On increasing the hydrogen concentration, we start depositing crystallites, rapidly increasing the crystalline volume fraction until layers that are essentially microcrystalline are obtained. Increasing even further the hydrogen dilution of the plasma, the microstructure of the layers is varied; high columns separated by cracks appear at high values of hydrogen dilution. The TEM (transmission electron microscope) micrograph diagram shown in figure 1-7 illustrates the trend for layers deposited by VHF plasma on glass substrates. Percentage values refer to concentration of silane in total gas flow (hydrogen + silane). These values decrease for increasing hydrogen value, hence the hydrogen concentration as illustrated in the diagram increases to the left hence micro crystallization too.

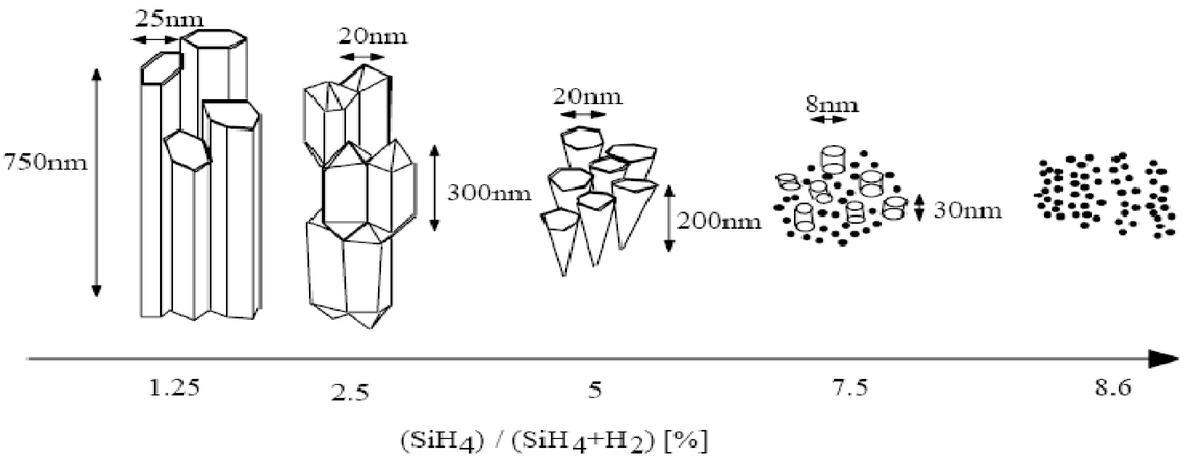

Figure 1-7: Evolution of microstructure in micro crystalline silicon [9]

Very high values of hydrogen dilution have proved to form the best microcrystalline layers, however these very high hydrogen concentration deposited materials do not make good solar cells due to cracks that can induce shunts in the cells, and appear also to act as channels in which contamination such as oxygen can enter the layer.

It is important to note that because of nucleation phenomena, on the initial stages of layer growth, hydrogenated microcrystalline silicon layers are sensitively dependent on the substrate and on the underlying layers on which they are grown. Layers grown on microcrystalline under-layers tend to be much more crystalline than layers grown on glass [9]. The whole growth process depends not only on crystallinity, but on the chemical nature and crystalline orientation of underlying layers.

1.4.4 Material properties of microcrystalline layers

Absorption coefficient

As shown in figure 1-8, absorption coefficient of microcrystalline silicon layers, as a function of photon energy is compared to monocrystalline layers and intrinsic amorphous silicon layers. It can be noted that:

- The absorption coefficient of the microcrystalline layer closely follows the monocrystalline with a shift towards higher values of the absorption coefficient. This shift occurs as a result of light scattering due to rough surfaces in the microcrystalline layer. It could also be due to additional absorption from the amorphous fraction contained within the µc-Si:H layers, especially in spectral region where photon energy is greater than 1.8eV [10].
-

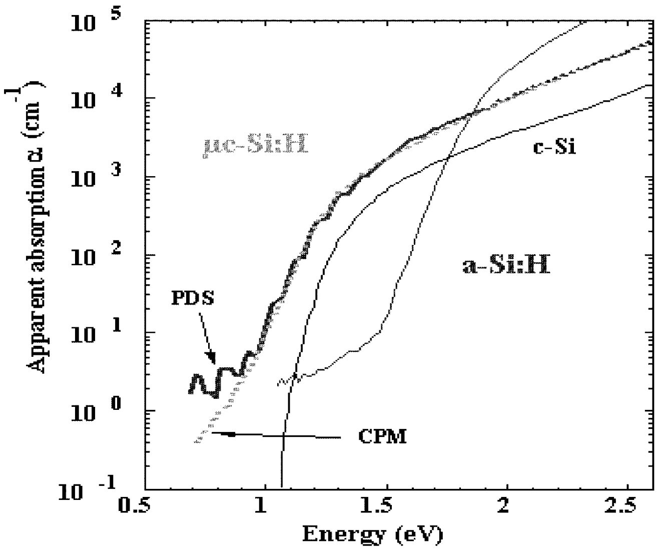

Figure 1-8: Typical curves for the optical absorption of photon energy, for crystalline silicon (c-Si), hydrogenated amorphous silicon (a-Si:H) and hydrogenated microcrystalline (µ-Si:H) silicon thin films. The low absorption region has been measured with the help of Photothermal Deflection Spectroscopy (PDS) and Constant Photocurrent Method (CPM) [8].

- Although the band gap of μc-Si:H seems to be greater than that of c-Si, the effect is solely due to light scattering. If a correction for the scattered light is carried out, the same band gap of 1.12eV can be seen for both c-Si and μc-Si:H [10].
- As can be shown both by optical modeling and mechanical polishing of the surface, sub-band gap absorption (photon energies between 0.6 to 0.8eV) of device quality μc-Si:H layers is very low, because light scattering on the rough μc-Si:H layer surface increases the measured absorption coefficient, hence the true absorption coefficient is often a factor of 10 lower. Such low values of sub-band gap absorption are indication that defect densities in these layers are relatively low, and certainly an indication that grain boundaries are passivated by hydrogen in these layers [10].

In μc-Si:H applications for solar cells, the increase in effective optical absorption due to light scattering by the rough surfaces is beneficial, it allows reduction in solar cell thickness, hence reduction of bulk and manufacturing costs.

Light induced degradation

Unlike a-Si:H layers, which are known to suffer from a light-induced degradation effect also known as the Staebler-Wronski effect, μc-Si: layers fortunately have shown not to bear light-induced degradation characteristics. However, due to the large range of different materials having notably different microstructures, researches done by H. Liu and M. Xu, [10], indicate that light induced degradation should not be ruled out completely. Figure 1-9 shows the comparative behavior under strong light exposure of μc-Si:H solar cells and an a-Si:H solar cell, both with relatively thick i-Layers.

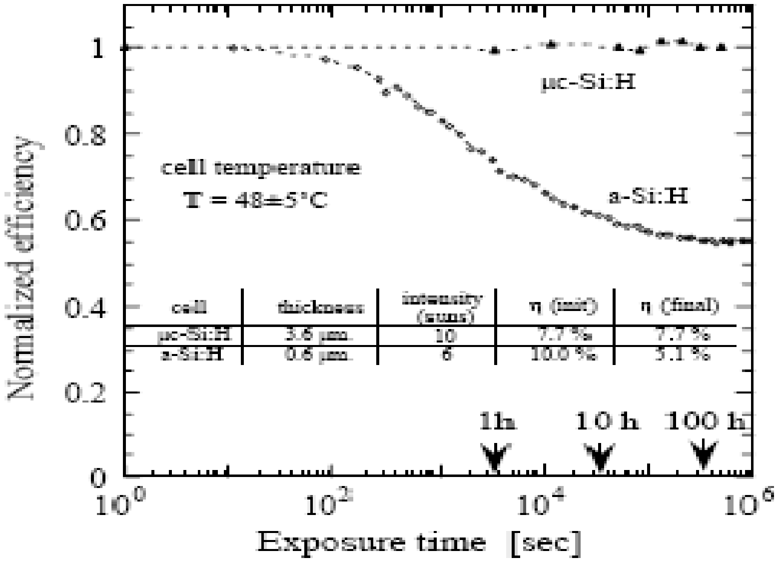

Figure 1-9: Comparative behavior of a microcrystalline silicon solar cell and an amorphous silicon solar cell under intensive light illumination, from a sodium lamp [10].

However, μc-Si:H layers suffer from another possible source of instability, which arises from an increasing contamination by oxygen, when exposed to air over a period of time. This effect, known as the post oxidation effect induces a change in Fermi level which is thereby pushed towards the conduction band edge. Because of this, long term electrical transport and conductivity measurements on μc-Si:H layers could be said to be delicate and not perfectly conclusive or accurate. This leads to detected variations in measured values after weeks of e.g. photoconductivity or dark conductivity, which are due to post oxidation and completely mask whatever other effect one wishes to observe [10]. The group at IMT Neuchatel suspect that μc-Si:H layers produced with high plasma power and strong hydrogen dilution are more susceptible to the post-oxidation effect, because of the cracks present in them. Although post-oxidation is a severe problem for μc-Si:H measurements, μc-Si:H solar cells have shown to be unaffected by this problem. This is suspected to be due to the type of μc-Si:H material used for entire solar cells. However, it has been shown that in full pin-type μc-Si:H solar cells, the back contact acts as a diffusion barrier and prevents post-oxidation.

Hydrogenation of μc-Si is very necessary because the addition of hydrogen plays the role of grain boundary passivation in μc-Si:H layers or solar cells. It is observed that there is much less hydrogen in μc-Si:H than in corresponding a-Si:H layers. In μc-Si:H layers, the hydrogen is preferentially bonded at the surface of the microcrystalline grains, and to a lesser extent in the amorphous fraction of the volume [8].

1.4.5 Requirements for intrinsic μc-Si:H layers for pin / nip solar cells

The following requirements have to be fulfilled in order for intrinsic microcrystalline silicon layers to be useful for solar cells in the pin / nip context [8].

- The μc-Si:H material should be truly intrinsic, with the Fermi level position E_F at mid-gap, i.e.:

  $$E_F \approx ½(E_c - E_v) \qquad (1.12)$$

  where E_c and E_v denote the energy levels of the conduction and valence band-edges, respectively. Microcrystalline silicon layers normally have a pronounced n-type behavior, this type of mid-gap material can be obtained by low level doping, or by a reduction in the inherent oxygen content of the material [8] to values below 10^{19} atoms/cm^3. In order to monitor the Fermi level position, the dark conductivity activation energy can be by measured, it should be higher than 0.5 eV [8], and the dark conductivity itself could also be measured.
- Passivation of grain boundaries and other defects by hydrogen should be carried out.
- Layer surface of the microcrystalline silicon should be rough.
- Crystalline volume fraction should be at least 70% [8].

1.5 Micromorph (μc-Si:H / a-Si:H) tandem solar cells

At different wavelengths of the solar spectrum, microcrystalline and amorphous silicon layers have an edge over each other for either long wavelength regions or short wavelength regions. It was thought that combining both of them in tandem will further maximize the efficiencies of solar cells, this proved to be true and hence the reason why wide studies on microcrystalline silicon layers are being carried out today. This tandem structure is of great importance in thin film solar cells. From a practical point of view, tandem cells are interesting, if the same deposition temperature and process can be used for both the top and the bottom cell. This is also the case when using VHF-PECVD as deposition process, with deposition temperature set to 200°C. The actual band-gap combination for µc-Si:H bottom cell and a-Si:H top cell is in reality very close to the optimal calculated value for the tandem cell which is top = 1.73eV and bottom = 1.16eV[11]. Hence, if all technological problems can be overcome, cell efficiencies obtained from the tandem configuration will be significantly higher than those for single junction µc-SiH:H cells. An example of a micromorph tandem solar cell can be seen in Figure 1-10 below, which shows a double junction micromorph a-Si:H/uc-Si:H thin film silicon solar cell.

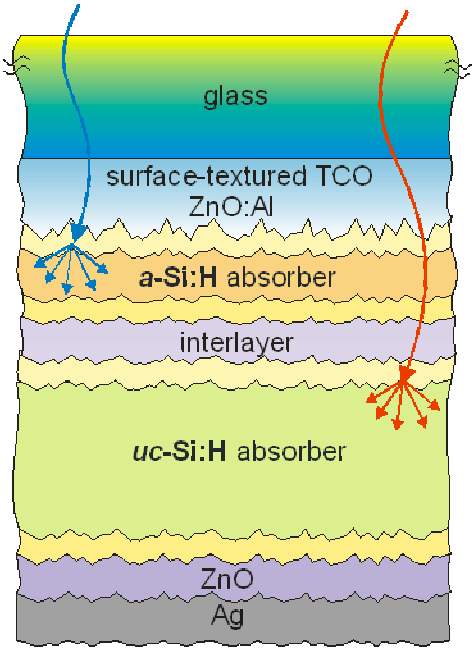

Figure 1-10: Double-junction micromorph a-Si:H/uc-Si:H [11]

1.6 Groups researching microcrystalline solar cells

At present, at least six laboratories worldwide are in the process of producing state of the art µc-Si:H solar cells. IMT Neuchatel (carry out simulations);

- Forschungsanstalt Julich (D)
- ECD (USA)
- Canon (J)
- Uni-solar
- ETL (J) and
- Kaneka (J).

Other institutions not mentioned above include

- University of Ljubljana, (Faculty of Electrical Engineering) (carry out simulations),
- Institute of photovoltaics, forschungszentrum Julich, Germany.
- Department of photonics, Faculty of science and Engineering, Ritsumeikan University, Japan.

Some of these institutions mentioned above are involved in using simulations and modeling to further study the µc-Si:H materials. Computer modeling is required to analyze and optimize a complex optical situation in a solar cell with either flat or rough interfaces [12]. Coherent or incoherent incident light may enter the thin-film solar cell, at each rough interface the light is scattered under different angles, multiple scattering processes at internal rough interfaces need to be taken into account.

1.7 Motivation and objectives of the thesis

Hydrogenated micro crystalline silicon is a mixed phase material, consisting of a crystalline phase, an amorphous phase and some voids. This complex structure makes the experimental study of μc-Si:H a challenge. To overcome some of these challenges in the study of μc-Si:H, optical and electrical modeling and simulations are being employed to study the film properties and their impact on the performance of the solar cell. Modeling and simulations has the advantage of investigating properties with experimental limitations. This is done in very little time.

My thesis is aimed at understanding the operation of microcrystalline silicon solar cells in view of optimizing its performance by modeling in order to create a better tandem solar cell. Both the optical and electrical properties of the μc-Si:H solar cell will be investigated in my work using modeling. The results of the simulations and modeling will be experimented in single junction μc-Si:H solar cells.

For the simulations carried out in this thesis, we will make use of the Advanced Semiconductor Analysis (ASA). The ASA simulator was developed by the solar cells group in DIMES TU Delft. It is a one dimensional simulation program with the capability of simulating both the electrical and the optical parameters of a solar cell.

1.8 Outline of the thesis

A general literature review ranging from a brief introduction of renewable energy to the basics of solar cells, thin-film silicon solar cells and work done by other groups researching μc-Si:H solar cells is given in this first chapter. Chapter 2 discusses light trapping by scattering hence the need to investigate optical properties by modeling. Also discussed is optical modeling, electrical modeling and the ASA simulator. Chapter 3 discusses the process of achieving roughness in the experimental solar cell. Also discussed are the steps taken in calibrating my model. The calibrated model is shown. Chapter 4 is dedicated to the sensitivity studies. A sensitivity study of the optical parameters is done, followed by a sensitivity study of the electrical parameters of the solar cell. Chapter 5 discusses the conclusions and recommendations for an optimized solar cell.

2 Modeling

2.1 Why modeling

Modeling is a very important aspect of research on solar cells and materials used in making solar cells. Using numerical computer modeling or simulations enables researchers to investigate properties of materials that cannot be investigated by means of practical measurements. Most if not all simulators used for solar cells are built on the bases of the Poisson equation and the continuity equations. In solar cells, there are two main properties you look at in order to determine the solar cell functionality and efficiency, these are the optical and the electrical properties. These properties can be investigated using simulations, in this thesis, this will be done using the ASA (Advanced Semiconductor Analysis) simulator which will be discussed later on. ASA is a simulator developed here in the TU Delft solar cell research group.

2.2 Optical modeling and simulations

Modeling and simulations have proven to be good tools in the study of solar cells. Optical modeling and simulations has to do with using computer models to imitate and investigate the optical properties of the solar cells. With these simulations, one can;

- Analyze optical phenomena,
- Look at the losses in different layers of the solar cell,
- Carry out simulations changing the cell parameters and hence optimizing the solar cell.
- Study light trapping and management in the cell.

The afore mentioned investigations are aimed at;

- Reducing the total reflection losses,
- Enhancing light absorption by prolonging the average optical path of light waves in the PV active layers,
- Reducing the absorption in the PV inactive layers.

Adopted in the models are: Anti-reflective coatings, rough interfaces (random nano-scale roughness), novel concepts such as 1-D photonic-crystal-like structures, diffraction gratings, embedded scattering and increased absorption (nanoparticles), etc.

Optical models are achieved by Micro optical design by numerical approaches e.g. rigorously solving of Maxwell's equations, Macro optical design by geometrical optics like ray tracing in 3-D, hybrid optical designs e.g. applying scalar scattering theory. Input parameters used in these models include

- Light sources
- Geometries of objects
- Complex refractive indexes of media

Examples of Numerical simulators include ASA, CELL, Sunshine, etc.

2.2.1 Light trapping

Light trapping techniques are used to enhance absorption of incident light in thin-film silicon solar cells. One of the possible ways to achieve efficient light trapping is scattering of light at rough interfaces [19].

Typically, a substrate with a textured surface is utilized to introduce roughness to the interfaces in the thin-film structures. In the case of solar cells in superstrate configuration, glass/transparent conductive oxide (TCO) substrates with native or post-fabricated TCO surface roughness obtained by wet chemical etching in diluted hydrochloric acid are employed. Different TCO materials Such as ITO, SnO2:F and ZnO are used as a front contact of the thin-film silicon solar cell. Besides high Conductivity and low optical absorption, scattering properties of the TCO layer are important in order to scatter incident light more efficiently.

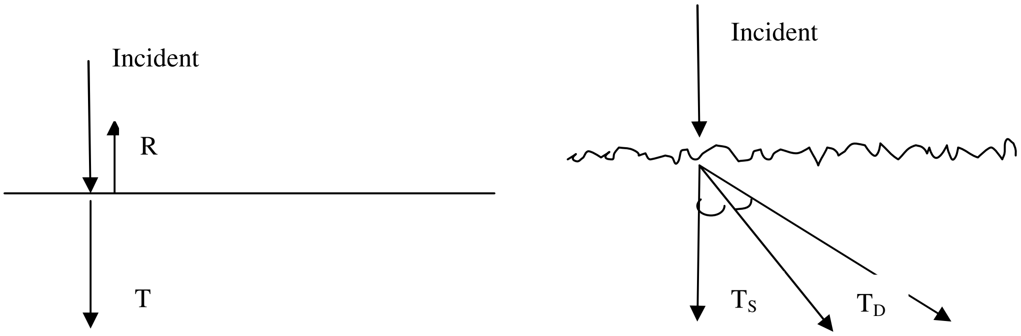

Figure 2-1: Incident light beams, on a smooth surface and on a textured surface showing scattering.

As illustrated in Figure 2-2, when a ray of light photons hit a smooth plane, it just passes through and little absorption takes place, also a lot of photons will be reflected off the surface. But as illustrated also, when light photons hit a rough surface, they have higher angles of refraction and hence spend more time to travel through, increasing the amount of absorption that takes place. Also on rough surfaces, much fewer photons are reflected off the surface hence more photons are absorbed inside, increasing light scattering and trapping.

Modeling is required to analyze scattering at the various interfaces of the solar cell. In order to describe the scattered light in relation to rough interface morphology, two scattering parameters will be discussed; Haze and ADF. In general, high haze and ADF are necessary for enhanced light scattering in the solar cell.

Haze describes how much of light is scattered outside of specular direction.

The Haze parameters for reflected and transmitted light can be calculated as shown

$$H_R = \frac{R_{diff}}{R_{tot}} \qquad (2.1)$$

$$H_T = \frac{T_{diff}}{T_{tot}} \tag{2.2}$$

Where R_{diff} is the diffused component of the reflected light, T_{diff} is the diffused component of the transmitted light, R_{tot} and T_{tot} are expressed as

$$R_{tot} = R_{spec} + R_{diff}\,, \qquad T_{tot} = T_{spec} + T_{diff} \tag{2.3}$$

And spec implies specular component of reflected and transmitted light [21]. The haze parameters are dependent on refractive indices, roughness of the surface, incident angle of the light photons and wavelength. These parameters, characterize the optical quality of texturized front TCO, that has to exhibit high H_T, or texturized back reflector, that has to exhibit high H_R.
Angular Distribution Function (ADF) as the name implies signifies how light is scattered from the surface, and in which direction it is scattered. ADF is also dependent on the same parameters listed above for haze. This parameter can be measured by the so-called angular resolved scattering setup (ARS), which provides angular distribution functions for both reflected and transmitted light (ADF_R and ADF_T, respectively).

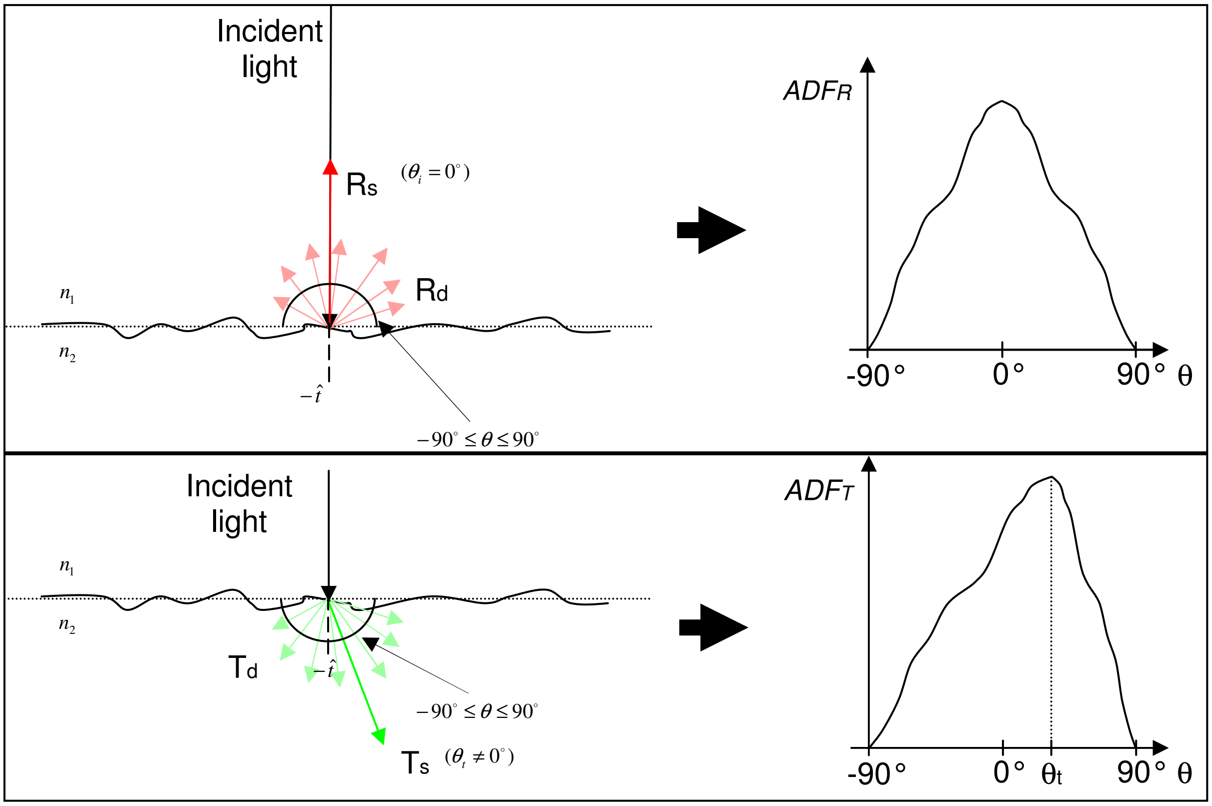

Figure 2-3: Angular distribution of incident light, the greater the angle the better light is scattered and the more the absorption attained.

Periodic gratings enable light scattering in selective angles which are determined by positive or negative integer values m. In order to achieve higher photo currents, the textured layers have to lead to light scattering spectra better than those obtained by the conventional randomly surface-textured substrates. The surface texture of the rough interfaces has to be designed in a way that light is scattered into pre-selected angles. These designs of periodic rough textured surfaces are the gratings. Periodic diffraction gratings enable efficient light scattering to high angles. They are based on periodic gratings (could have different shapes, e.g. rectangular) on a surface. The period P of these gratings should be in the range of the wavelength of light in order to achieve desired diffraction effects. The grating equation below can be used to calculate scattering angles.

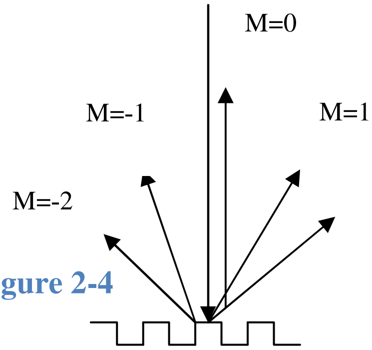

Figure 2-4

$$\varphi_{scatt} = \arcsin\left(\frac{m \cdot \lambda}{n \cdot p} - \sin \varphi_{inc}\right) \tag{2.4}$$

Where m represents the diffraction order, λ is the wavelength of light, n is the refractive index of the incident medium, p is the grating period and φ_{inc} is the angle of the incident light.

2.3 Need for light trapping and management

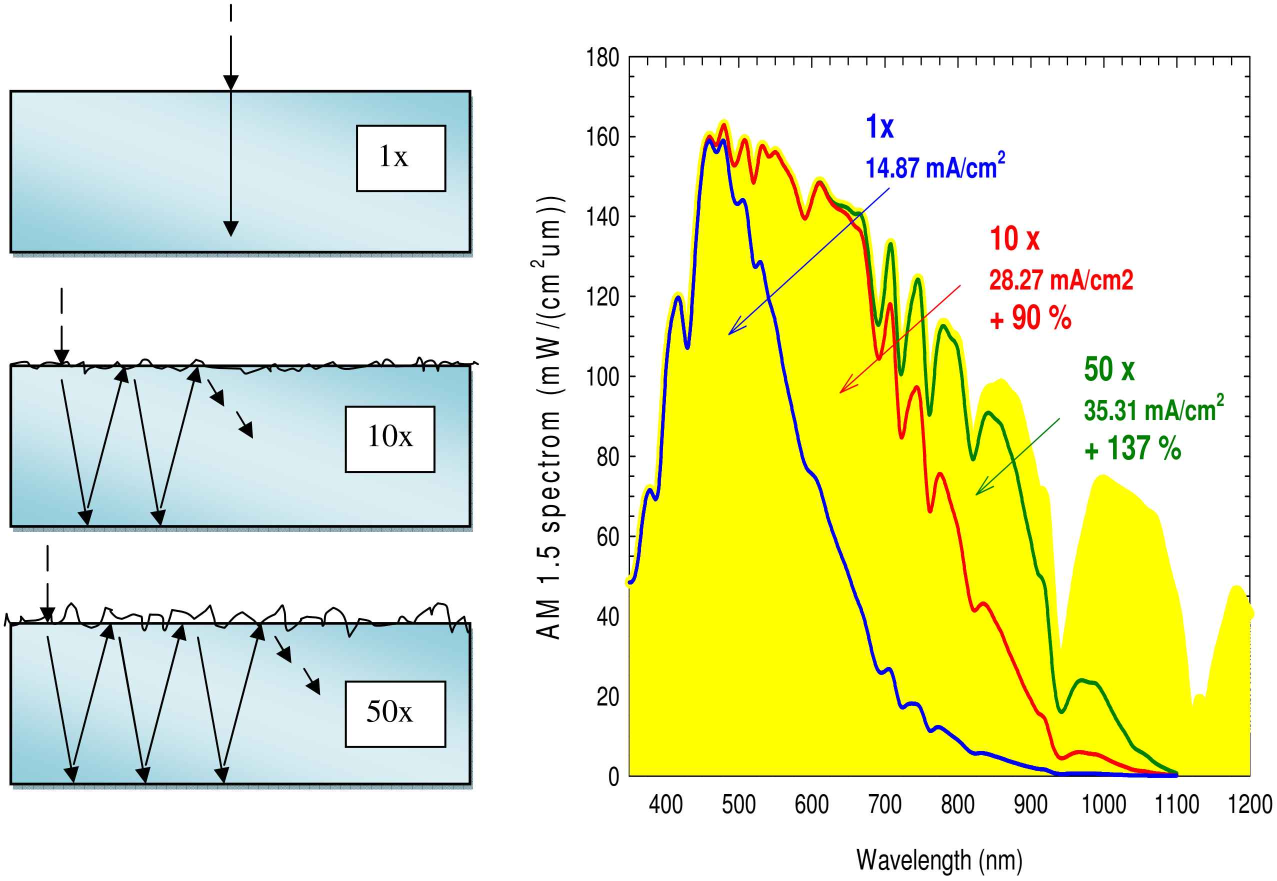

Figure 2-5: Light absorption in µc-Si:H solar cell after 1, 10 and 50 passes

Light management is a very important aspect of solar cells. The more light you can trap, the better the QE and Jsc of the solar cell. Proper light trapping and management techniques make use of the possibility of having multiple passes of light in the absorber layer. The effect of having multiple passes of light is like increasing the thickness of the i-layer of the solar cell by the number of passes achieved. There are many techniques of improving light trapping in a solar cell, of which some are; implementation of rough interfaces, optimized diffraction gratings, anti reflective coatings, highly reflective back contacts, photonic crystals, inter layers, etc. simulations were carried out by increasing the thickness of the solar cell by 10 and 50 times, this is like having 10 and 50 passes of light in the cell. Figure 4-0 shows the results of the simulations and the depiction of multiple passes of light.

2.3.1 Electrical modeling

By electrical modeling, the electrical properties of a solar cell can be investigated, hence enabling solar cell optimizations. As mentioned above, the bases of electrical modeling are the Poisson equation and the continuity equation for electrons and holes. Using electrical modeling, the dark and light J-V characteristics of a solar cell can be investigated and optimized. Also the way different properties of materials such as the band gap, mobility gap, activation energy, defect densities, etc, affect the external properties (open circuit voltage, Fill factor, short circuit current and the overall efficiency) of solar cells can be investigated.

2.4 Some Research groups using modeling and simulations to study solar cells

The Ljubljana group, Janez Krc et al in a paper (improving thin-film solar cells through optical modeling) explained that a simulator called "sunshine" was used, to perform optical model simulations of different types of thin film solar cells. The sunshine model was used to explore ways to optimize the efficiency of the micromorph tandem solar cell. The scatter levels were calibrated by the optical parameters of realistic state of the art micromorph solar cells, which typically achieve efficiency of about 10% [13]. The simulated optimized solar cell has a J_{sc} potential above 16mA/cm^2, from the simulations, which suggests possibility of efficiency exceeding 15%. In order to increase the simulated efficiency, several modifications were made. These include, improved back reflector reflectance and decreased supporting layer absorptance. Also implemented were tweaks to interface scattering levels, broaden scattered light angular distribution (lambertian), and optimize antireflective coatings on the front glass substrate. Further modifications also provided wavelength-selective properties for intermediate reflector between top and bottom cells [13].

Sunshine was also used to design a highly reflective back reflector. In reality, back reflectors from textured metals such as aluminum, and silver are typically used for this purpose. Properties of a non metallic back reflector were simulated using one dimensional photonic-crystal-like structures with high reflectivity, these materials were based on thin films which can be deposited at low temperatures and are compatible with the deposition process of thin-film solar cells, these structures were modeled as four pair layers of intrinsic amorphous silicon [13] and silicon dioxide. Nearly 100% reflectance was achieved in the wavelength range of interest for silicon micromorph solar cells [13]. In another paper by Janez Krc, F. Smole and M. Topic, (Optical simulation of the role of reflecting interlayers in tandem micromorph silicon solar cells) investigated the role of an interlayer in the micromorph silicon solar cell from an optical point of view. Simulation results using a single interlayer showed that the refractive index of the interlayer plays an important role [14]. Interlayers with low refractive indexes are desired (below n_{zno} =2.0), since they render a higher internal reflectance, leading to improved quantum efficiency and short circuit current density of the top cell [14]. It was noted that optical losses due to reflected light from the solar cell are enhanced for the interlayers with high internal reflectance, since the reflected light cannot be fully trapped in the top solar cell [14]. However the quantum efficiency and short circuit current of the bottom cell are in general decreased if the interlayer is introduced, due to decreased transmission of light to the bottom cell.

The group at the Department of photonics, Faculty of science and Engineering, Ritsumeikan University, Japan carried out device modeling for p-i-n junction basis thin film microcrystalline Si solar cells, examined with a simple model of columnar grain structure utilizing two dimensional device simulator. They found that the grain size and grain boundary passivation are of great importance. It is also found that conversion efficiency of more than 16% is expected with 3.0 µm thick cell if incident light can be well confined [15]. The results of numerical device simulations for p-i-n diodes and the closed-form expression of the current-voltage characteristics developed for p-n diodes are compared by T. Brammer and H. Stiebig of forschungszentrum Julich, Germany. It is shown that the closed form expression correctly predicts the functional relationship between material parameters and device performance of p-i-n diodes [16]. The ideality factor between 1 and 2 is analyzed in detail. The effect of the defect density, the intrinsic carrier concentration, the mobility and the built-in potential on device performance is demonstrated. These insights are applied to analyze microcrystalline silicon thin-film solar cells deposited by chemical vapor deposition at temperatures below 250 degrees centigrade [16].

2.5 The ASA simulator

The ASA (Advanced Semiconductor Analysis) simulator is a one dimensional device simulator which is based on the adapted drift-diffusion model [22]. ASA program uses the electrostatic potential, the free electron concentration n, and the free hole concentration p, as variables. The continuity equations for electron and holes and the Poisson equation form the basis for the model equations. The ASA program has the capability of simulating both the optical and the electrical properties of solar cells.

A typical input file for an integrated optical and electrical simulation would include but are not limited to:

- The grid layers, indicating the number of spaces for each layer
- The “nk” files
- The Haze and ADF parameters
- The properties in the bands: mobility gap, electron affinity, etc.
- The doping concentrations
- The Valence band tail definition states
- The conduction band tail definition states
- Settings for temperature, number of iterations, e.t.c
- The print statements for output files.

A sample input file for ASA can be seen in the appendix. In the ASA simulator, the optical properties are defined by the “lnk” which are wavelength, refractive index and the extinction coefficient. The main features of the ASA program are summarized below [22]:

- Modeling of multi heterojunction amorphous and crystalline silicon devices
- Models describing a complete density of states distribution as function of energy, which include both the extended and localized (tail and defect) states with corresponding recombination-generation statistics

- Calculation of the defect-state distribution using the defect pool models
- Calculation of the absorption profile in a device with flat and rough interfaces
- Model for the tunnel-recombination junction
- Continuous change (grading) of all input parameters as a function of position in the device or energy level in the gap
- Degradation of a-Si:H solar cells can be simulated by using position dependent coefficients (k_h, k_z, k_e), which effect the density of D_h, D_z, and D_e states
- It is written in the ANSI C language
- Runs under UNIX, LINUX and WIN32 operating systems.

The basic set of semiconductor equations which are the building blocks of the ASA simulator are given below:

The Poisson equation:

$$div(\varepsilon grad\psi) = -\rho \tag{2.5}$$

The continuity equations for electrons:

$$\frac{\partial n}{\partial t} = \frac{1}{q} divJ_n + G_{opt} - R_{net} \tag{2.6}$$

The continuity equations for holes

$$\frac{\partial p}{\partial t} = -\frac{1}{q} divJ_p + G_{opt} - R_{net} \tag{2.7}$$

The electron current density:

$$J_n = n\mu_n gradE_{FN} \tag{2.8}$$

The hole current density:

$$J_p = -n\mu_p gradE_{FP} \tag{2.9}$$

where the permittivity of the semiconductor is ε , ψ is the electrostatic potential, ρ is the space charge density, G_{opt} is the optical generation rate and R_{net} is the net recombination-generation rate of electrons and holes. E_{FP} is the hole quasi Fermi energy level and $\frac{\partial n}{\partial t}$ is the time rate of change in the electron concentration.

To calculate the free carrier concentrations as a function of the quasi Fermi levels and the effective density of states in the valance and conduction bands, N_c and N_v respectively, the Maxwell-Boltzmann approximation is used to obtain the following expressions;

$$n = N_C \exp\left(\frac{E_{FN} - E_C}{KT}\right) = N_C \exp\left(\frac{E_{FN} - (E_{vac} - qx)}{KT}\right) \tag{2.10}$$

$$p = N_V \exp\left(\frac{E_V - E_{FP}}{KT}\right) = N_V \exp\left(\frac{(E_{vac} - qx - E_\mu) - E_{FP}}{KT}\right) \tag{2.11}$$

where E_{vac} is the vacuum potential, x is the electron affinity and E_μ is the mobility gap.

For a one dimensional model, under steady state condition and using the Einstein relations for the diffusion coefficient for electrons and holes, the set of model equations become:

$$\frac{d}{dx}\left(\varepsilon\frac{d\psi}{dx}\right)=-\rho \tag{2.12}$$

$$\frac{1}{q}\frac{dJ_n}{dx}+G_{opt}-R_{net}=0 \tag{2.13}$$

$$-\frac{1}{q}\frac{dJ_p}{dx}+G_{opt}-R_{net}=0 \tag{2.14}$$

$$J_n=qD_n\frac{dn}{dx}+\mu_n n\left[-q\frac{d\psi}{dx}-\frac{dx}{dx}-\frac{KT}{N_C}\frac{dN_C}{dx}\right] \tag{2.15}$$

$$J_p=-qD_p\frac{dp}{dx}+\mu_p p\left[-q\frac{d\psi}{dx}-\frac{dx}{dx}-\frac{dE_G}{dx}+\frac{KT}{N_V}\frac{dN_V}{dx}\right] \tag{2.16}$$

Where the space charge density ρ is given by

$$\rho=q(p-n+p_{loc}-n_{loc}+N_{don}-N_{acc}) \tag{2.17}$$

and takes free and localized carriers and ionized donors and acceptors into account.

3 Solar cell calibration

3.1 Model calibration

The solar cell model calibration can be seen as an exercise that aims at matching experimentally obtained results with results obtained by simulations, thereby validating the simulation model. To calibrate a solar cell fully, both the optical and electrical calibrations have to be done.

3.2 Optical calibration

3.2.1 Achieving rough interfaces

ZnO TCO was deposited on a glass substrate, yielding a flat surface. In order to achieve roughness, the TCO was etched with diluted hydrochloric acid. In order to obtain various surface roughnesses, the etching time is varied. In order to obtain the root mean square of 140nm implemented in our own solar cells and in my model, the etching time was set at 40s. Etching of the TCO depending on etching time can reduce the layer thickness by up to 400nm.

Atomic force microscopy (AFM) and scanning electron microscopy (SEM) are used to obtain the layer surface roughness and hence achieving layer characterization. Haze increases with increasing root mean square roughness and decreases with increasing wavelength for both transmitted and reflected light. It can then be inferred that scattering at the glass/TCO substrate is most efficient for the short wavelength light and high root mean square roughness. Also inferred is that haze reflectance parameter has higher values than haze transmittance for the same substrate showing scattering is less pronounced in transmission and more pronounced in reflection [23].

Angular resolved scattering (ARS) measurements were used at the rough interfaces to determine the angular distribution functions, ADF_T and ADF_R. J. Krc et al reported in [23] that for glass/TCO:Al substrates with higher root mean square roughness, scattering into smaller angles around the specula direction is large, whereas for substrates with lower root mean square roughness, light scatters greatly into shallow angles ($\varphi > 30^o$) . The ADF and haze parameters are used as input parameters to describe scattering at rough interfaces. Real life measured values of haze and ADF are incorporated in the model while carrying out the calibration. The coherent (specular) and incoherent (diffused) components of light were taken into account. In order to get scattering parameters of the internal interfaces, we estimated using the modified equations of scalar scattering theory given in equations 3.1 and 3.2 below. The rms roughness values are given in Table 1 below were used.

The optical calibration of the solar cell defines the scattering parameters implementation in the simulation to reflect the scattering at the interfaces in the solar cell. . The two parameters responsible for the this are the Haze (T,R) parameter and the Angular Distribution Function (ADF).

The Haze H is the ratio between diffused and total diffused (diffused + specular) light. The Haze for reflectance is given by:

$$H_R = 1 - e^{-\left(\frac{4\Pi \sigma_{RMS} n_1 \cos\psi}{\lambda}\right)^2} \tag{3.1}$$

Where σ_{RMS} , is the root mean square roughness parameter of the interface and is used to describe roughness, and n_1 is the refractive index of the incident medium. For the transmission, the Haze is given by

$$H_T = 1 - e^{-\left(\frac{2\Pi \sigma_{RMS} \left|n_1 \cos\psi_1 - n_2 \cos\psi_2\right|}{\lambda}\right)^{1.8}} \tag{3.2}$$

In the above, it is important to note that we assumed $\psi = 0$ in all cases, ψ being the incident angle.

The Angular Distribution Function ADF of the scattered light is given by

$$ADF_{R,T} = \frac{2b^2}{\cos\psi_{scatt}\left(b^2 + \tan^2\psi_{scatt}\right)}.\sin\psi_{scatt} \tag{3.3}$$

Where ψ_{scatt} is the scattering angle and b is the vertical radius of the ellipse. For ADF transmission, b was taken to be 0.4 and for ADF reflection, b was taken to be 0.5. For the lambertian case, b=1.

Table 1 below shows the values of root mean square roughness I used for my calibration, for both a rough and a flat solar cell at the different interfaces of the cell.

Table 1. Root mean square roughness values of the interfaces used for the calibration

INTERNAL INTERFACES	σ_{RMS} ROUGH (nm)	σ_{RMS} FLAT (nm)
TCO/P	140	10
P/I	140	10
I/N	50	10
BUFFER/Ag	50	10
Ag/AIR		10

In calibrating the model, the root mean square roughnesses in Table 1 were inserted into the haze equations above. The result of the haze calculations for different wavelengths and the result of the ADF calculation were used to build the interface files for the simulations. The nk files are built by extracting the data from the mini RT after the reflection and transmission measurements. These exported data are arranged in the way the ASA simulator could use them. An input file for ASA simulation is built having a cell configuration as the p-i-n structure, with glass thickness of 1.5 mm, TCO thickness of 800 nm, p-layer thickness of 24 nm, i-layer thickness of 1230 nm, n-layer thickness of 20 nm and back reflector thickness of 300 nm. The optically calibrated model as a result of the above calculations, solar cell structure and input parameters was verified by comparing the plot of the quantum efficiencies of the experimental solar cell with the calibrated one. The figures below show a comparison between the QE of the calibrated model and the measured QE of a solar cell deposited in DIMES.

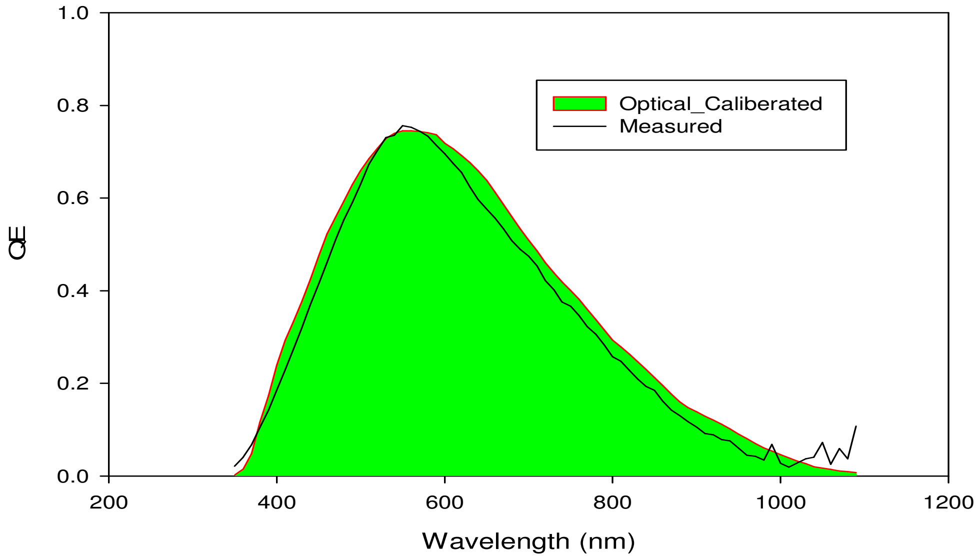

Figure 3-1: Quantum efficiency of the calibrated rough solar cell compared with the measured.

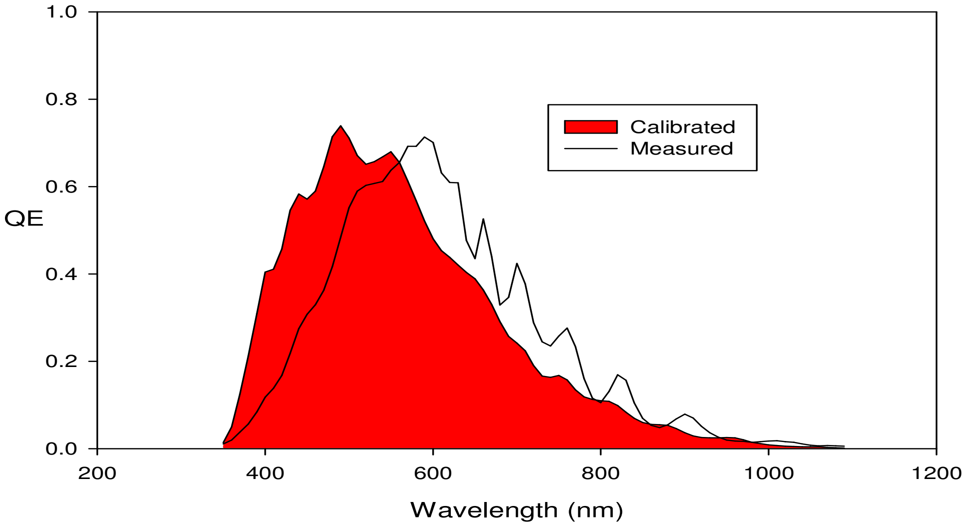

Figure 3-2: Quantum efficiency plot for a flat solar cell. The calibrated curve is compared to the measured.

From figure 3-1, we can see that a good agreement was reached between the measured QE and the simulated one, hence our model being calibrated. The large difference in measured and simulated solar cells QE for the case of the flat cell shown in figure 3-2 is suspected to be as a result of the simulation nk files used, but I was not able to reach a clear conclusion as to where the difference came from.

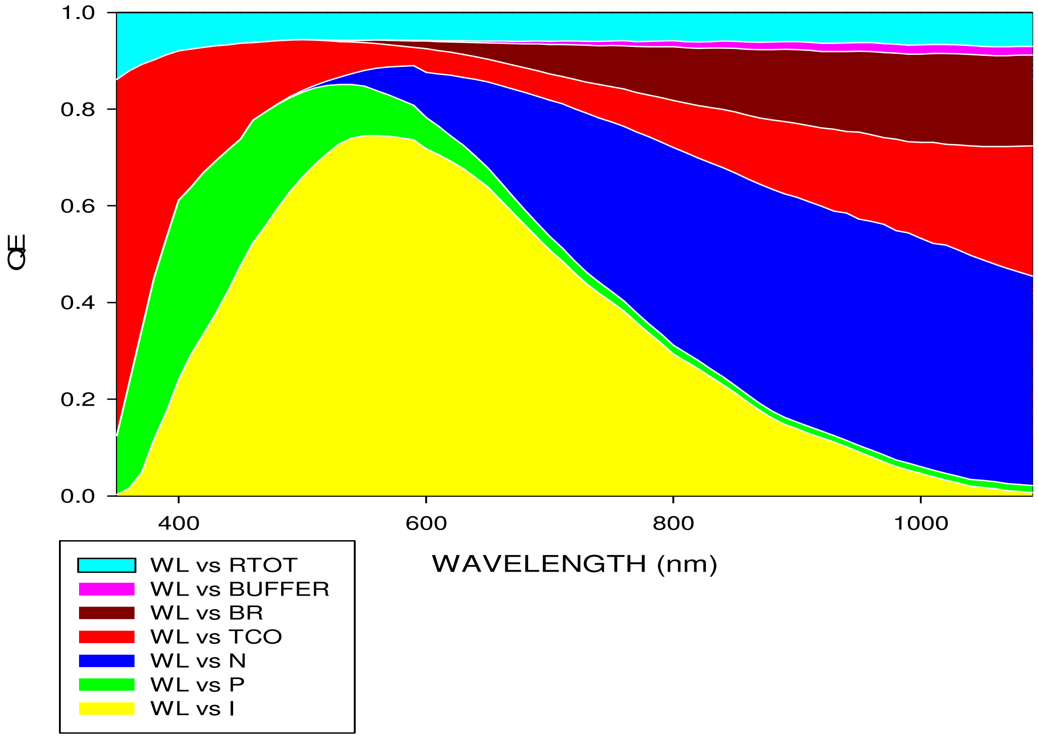

Figure 3-3: Simulated plot of optical absorption in different layers of a solar cell

Figure 3-3 above shows absorption in all the optical layers of the simulated solar cell. The graph shows most of the absorption to be in the i-layer. The absorption in the other layers of the solar cell can be seen as losses, as absorption is desired most in the i-absorber layer. We observe that due to the thickness of the TCO, a lot of absorption takes place in that layer. Surprisingly, there is a lot of absorption in the n-layer. In reality however, there is relatively little absorption in the n-layer of the solar cell.

3.3 Electrical calibration

Extensive work has been done on the electrical calibration of thin film microcrystalline silicon solar cell in the thesis “Characterization of Thin-Film Silicon Solar Cells through Numerical Modeling” by Bart Pieters. Some of the model parameters used in this calibration are based on the earlier input parameters obtained by B. Pieters [18].The table below shows a list of some models parameters and their values. The electrical calibration involves the matching of the electrical input parameters of the solar cell with realistic values to obtain simulation results close to those obtained from measurements. The result of the electrical calibration should give a close matching with the solar cell external parameters of a measured cell.

Table 2: list of model parameters

PARAMETER	p-layer	i-layer	n-layer	unit
STRUCTURE				
thickness	24e-09	1230e-09	20e-09	m
TRANSPORT, DOPING AND EXTENDED STATES				
E_μ (e.mob)	1.18	1.18	1.75	eV
E_r (epsilon)	11.9	11.9	11.9	–
χ (chi)	4.05	4.05	3.90	eV
N_v (nv)	0.62E+25	0.62E+25	4.0E+26	m^{-3}
N_c (nc)	1.25E+25	1.25E+25	4.0E+26	m^{-3}
μ_n (mu.e)	5.0e-3	5.0e-3	2.0e-3	$m^2V^{-1}s^{-1}$
μ_p (mu.h)	1.5e-3	1.5e-3	0.5e-3	$m^2V^{-1}s^{-1}$
E_a (e.act)	0.01	–	0.05	eV
VALENCE BAND TAIL STATES				
E_{v0} (e.char)	0.031	0.031	0.080	eV
n.emob	1.04e26	1.04e26	5.00e27	m-^{3}eV^{-1}
c.neut	5.0e-15	5.0e-15	0.7e-15	m^3s^{-1}
c.pos	50.0e-15	50.0e-15	07.0e-15	m^3s^{-1}
CONDUCTION BAND TAIL STATES				
E_{c0}	0.031	0.031	0.070	eV
n.emob	2.8E+26	2.8E+26	7.0E+27	m-^{3}eV^{-1}
c.neut	5.0e-15	5.0e-15	0.70e-15	m^3s^{-1}

c.neg	50.0e-15	50.0e-15	7.0e-15	$m^3 s^{-1}$
DANGLING BONDS STATES				
e.corr	0.2	0.2	0.2	eV
N_{db} (n)	3e22	2e22	2e22	m^{-3}
ce.neut	3.0e-15	3.0e-15	0.7e-15	$m^3 s^{-1}$
ce.pos	30.0e-15	30.0e-15	7.0e-15	$m^3 s^{-1}$
ch.neut	3.0e-15	3.0e-15	0.7e-15	$m^3 s^{-1}$
ch.neg	30.0e-15	30.0e-15	7e-15	$m^3 s^{-1}$

The figure below shows the J-V and the quantum efficiency plots of the simulated integrated electrical and optical cell compared to the measured solar cell.

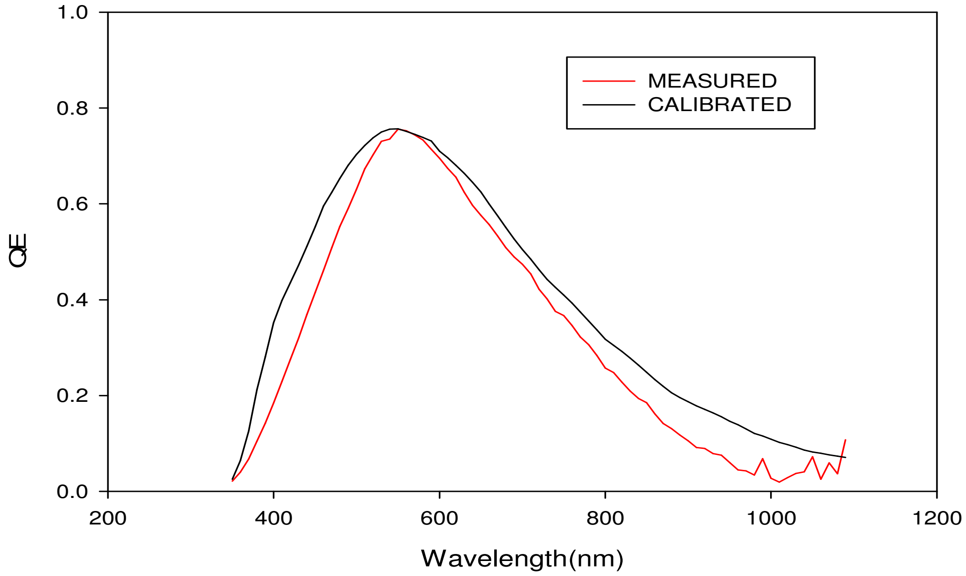

Figure 3-4: The simulated QE compared with the measured.

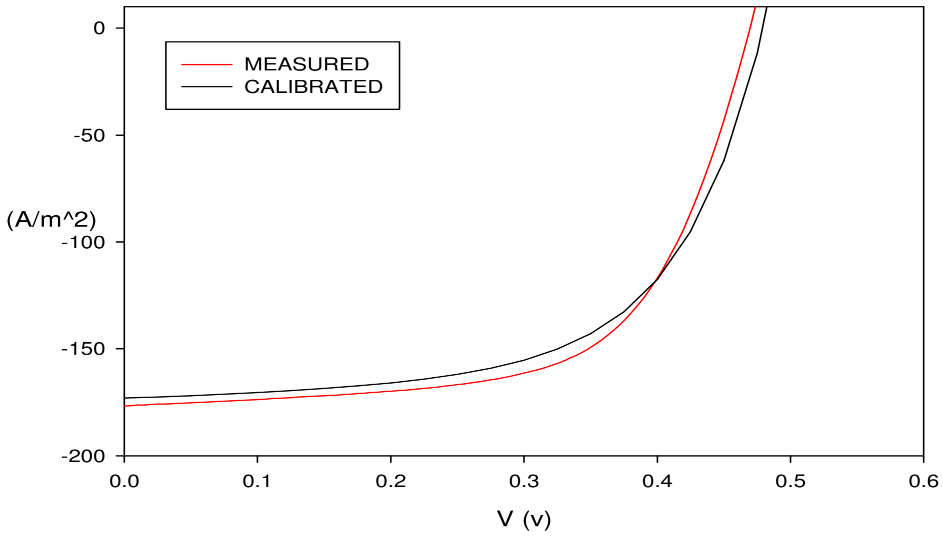

Figure 3-5: The simulated JV plot compared with the measured.

The results of the simulation show a reasonable amount of matching with the experimental cell and can therefore be used as a model to simulate and study the behavior and properties of a hydrogenated microcrystalline silicon solar cell. The next chapter treats a sensitivity study of the parameters and structure of the model solar cell made in this chapter. The table below shows a comparison of the calibrated solar cell characteristics and the measured cell.

Table 3. Comparison of calibrated solar cell parameters with measured

PARAMETER	MEASURED	CALIBRATED
J_{sc}(A/m$^{2)}$	-177	-172.7
V_{oc} (V)	0.47	0.4774
FF	0.63	0.6095

3.4 Conclusion

The method of achieving rough surfaces by etching of the TCO was described, it was also mentioned that layer characterization is performed by AFM and SEM measurements for the haze and ARS measurements were used to determine the ADF. The optical calibration of the solar cell was performed using the haze and ADF and the results matched closely with experimental data for the rough. Electrical calibration was also achieved using the results from the optical calibrated model. The table 2 presents the list of model parameters for the calibrated cell. The electrical calibrated model was also matched with experimental data.

4 Sensitivity study

4.1 Sensitivity studies

In order to understand how hydrogenated microcrystalline silicon solar cells work, the effects of various input parameters on the solar cell was investigated. In this study, the sensitivity of the solar cells J-V characteristics and the quantum efficiency to the various input parameters were analyzed in ASA. Also recombination in the solar cell was investigated as well as the effect of various input model parameters on the open circuit voltage.

Methods describing how the ASA simulator combines a forward model with inverse modeling to extract values of input parameters for the forward model have been shown in [1]. In this study, we tried to investigate the solar cells sensitivity to input parameters. For the sensitivity study, the solar cell calibrated in chapter three was used as a reference solar cell. The structure of the solar cell is the same as the structure explained in chapter 3, except for the optical simulation where a buffer layer was put in-between the i and n layers. The figure below shows the QE of the calibrated cell used as a reference.

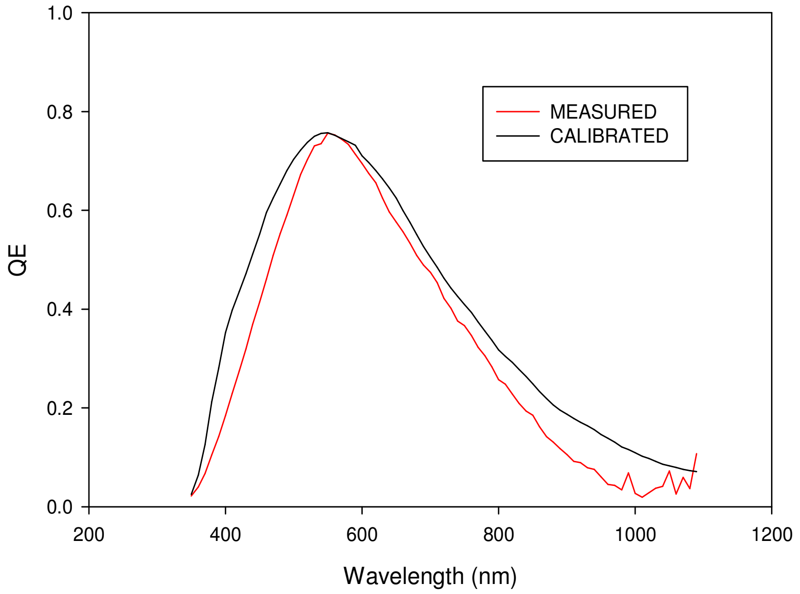

Figure 4-1: Plot of external QE of a simulated solar cell vs. that of the measured solar cell.

4.2 Optical sensitivity studies

The optical properties of the solar cell are very important and cannot be ignored; they have to do with the solar cell's absorption of light and the generation of the electron hole pairs. The quantum efficiency and the short circuit current density of the solar cell are largely dependent on the optical properties of the solar cell. Light trapping and light management techniques in the solar cell have been and are still being researched extensively to improve the cells optical properties. In this section of the thesis, a sensitivity study of some of the optical properties of the solar cell was conducted. Parameters such as absorption coefficient, the root mean square roughness of the layer interfaces, and thicknesses of the various layers were studied, to see their effects on the solar cell.

4.2.1 Absorption coefficient

The absorption coefficient of a material determines how far light of a particular wavelength will penetrate that material before it is absorbed. Light is poorly absorbed in materials with low absorption coefficient and in case of very thin layers, the material can serve as a transparent layer to certain light wavelengths. Absorption coefficient is dependent on wavelength as well as the material absorbing the light. In hydrogenated microcrystalline silicon as well as in other semiconductor materials, light rays with energy lower than the band gap, cannot cause the creation of an electron hole pair and hence the light is not absorbed. As just explained, absorption is dependent on the wavelength and the band gap of the material, hence if the band gap of a material can be varied, the absorption coefficient or the materials ability to absorb light can be varied.

The absorption coefficients of different layers in the solar cell of the calibrated model were varied.

The effects of the absorption coefficient of the p, n and TCO layers on the quantum efficiency of the solar cell were investigated. Figure 4-2 shows the results obtained. The figures show that reducing the absorption in the p, n and TCO increases the absorption in the absorber layer.

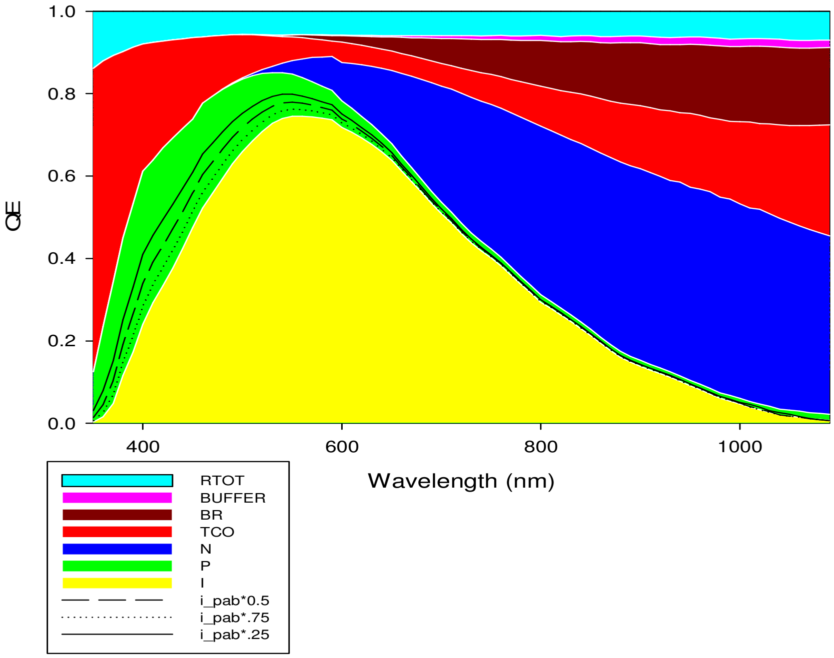
1.0
0.8
0.6
0.4
0.2
0.0
QE
400
600
800
1000
Wavelength (nm)
RTOT
BUFFER
BR
TCO
N
P
I
i_pab*0.5
i_pab*.75
i_pab*.25

(a)

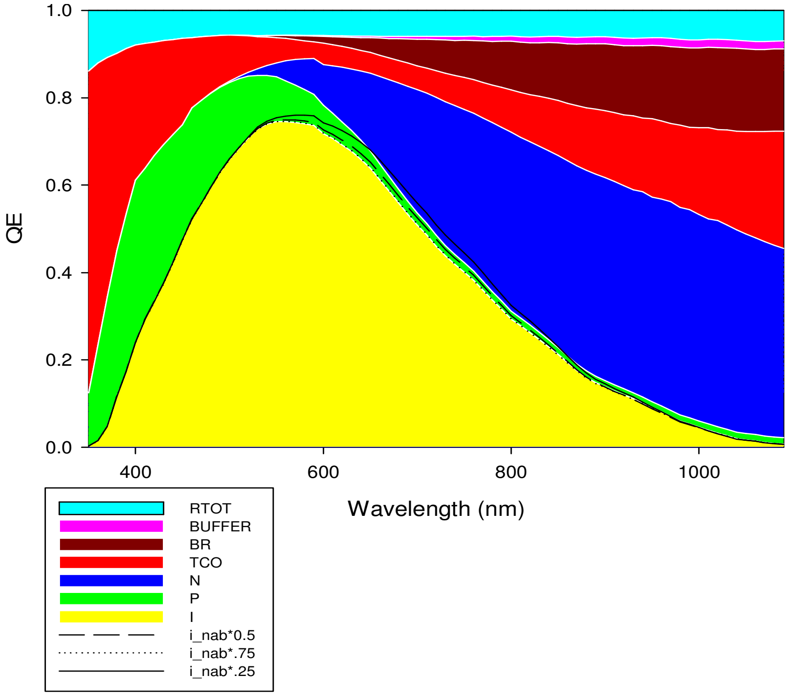
1.0
0.8
0.6
0.4
0.2
0.0
QE
400
600
800
1000
Wavelength (nm)
RTOT
BUFFER
BR
TCO
N
P
I
i_nab*0.5
i_nab*.75
i_nab*.25

(b)

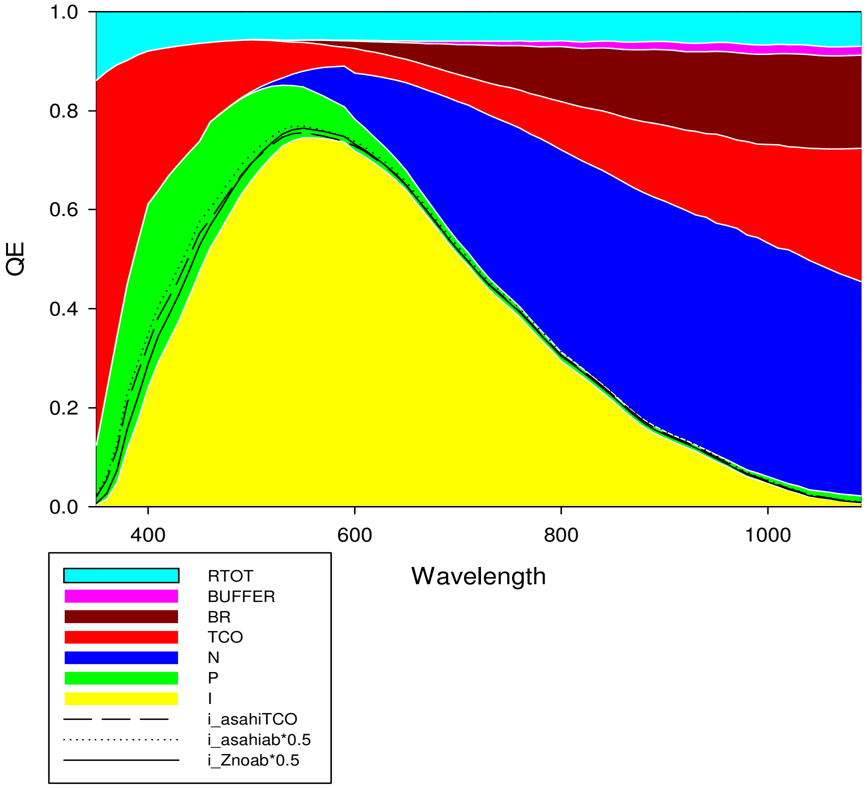

(c)

Figure 4-2: (a) Plot of the effect of a reduced p-layer absorption coefficient. (b) plot of a reduced n-layer absorption coefficient. (c) varied TCO ZnO and Asahi absorption coefficients.

A reduced absorption coefficient of the p-layer causes a reduced absorption in the p-layer and consequently, increased i- layer absorption for the short and mid wavelength range as seen in the figure. Reduced absorption coefficient of the n-layer also has a significant effect, even though not as significant as the p-layer and TCO. The increased i-layer QE can be seen in the long wavelength region. The effect of reduced TCO absorption coefficient can be seen in both the long and short wavelength regions, with majority of the effect though in the short wavelength region.

4.2.2 Root mean square roughness of solar cell interfaces

4.2.2.1 Haze

As discussed in chapter 1, roughness in solar cells is a very important aspect of optimizing light trapping in a solar cell and increasing the current density of the solar cell and hence its quantum efficiency. The more roughness an interface attains, the better the scattering in the cell will be and the higher the values of the QE and Jsc. In order to have a feel of the effect surface roughness creates on the Jsc and the QE of a solar cell, the Root mean square roughness of the TCO/P interface was varied. The roughness was set at RMS = 10, 50, 140 and 200 nm. The results are shown in the graphs below. In the graphs, we observe that as the RMS roughness of the TCO/P interface increases, the QE and Jsc increase. Figure 4-4 shows that a point is reached where the increment in the Jsc and QE tends to saturate, hence we see that a point is reached where roughness cannot be increased further. Roughness is achieved by etching in acids like dilute HCl. There is a limit in which you can etch the TCO layer to, else you start obtaining losses in the thickness of the layer.

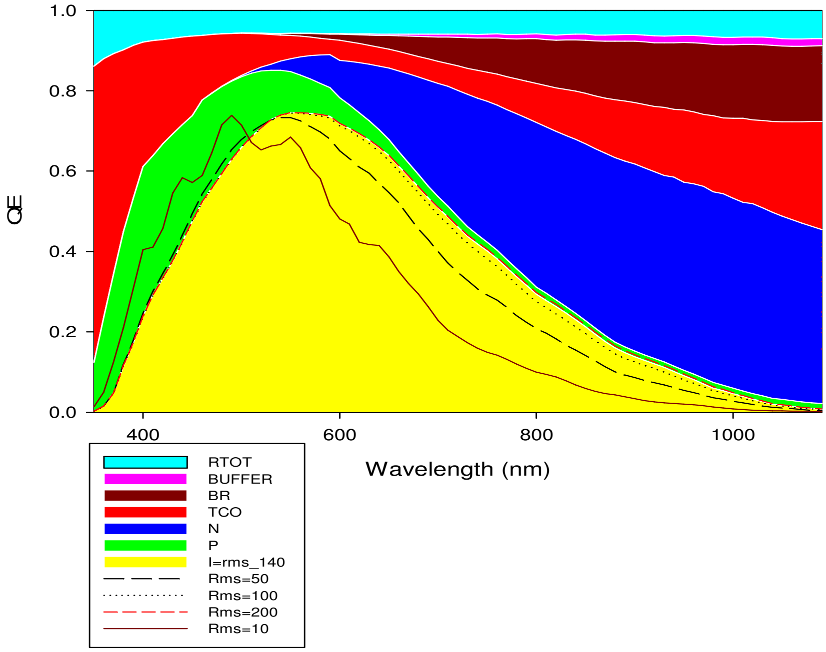

Figure 4-3: QE for various RMS roughness roughness of the TCO/P interface.

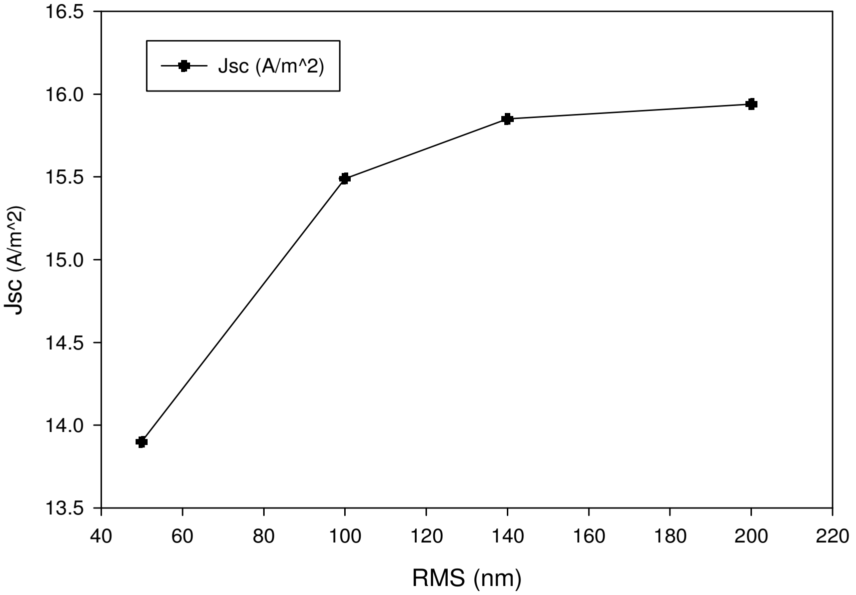

Figure 4-4: Jsc for various RMS roughness of the TCO/P interface.

The J_{sc} current densities represented in figure 4-4 were calculated by multiplying the quantum efficiency values for all wavelengths by the AM 1.5 spectrum and the elementary charge (1.6E-19) and summing the results for all the wavelength values.

4.2.2.2 ADF: radius of the ellipse

In this section, the radius of the ellipse in the angular distribution function (ADF) calculation is varied. It is believed that the larger the radius of the ellipse, the better the light scattering obtained in the solar cell. The figure 4-5 below, shows an incident ray of light and the scattering with respect to the radius of the ellipse. The smaller arc has a smaller radius “r1” and hence scattering is less. But the bigger arc or semicircle we can see has a higher radius “r” and we can say that scattering in the material is improved.

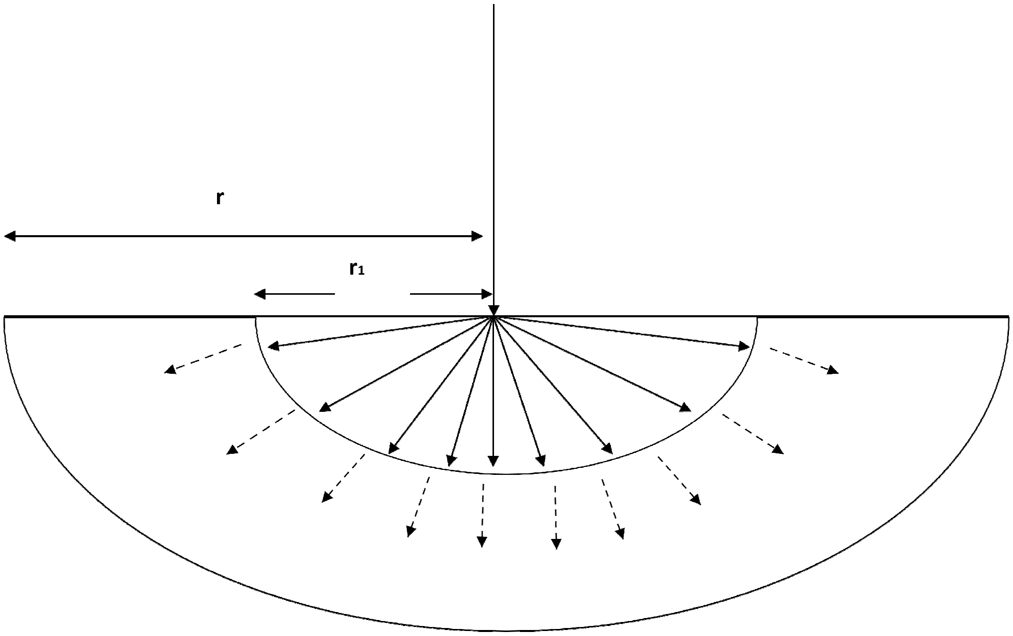

Figure 4-5: Radius of the ellipse in relation to scattering.

The effect of an increased radius of the ellipse was investigated for both the ADF transmittance and the ADF reflectance. It can be seen below in figure 4-6 (b) that there is a negligible change in the QE plot for a change in radius of the ellipse for the case of ADF reflectance. But for the case of the change in radius of the ellipse for ADF transmittance, figure 4-6 (a), we can really see for high values of the radius of the ellipse, implying high scattering, that there is an increase in the quantum efficiency, implying an increase also in the short circuit current density mostly in the long wavelength region. This supports the claim shown in figure 4-5 above.

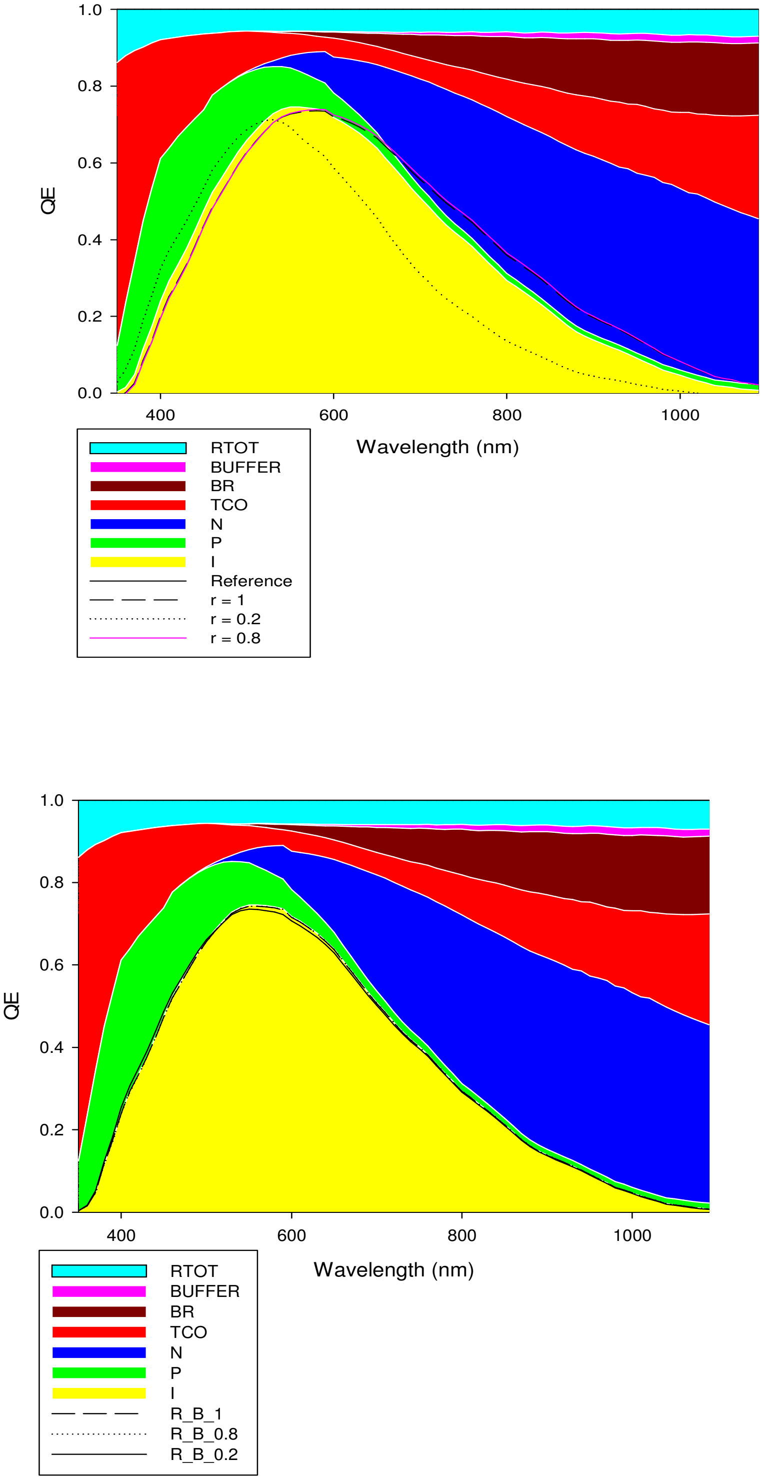

(a)

(b)

Figure 4-6: Variation of the radius of the ellipse in the ADF calculation for (a) ADF transmittance and (b) ADF Rwflectance.

4.2.3 Optical sensitivity studies for thickness of layers

A study of the effect of varied solar cell layer thicknesses was carried out. As shown in the graphs in figure 4-8, the QE and Jsc increase as thickness increases.

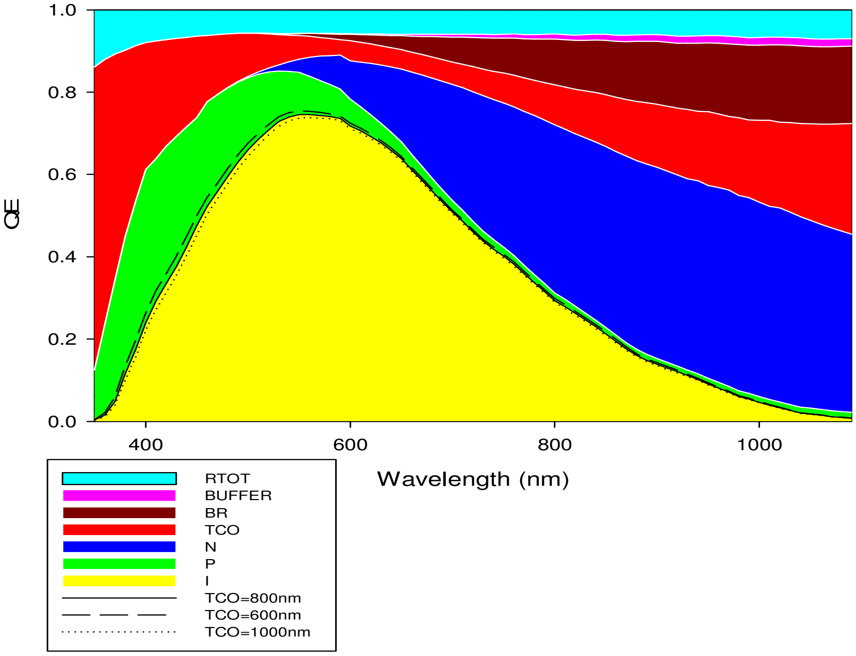

(a)

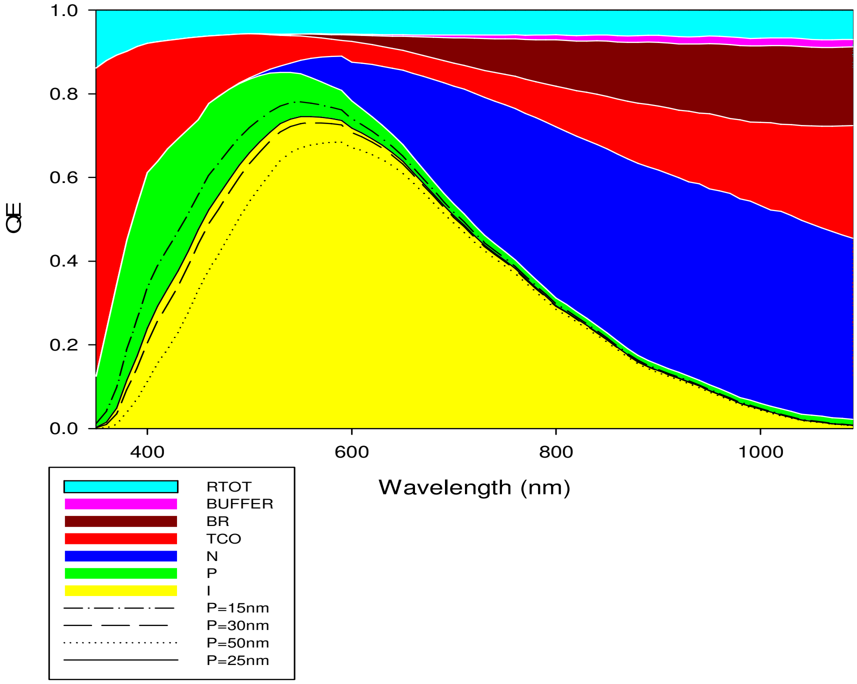

(b)

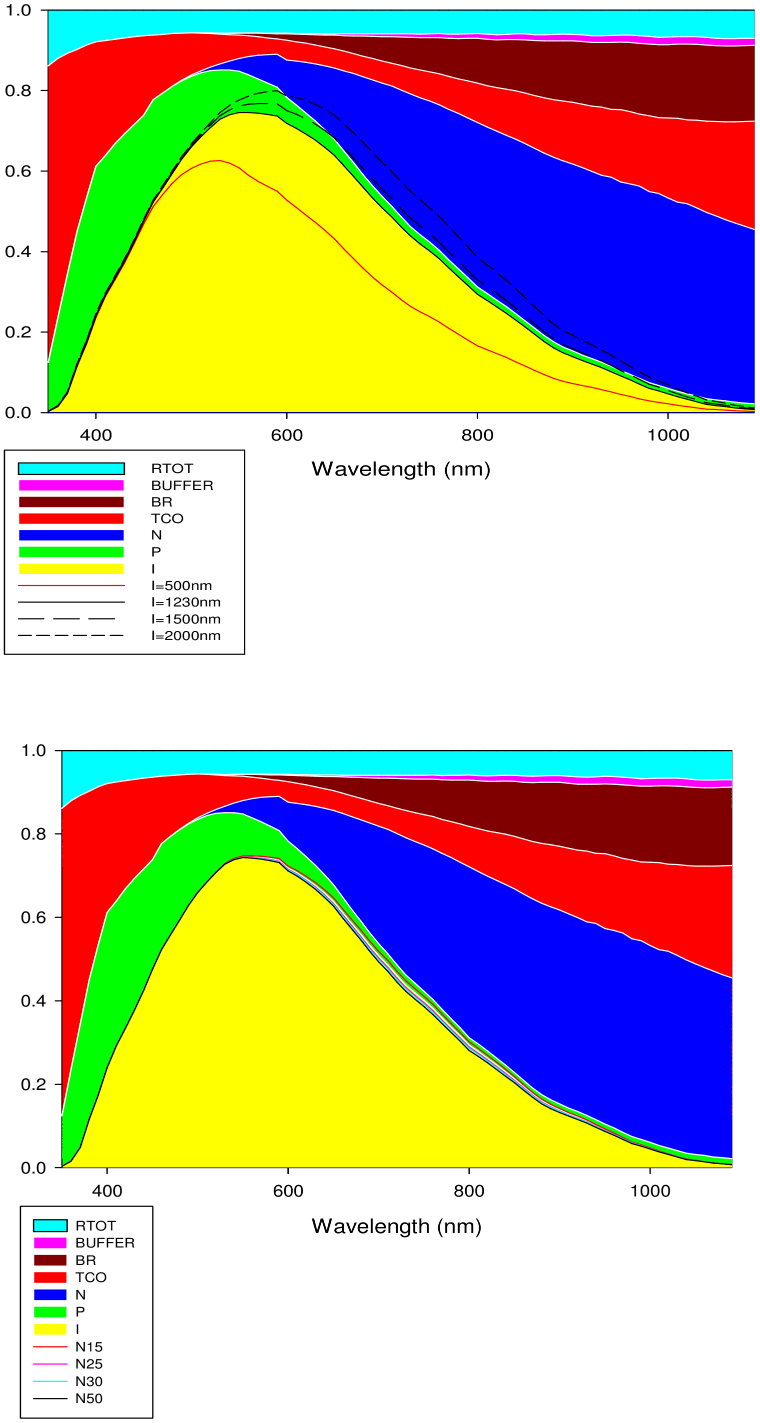

(c)

(d)

Figure 4-7: Results of varied thicknesses for different layers of the solar cell considering optical properties only (a) TCO thickness series, (b) p-layer thickness series, (c) i-layer thickness series, and (d) n-layer thickness series.

Figure 4-7 (a) shows the QE plots for three different TCO thickness values. Decreasing the TCO thickness slightly decreases absorption in the TCO layer, giving rise to slight increment of the absorption in the p and i-layers. The thickness of the p-layer greatly affects the external quantum efficiency and short circuit current density of a solar cell. Different thicknesses ranging from 15nm to 25nm were assigned the p-layer and simulations were carried out. Figure 4-7 (b) shows the increment in the QE of the solar cell in the short wavelength region for lower values of the p-layer thickness. Lower values of p-layer thickness translate to lower losses due to absorption in the p-layer. Figure 4-7 (c) shows increase in the solar cell QE in the long wavelength region for increments in the i-layer thickness. Similarly the n-layer thickness when reduced increases the QE in the long wavelength region. The plots show that reduction in thickness of layers other than the i-layer decrease the amount of losses in those layers, leading to improved absorption of light in the absorber layer of the solar cell.

4.3 Sensitivity of electrical parameters

A sensitivity study was carried out to understand how input parameters and different characteristics affect the solar cell electrically. Properties of the solar cell material such as the mobility gap, layer thicknesses, defect density, etc, were studied. This study enabled us attain a better understanding of microcrystalline silicon solar cell.

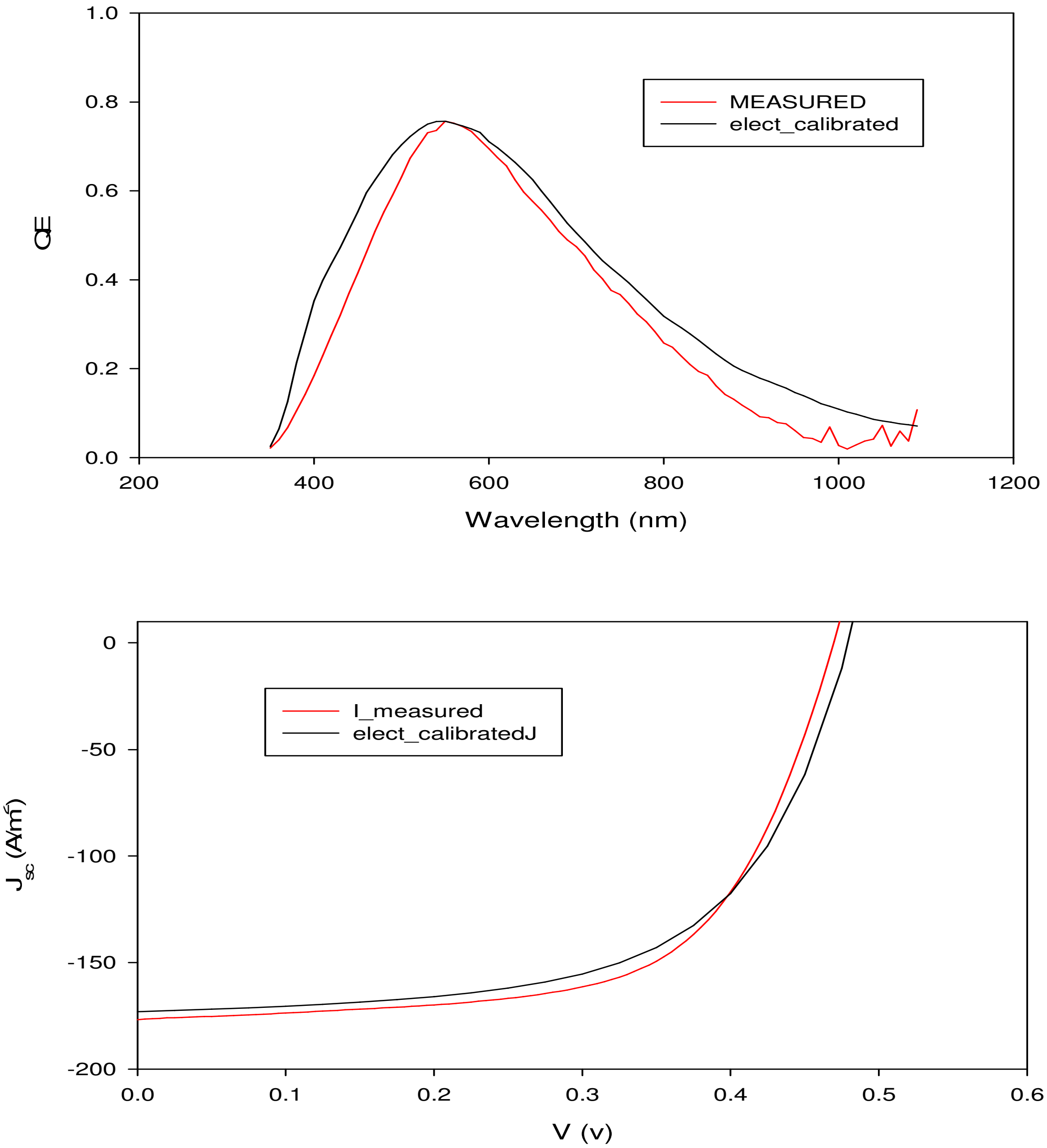

Figure 4-8: QE plot and Jsc plot for the calibrated solar cell.

4.3.1 Recombination in solar cells

In modeling of solar cells using ASA, the ASA simulator assumes that every absorbed photon generates an electron hole pair in the optical simulation. In the electrical simulation, ASA assumes that every electron hole pair generated is collected. In reality however, this is not the case, losses are expected due to recombination in the p, i and n layers as well as in the layer interfaces.

The impact of the above statement is that it is expected in reality that the external quantum efficiency will be smaller than the optical QE. In order to show this effect, as can been seen in the calibrated solar cell that this is not the case, the amount of defects in the layers of the solar cell were increased. The plots below show the recombination in the solar cell and show that the electrical QE is less than the optical QE due to recombination losses in a solar cell, incurred in this case by the increase in the defect densities of the solar cells layers.

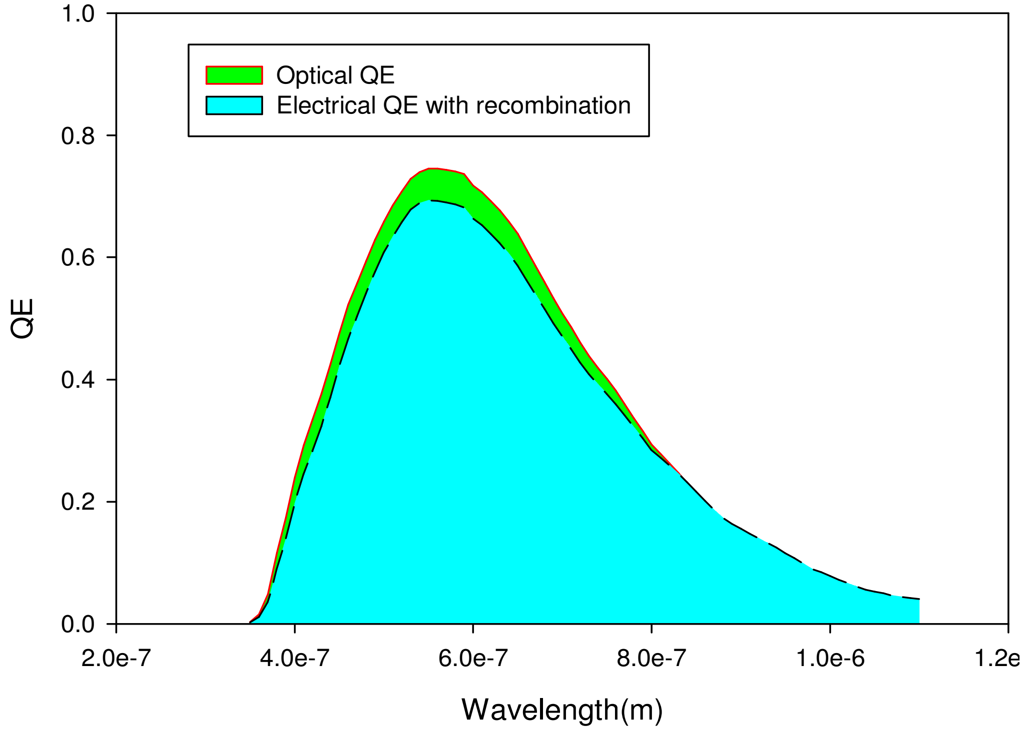

Figure 4-9: QE plots showing losses due to recombination in the electrical simulation.

4.3.2 P-layer mobility gap

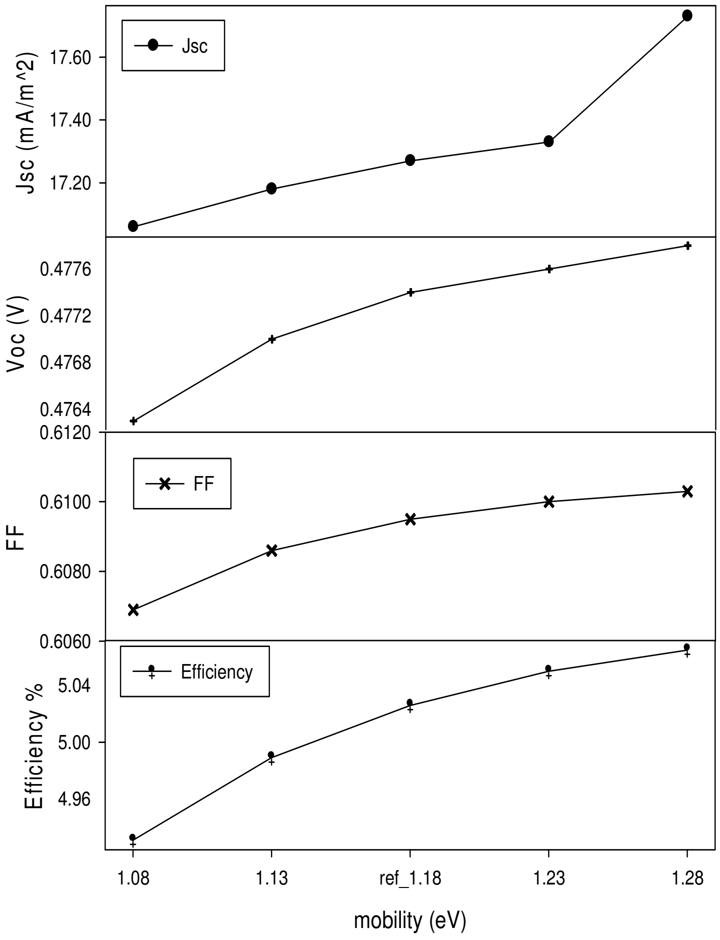

(a)

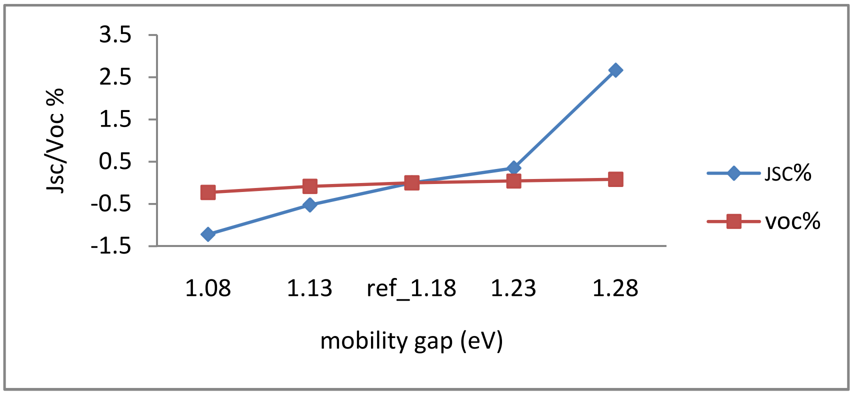

(b)

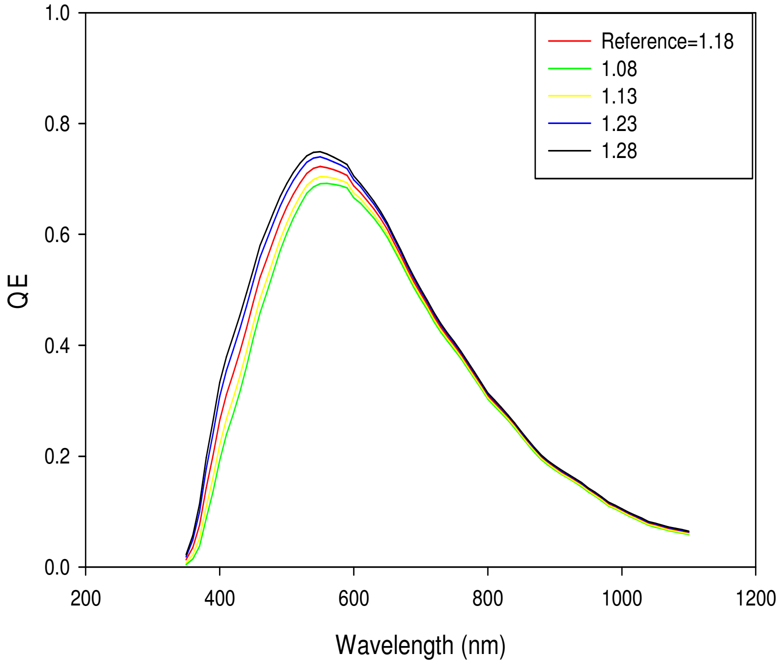

(c)

Figure: 4-10 (a) External parameters, (b)percentage change and (c)Quantum efficiency plots for sensitivity of the p-layer mobility gap.

The effect of the p-layer mobility gap on the solar cell was studied by varying the mobility gap. Figure 4-10 above shows the effect on the external parameters of the solar cell as well as the quantum efficiency. For lower values of the p-layer mobility gap, all external parameters decrease while for higher values the cells parameters increase. Part of the explanations for this effect arises from the fact that a higher mobility gap in the p-layer reduces the amount of absorption in the p-layer, giving rise to more absorption of photons in the absorber layer and hence an improved overall effect on the solar cell. The effect of this on the Voc and Jsc were compared in terms of percentage increase or decrease, and it is seen in figure 4-10 (b) that the Jsc is more affected by the changes in p-layer mobility gap.

4.3.3 Absorber layer mobility gap

A sensitivity study of the effect of the i-layer mobility gap on the external parameters of the solar cell as well as the quantum efficiency was carried out. As the mobility gap of the i-layer decreases, the absorption in the cell increases this implies that the short circuit current density also increases. On the other hand, as seen in figure 4-11, as the mobility gap of the i-layer increases, the Jsc reduces. The plot shows an increase in the Voc and fill factor with increasing values of mobility gap. Experimentally, the mobility gap can be changed by varying the substrate temperature [25].

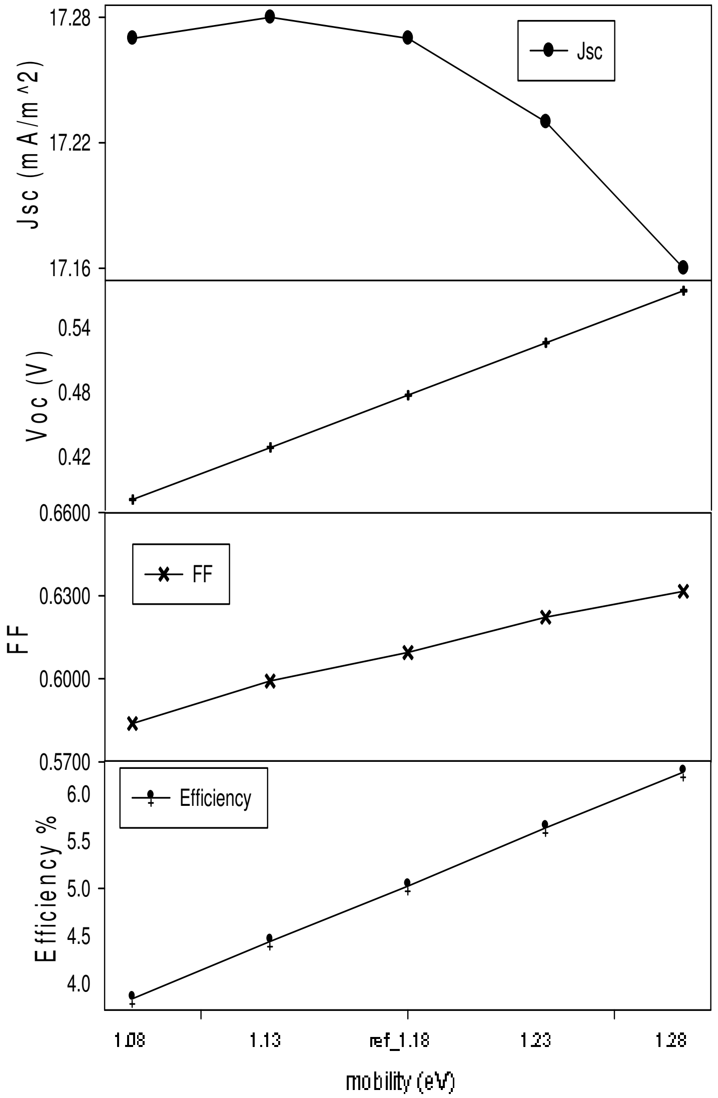

(a)

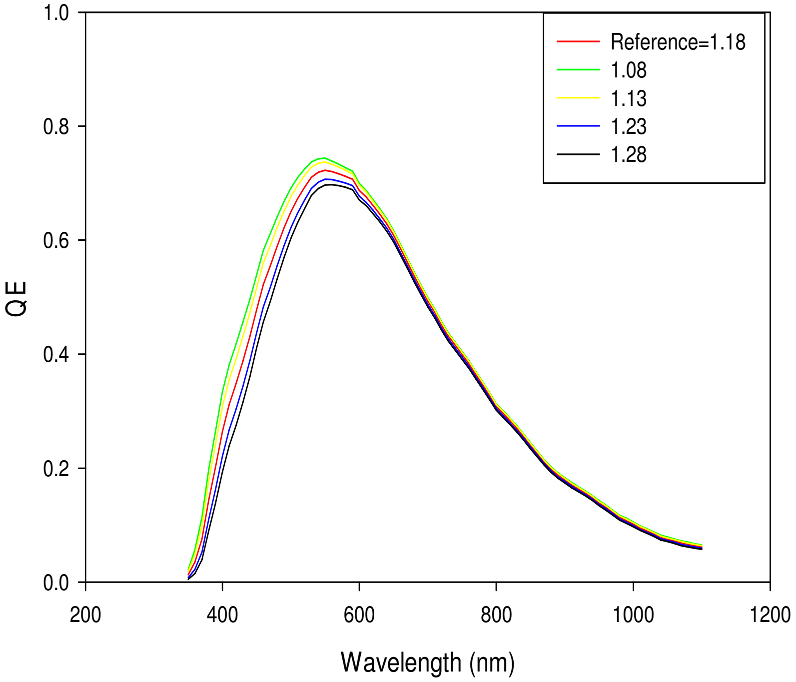

(b)

Figure 4-11: (a) External parameters, and (b) Quantum efficiency plots for sensitivity of the i-layer mobility gap.

4.3.4 n-layer mobility gap

The effect of the n-layer mobility gap on the solar cell was studied. The results show that the n-layer mobility gap had very little effect on the Jsc, while the fill factor and the Voc remained unchanged. The effect of the n-layer mobility gap led to a decrease in the efficiency of 3% and 9% for a mobility gap increase from the reference value of 0.10eV and 0.20eV respectively. One could conclude that for these variations to the n-layer mobility gap, there is no real effect on the solar.

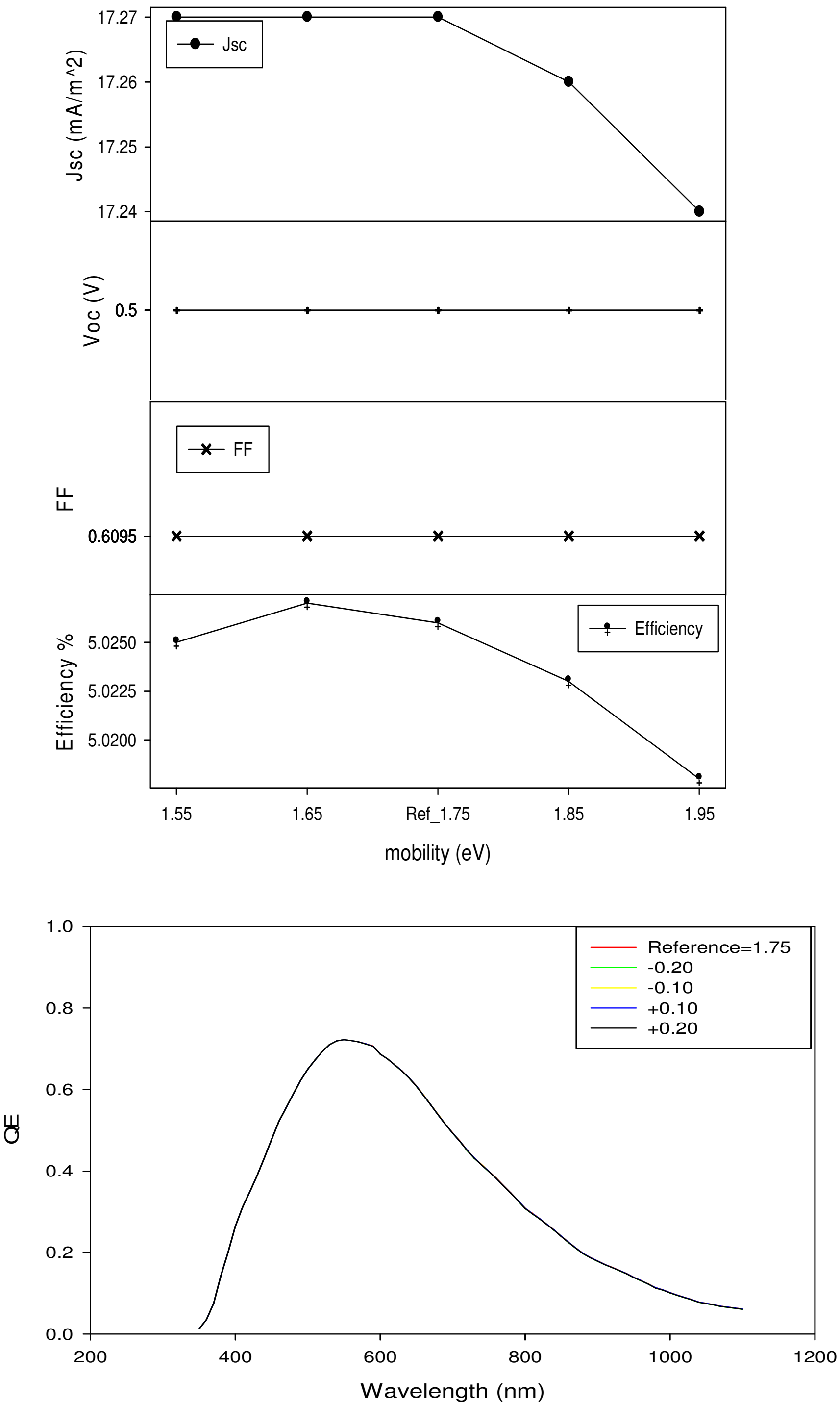

Figure 4-12: (a) External parameters, and (b) Quantum efficiency plots for sensitivity of the n-layer mobility gap.

4.3.5 P-layer activation energy

The p-layer activation energy was studied with respect to its effect on the solar cell. The results presented in figure 4-13 show that there was an increase in the Jsc for increasing activation energy values which led to a slight increase in the efficiency, whereas the Voc reduced as the activation energy was increased. This can be attributed to an increase in recombination due to increased carrier concentration with doping. Further investigation into the recombination profile of the solar cell as a function of p-layer activation energy confirms this as shown in figure 4-13. It was noticed that the p-layer activation energy had a stronger effect on the Voc, eventually leading to a decrease in the solar cells efficiency for higher values of the activation energy. The percentage comparison figure 4-13 (b) shows the p-layer activation energy is more sensitive to Voc.

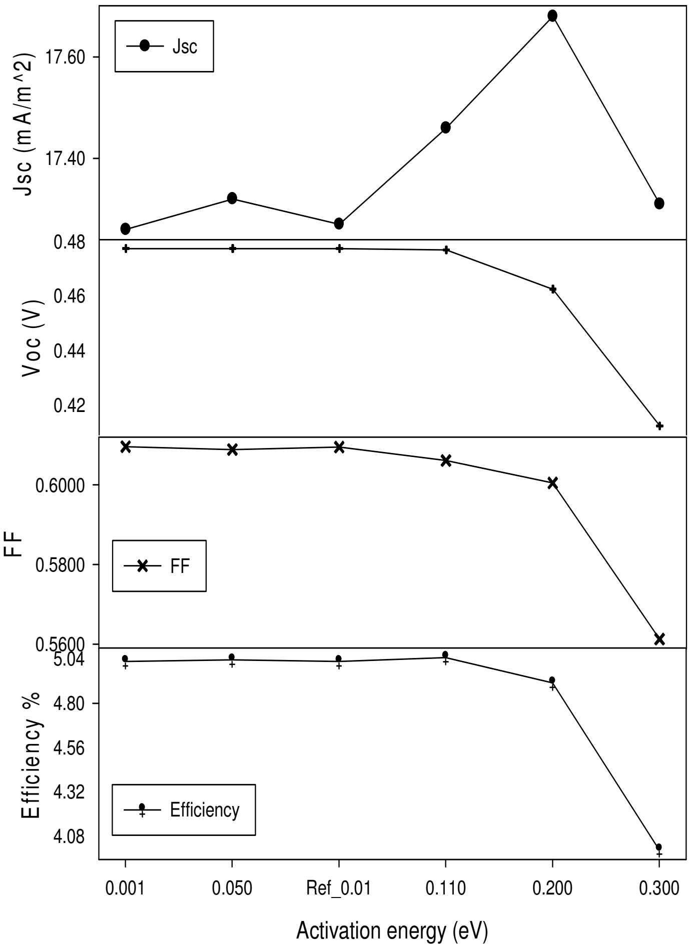

(a)

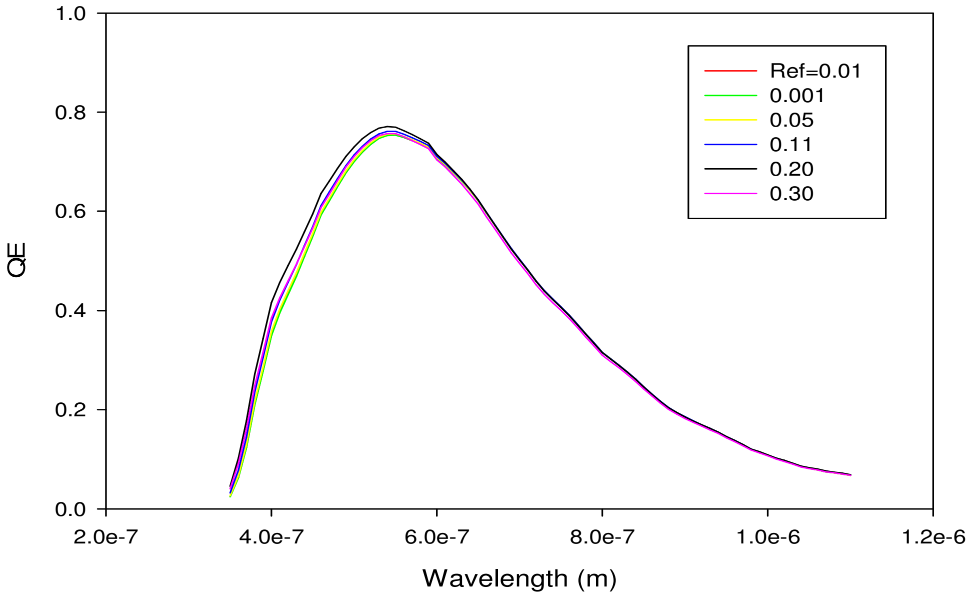

(b)

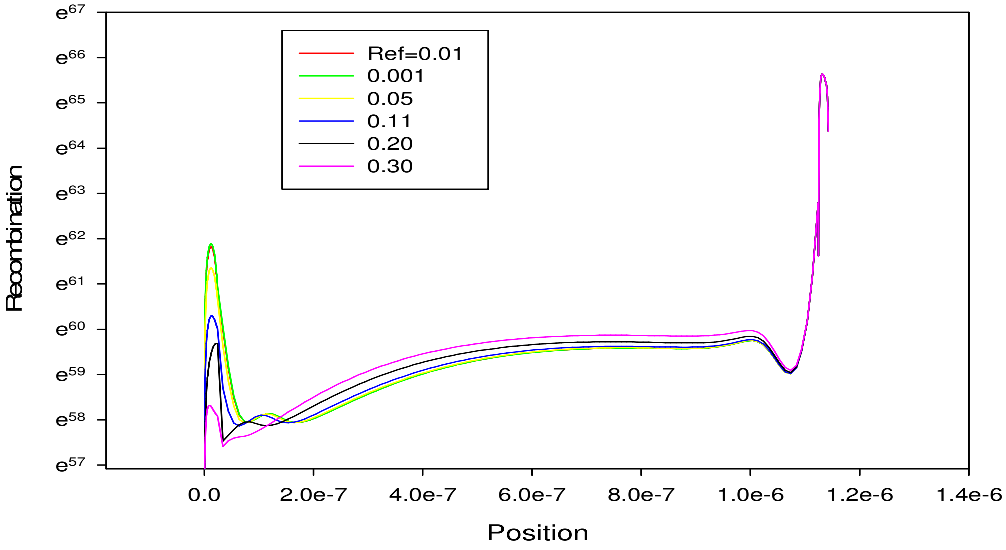

(c)

Figure 4-13: (a) External parameters, (b) Quantum efficiency plot and (c) recombination plots for sensitivity of the p-layer activation energy.

4.3.6 n-layer activation energy

The effect of the n-layer activation energy on the solar cell was studied. We notice changes in the long wavelength region of the QE plot. The n-layer causes an increase in the external parameters of the solar cell for increasing values of its activation energy.

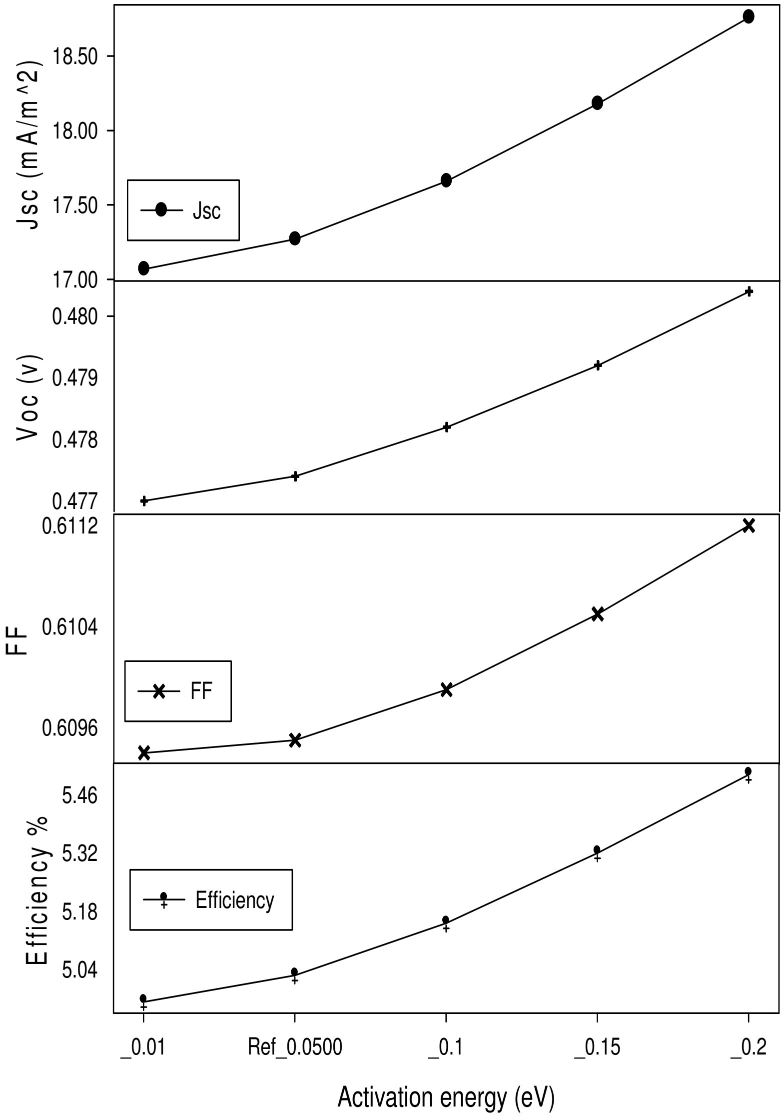

(a)

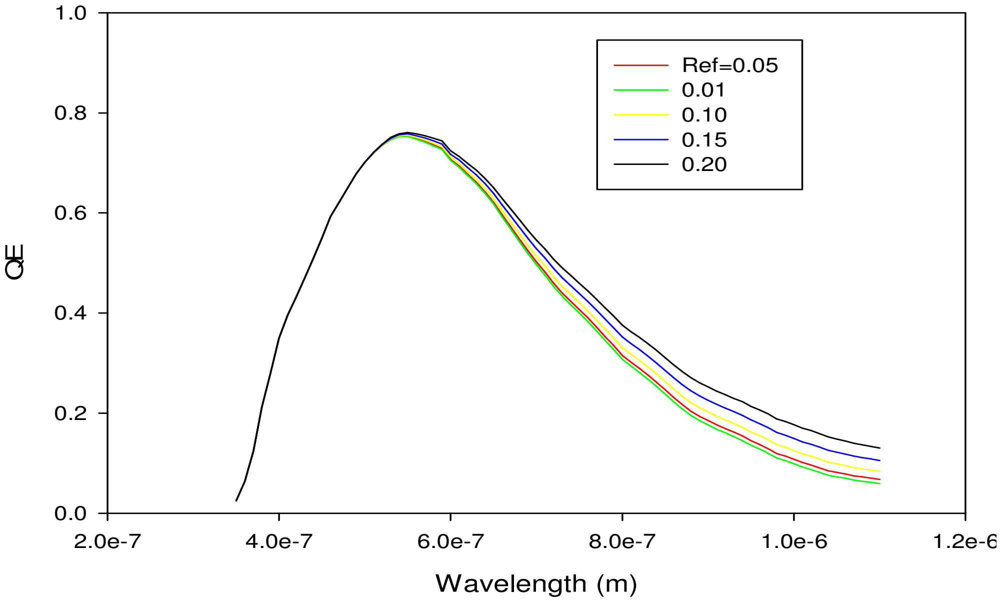

(b)

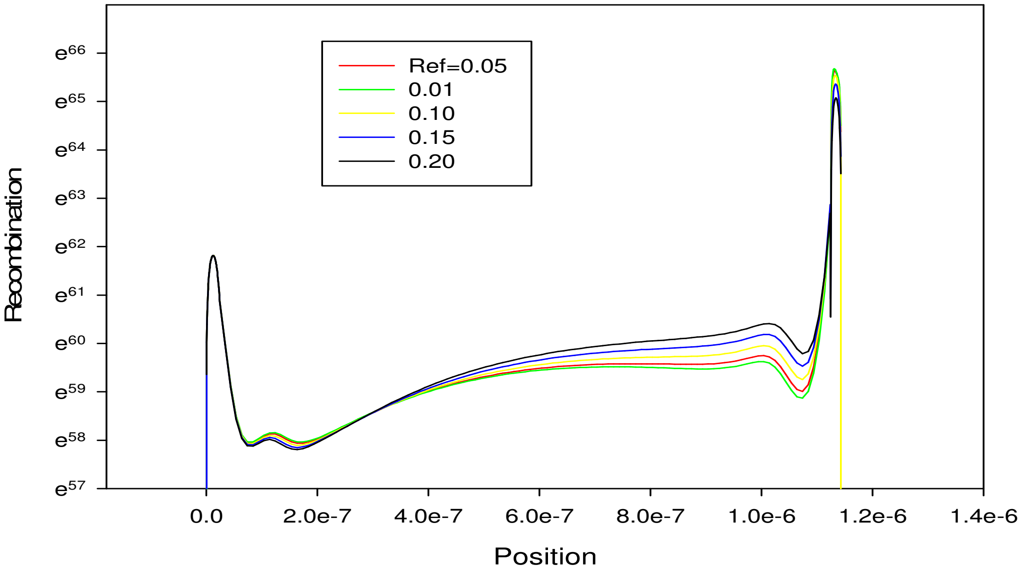

(c)

Figure 4-14: (a) External parameters, (b) Quantum efficiency and (c) recombination plots for sensitivity of the n-layer activation energy.

4.3.7 P-layer defect density

A study of the defect density of the p-layer was carried out by varying the total concentration of dangling bonds in the layer. The results in the figures for the external parameters and QE of the solar cell show a decrease in Jsc, Voc, FF, QE and efficiency for increased amount of defects in the p-layer. The Jsc is more sensitive to the defects than the Voc as inferred from figure 4-15 (b).

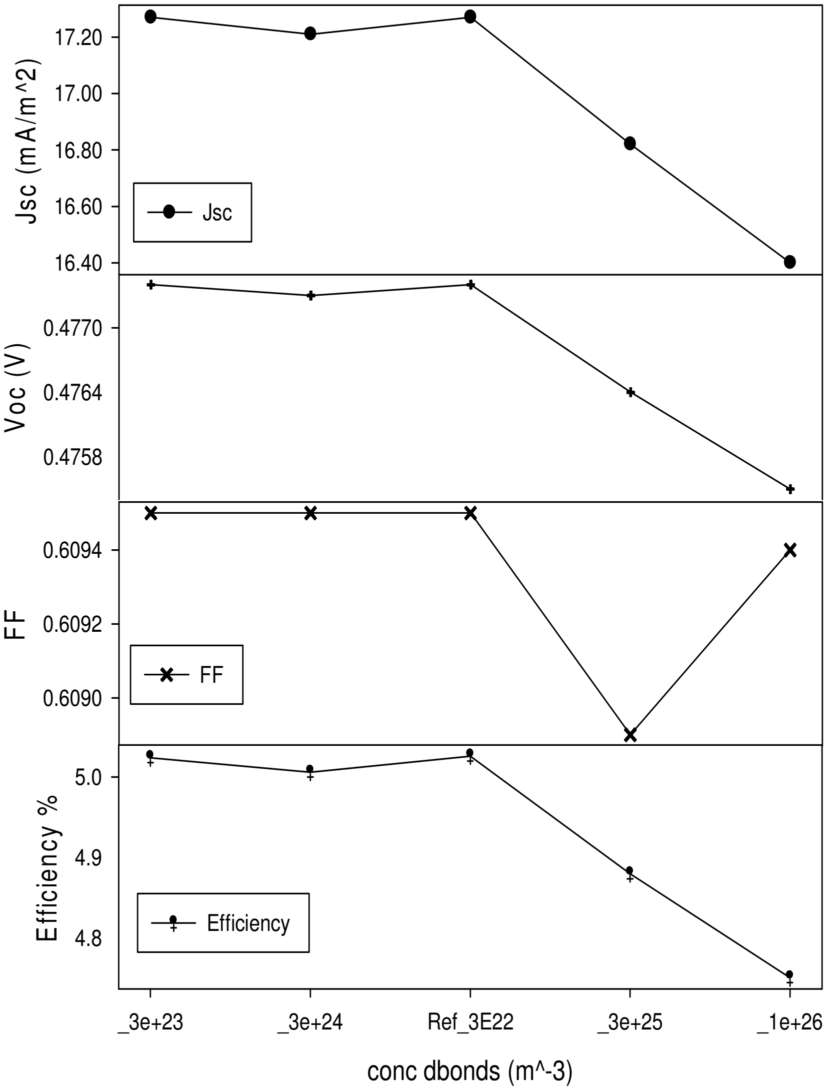

(a)

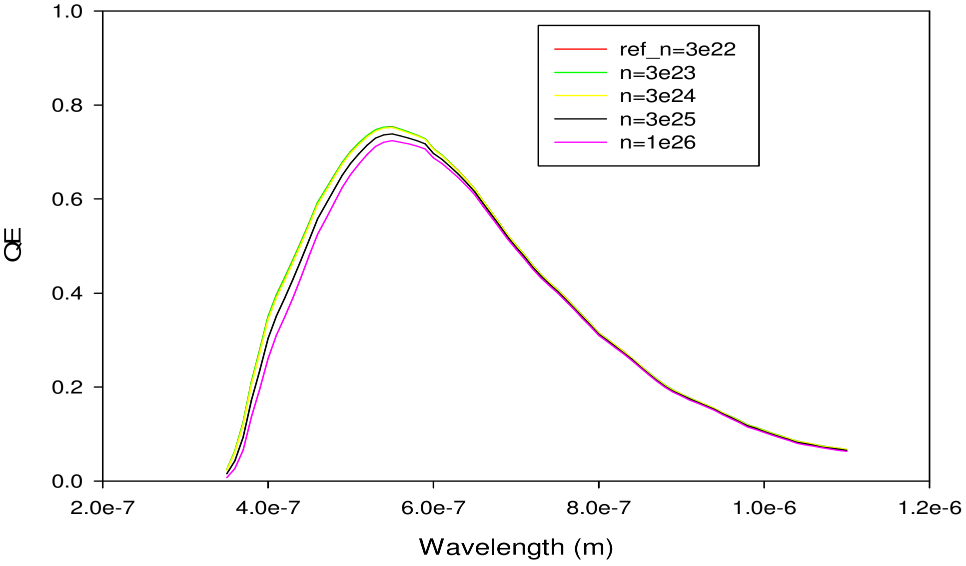

(b)

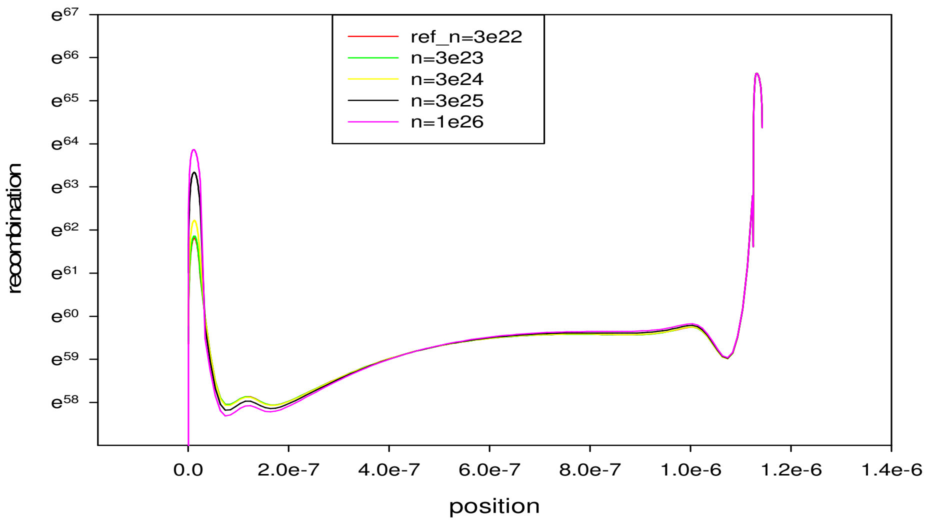

(c)

Figure 4-15: (a) External parameters, (b) Quantum efficiency and (c) recombination plots for sensitivity of the total concentration of dangling bonds in the p-layer.

4.3.8 I-layer defect density

Just as it was seen for the p-layer, the effects of defects in the i-layer was studied, the results follow logical reasoning that increased defects will lead to a reduction in the performance of the solar cell. The plots for recombination show increased recombination throughout the cell and not only at the interfaces as has been the case for most other parameters studied.

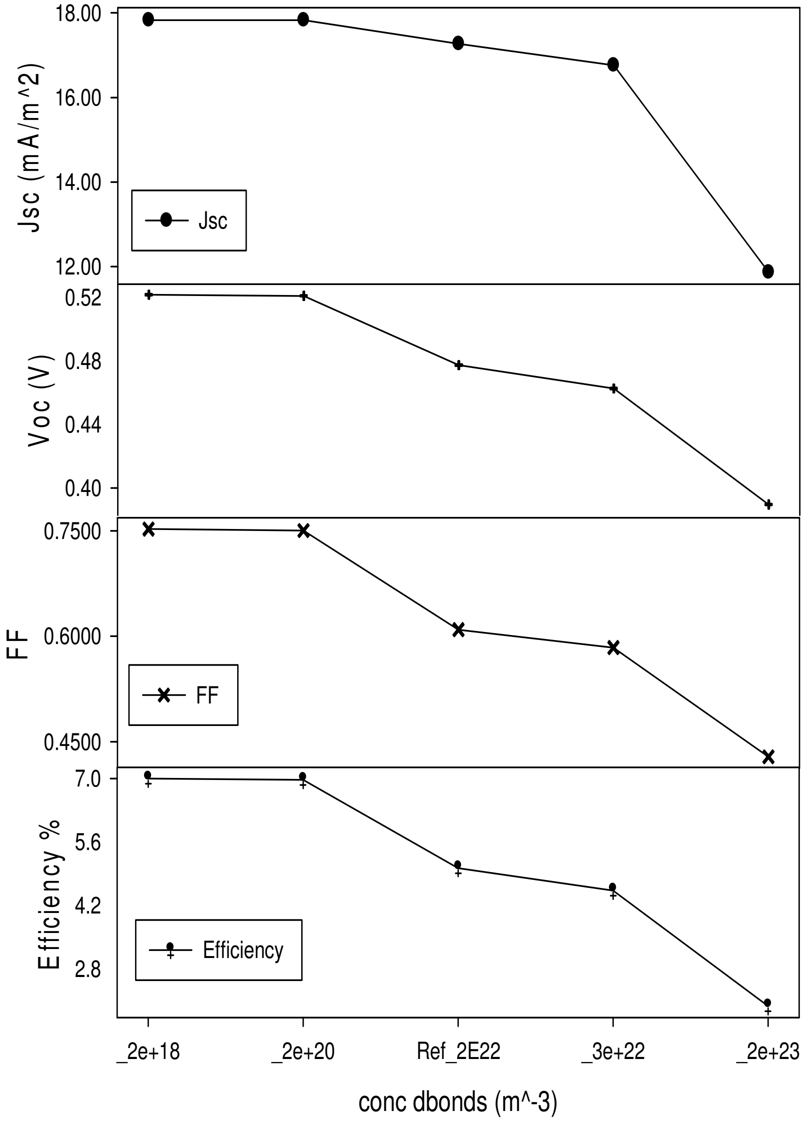

(a)

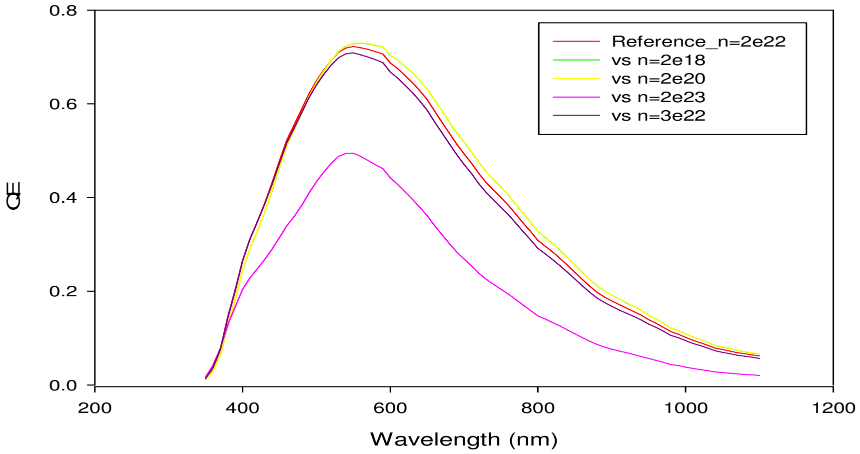

(b)

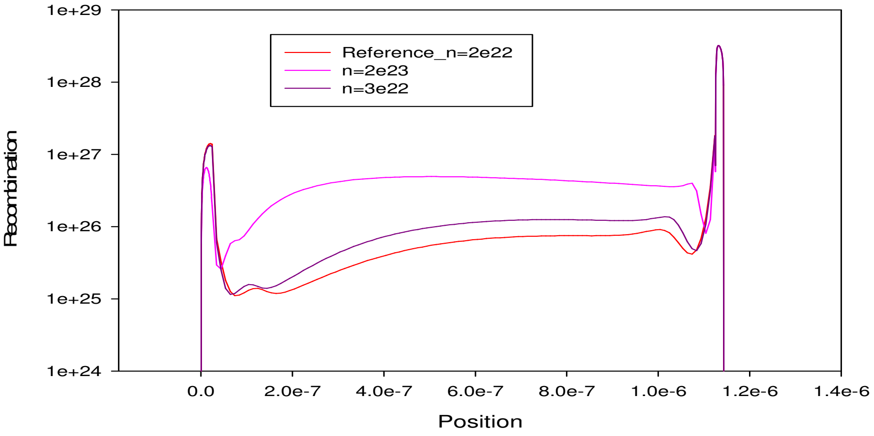

(c)

Figure 4-16: (a) External parameters, (b) Quantum efficiency and (c) recombination plots for sensitivity of the total concentration of dangling bonds in the i-layer.

4.3.9 Thickness series

A thickness sensitivity study was carried out for the TCO, p, i and n layers. As the thickness of the p-layer increases, the solar cell's Jsc decreases, so does the Voc, FF and its efficiency. For the i-layer however, Jsc and QE increase with increasing i-layer thickness. This is due to the fact that there will be more absorption with greater thickness of the i-layer. However, the other cell parameters and the efficiency of the solar cell decrease with increasing i-layer thickness.

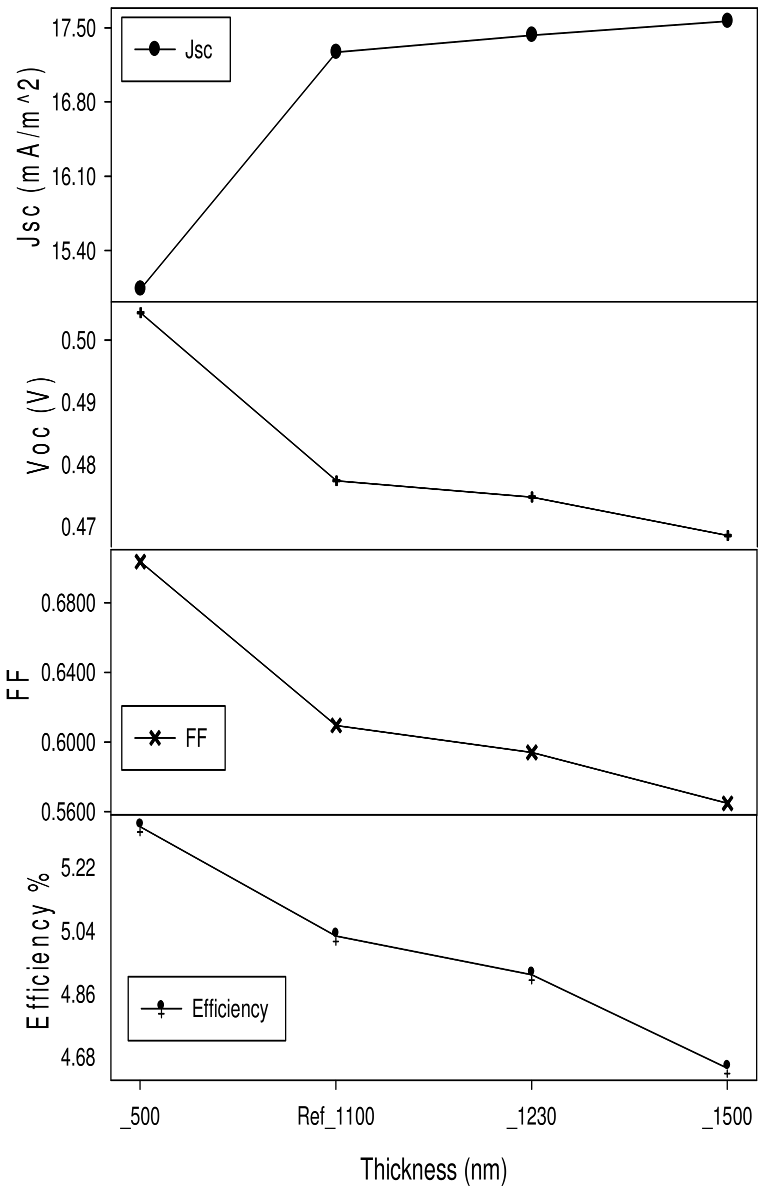
Jsc
Jsc (mA/m^2)
17.50
16.80
16.10
15.40
Voc (V)
0.50
0.49
0.48
0.47
FF
0.6800
0.6400
0.6000
0.5600
Efficiency %
5.22
5.04
4.86
4.68
Efficiency
_500
Ref_1100
_1230
_1500
Thickness (nm)

(a)

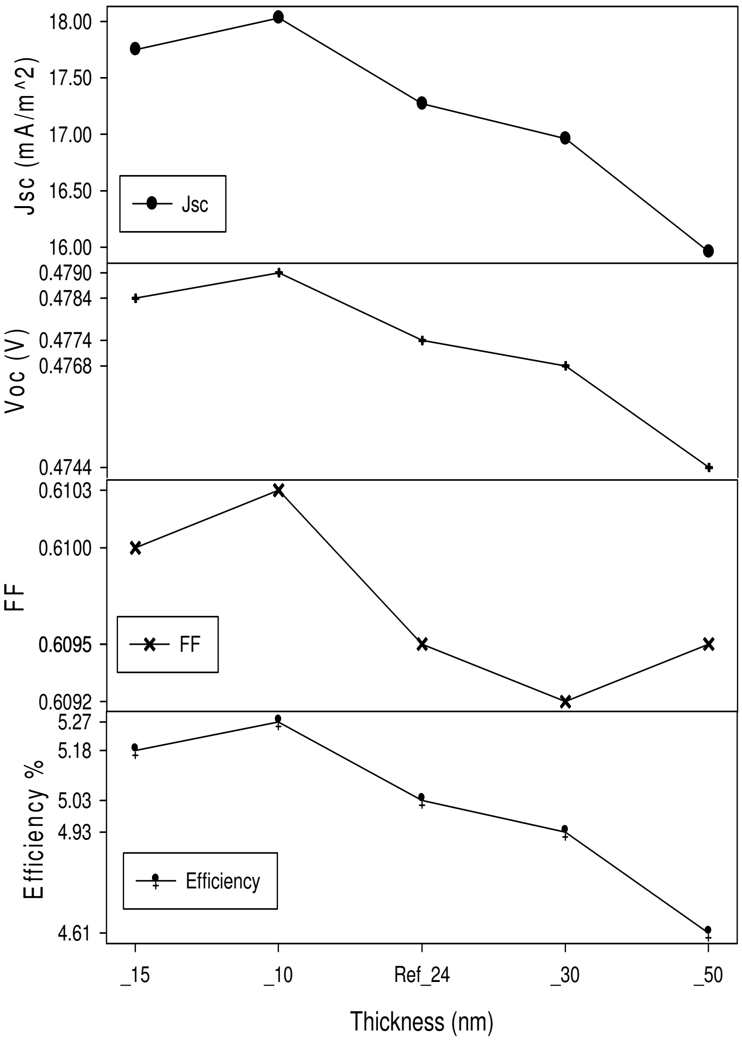

(b)

Figure 4-17: External parameters and efficiency plots for sensitivity study of the (a) i-layer, and (b) p-layer thicknesses.

The effect of varying the thickness of the n-layer and the TCO were studied. The effect turned out to be same for both cases. An increase in their thicknesses led to a reduction in value of the external parameters of the solar cell, increased thickness also leads to reduced efficiency for both cases. The short circuit current density proved to be more sensitive to the n-layer and TCO-layer thickness variations.

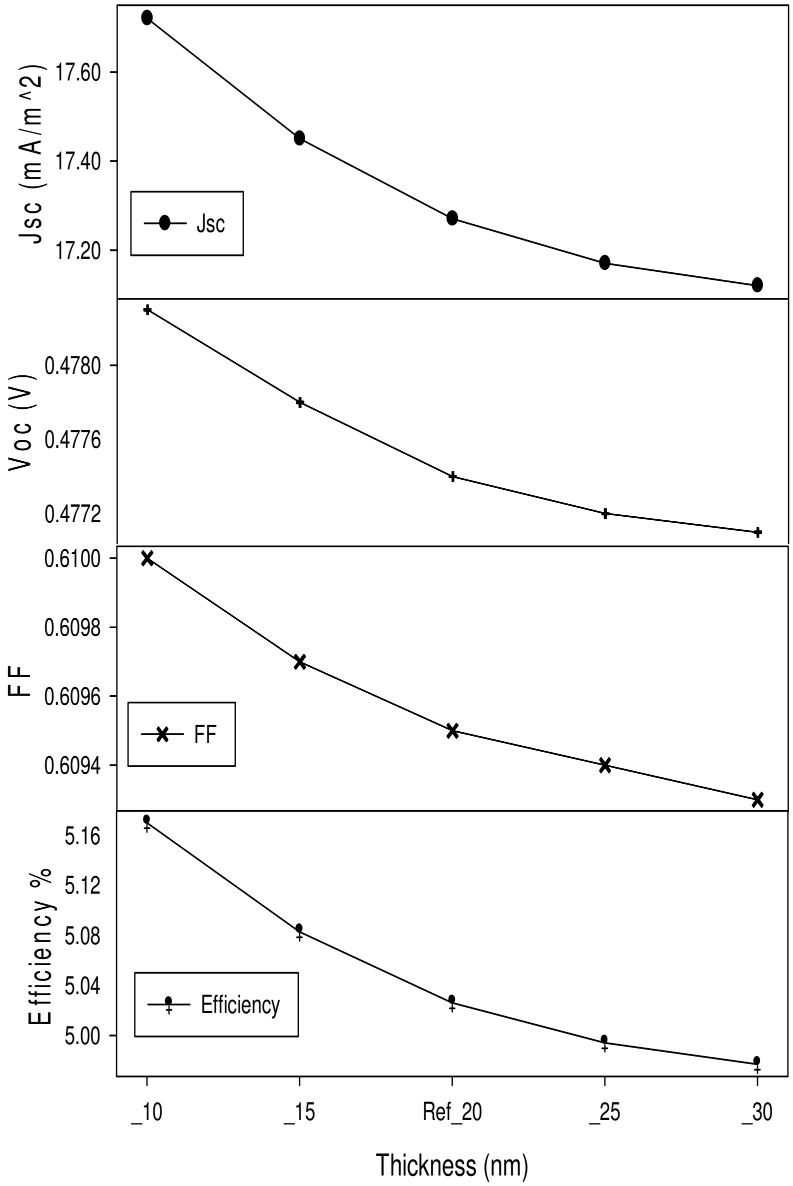
Jsc (mA/m^2)
17.60
17.40
17.20
Jsc
Voc (V)
0.4780
0.4776
0.4772
FF
0.6100
0.6098
0.6096
0.6094
FF
Efficiency %
5.16
5.12
5.08
5.04
5.00
Efficiency
_10
_15
Ref_20
_25
_30
Thickness (nm)

(a)

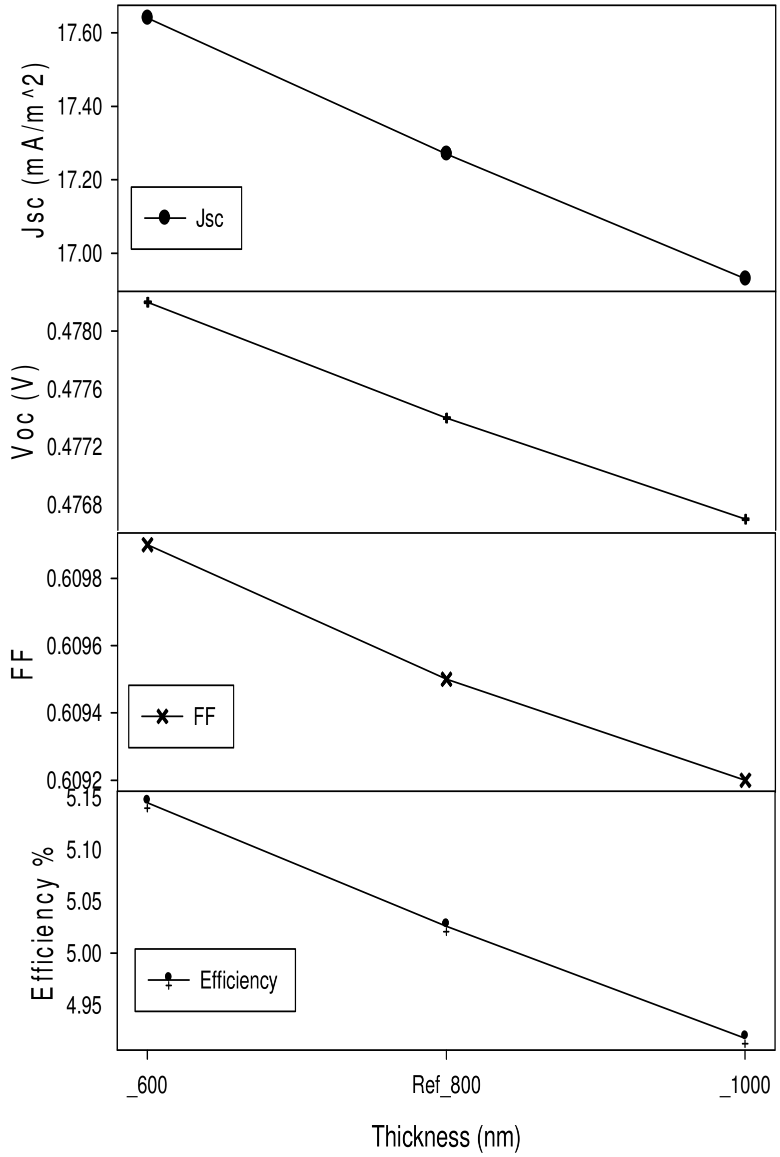

(b)

Figure 4-18: External parameters and efficiency plots for sensitivity study of the (a) n-layer, and (b) TCO-layer thicknesses.

4.4 P-i interface buffer layer

A p buffer layer was inserted at the p-i interface. It is believed that having a buffer layer with a higher mobility gap than the mobility gap of the i-layer in the p-i interface will improve the Voc of the solar cell as the Voc is proportional to the mobility gap [25]. In the case of a large difference between the mobility gap of the p-layer and the i absorber layer, there occurs a band offset. This band offset in the valence band prevents photo generated carriers (holes) from moving to the p-layer from the absorber layer.

The introduction of a buffer layer, with a mobility gap value lower than that of the p-layer but higher than that of the i-layer supposedly improves the p-I interface thereby improving the Voc, as the Voc is not only dependent on the i-layer but on the p-i interface also [25].

In our simulations, a p microcrystalline silicon buffer layer was inserted at the p-i interface. The mobility gap of the p-layer was set at 1.25eV, the buffer layer at 1.21eV and the i-layer at 1.18eV. a study of the buffer layer thickness was carried out as well as a study for different values of the mobility gap of the buffer layer. The results of our simulations are shown in the figures and tables below. For the structure we investigated, the buffer layer had a very little effect on the solar cell, even though for some values, it improved the Voc by very little amounts.

4.4.1 Thickness series for buffer layer

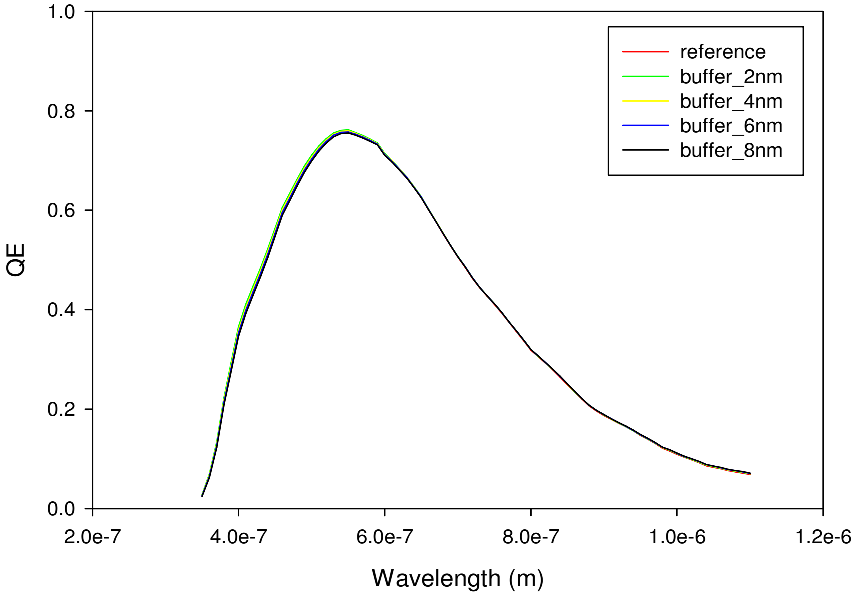

Figure 4-19: QE plot of buffer layer thickness series

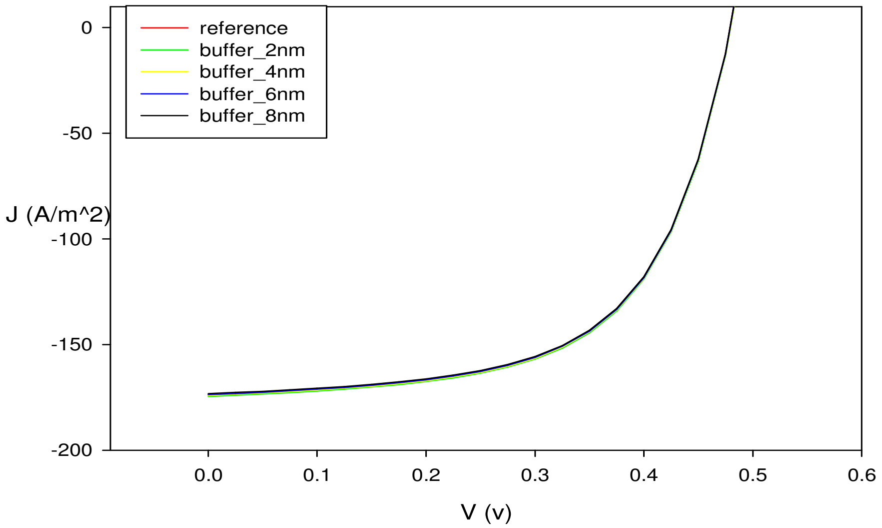

Figure 4-20: IV plot of buffer layer thickness series

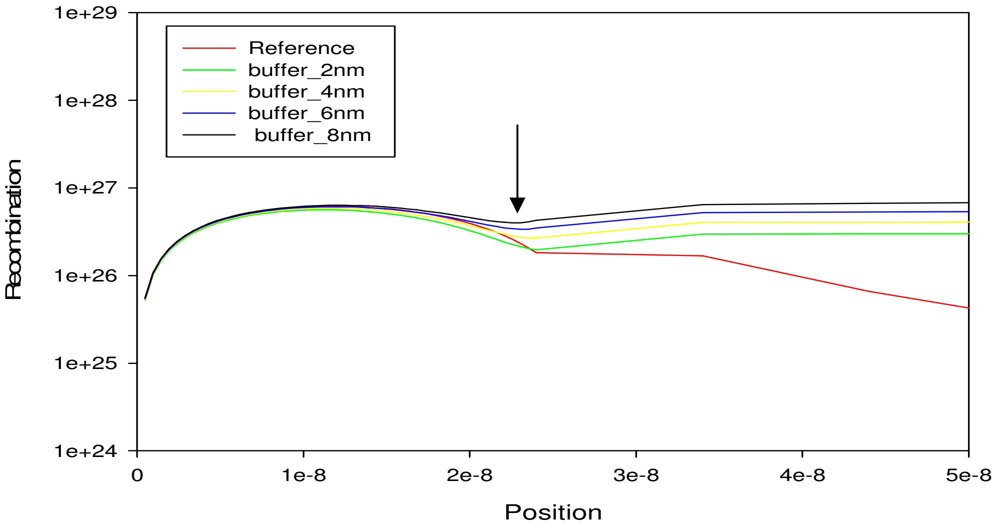

Figure 4-21 Recombination at the p/I interface for buffer layer thickness series

Figure 4-19 to 4-21 show the results of the simulations carried out for a thickness sensitivity study of the buffer layer. The results show very little change in the solar cell parameters, although for a buffer layer thickness of 2 nm, there was slight improvement in both the Voc and the Jsc. Figure 4-21 also shows a slight improvement in the recombination profile at the p-i interface for the 2nm thick buffer layer. Table 4 reports the exact values of external parameters obtained from the simulation.

Table 4. Buffer layer thickness series

Buffer thickness	voc	$j_{sc}(A/m^2)$	ff
No buffer	0.4791 V	-174.0	0.6141
2nm	0.4792 V	-174.8	0.6141
4nm	0.4792 V	-174.4	0.6140
6nm	0.4791 V	-173.9	0.6140
8nm	0.4790 V	-173.4	0.6139

4.4.2 Mobility gap series for buffer layer

The solar cells sensitivity to the mobility gap of the buffer layer was also investigated. The mobility gap of the buffer layer was varied from 1.19eV to 1.23eV. A buffer layer mobility gap value of 1.19eV proved to be the optimum of the values selected. Again a very little change from the case where there was no buffer was observed. In the plot for the recombination profile figure 4-24, we observe also a decrease in recombination at the p-i interface for a buffer layer mobility gap value of 1.19ev. Table 5 below shows actual results obtained from the simulations.

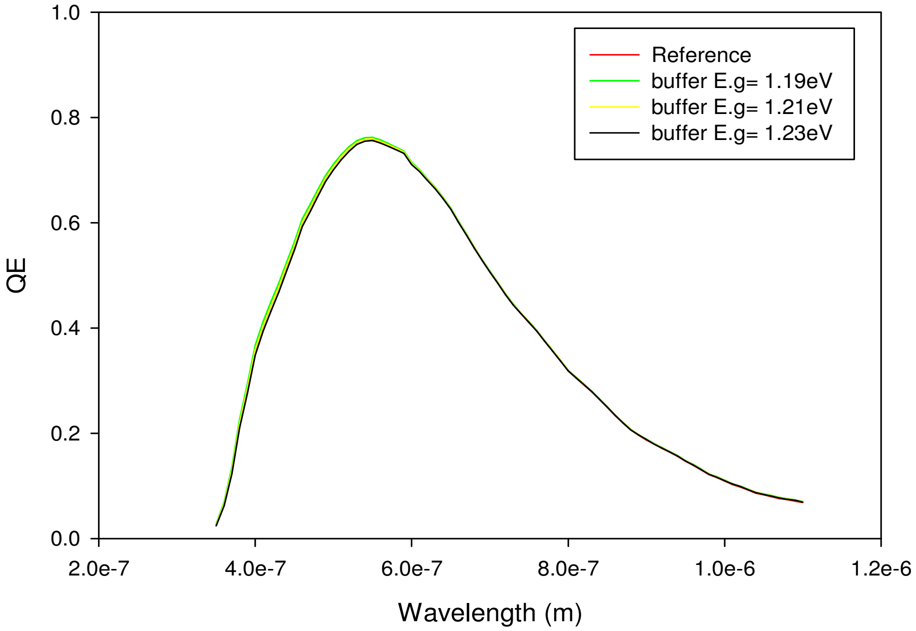

Figure 4-22: QE plot of buffer layer mobility gap series

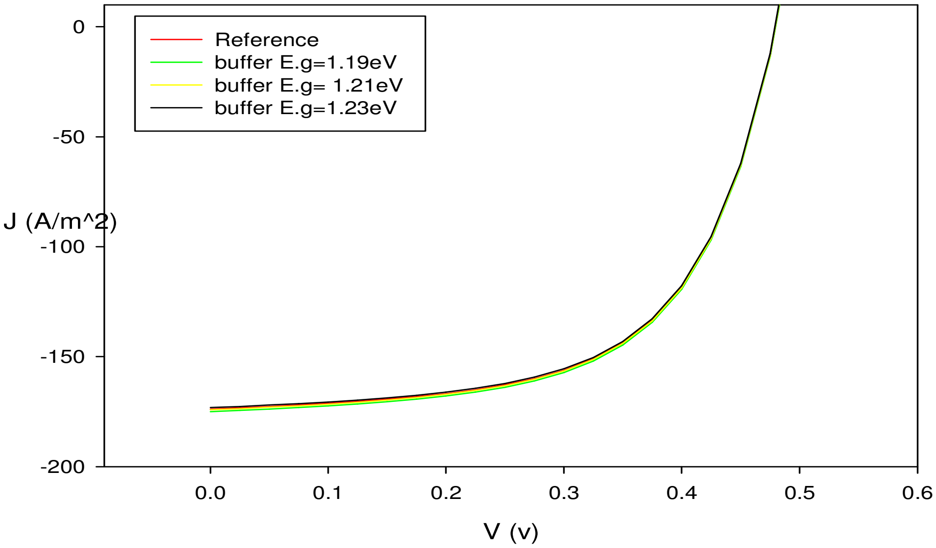

Figure 4-23: IV plot of buffer layer mobility gap series

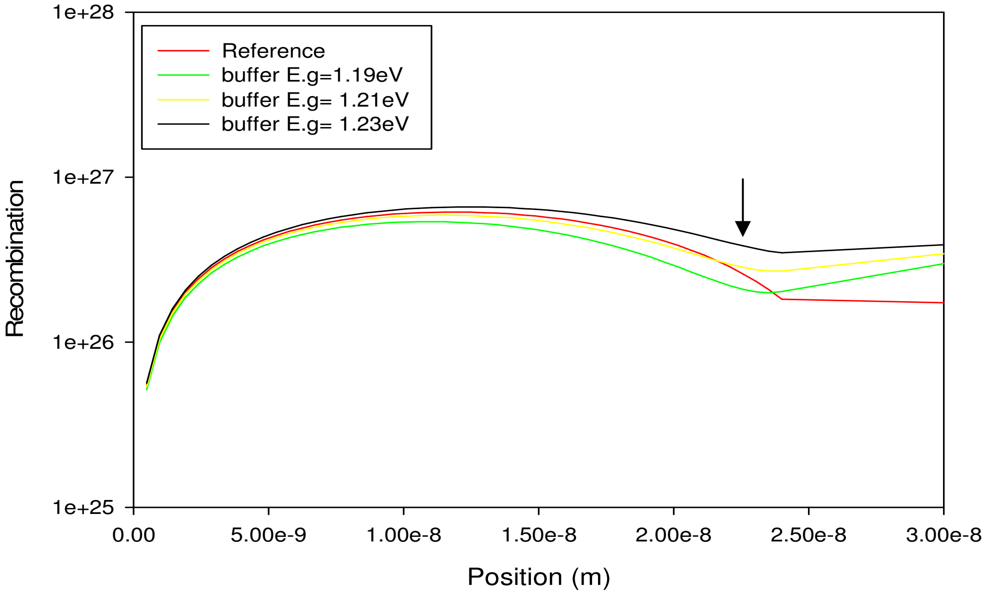

Figure 4-24 Recombination at the p/I interface for buffer layer thickness series

Table 5. Buffer layer mobility gap series

Buffer band gap	V_{oc}	J_{sc} (A/m^2)	FF
No buffer	0.4791 V	-174.0	0.6141
1.19eV	0.4793 V	-175.1	0.6140
1.21eV_buffer_4nm_ref	0.4792 V	-174.4	0.6140
1.23eV	0.4789 V	-173.3	0.6140

4.5 Amorphous silicon carbide buffer

An amorphous silicon carbide buffer layer was introduced at the p-i interface, this was done to investigate its effects on the external parameters of the solar cell especially the V_{oc}. As was mentioned in the previous section, the Voc is not only dependent on the absorber layer, but also on the p-i interface region. Results of the simulations carried out showed that implementing an amorphous silicon carbide buffer layer gave rise to an increase in the Jsc, Voc and for the 2nm thick buffer layer, the solar cell efficiency also increased. However, the fill factor was reduced significantly. Also observed was a spike in the QE plot in the visible light region of the spectrum, I was unable to find a reason for this spike. The QE plot however showed improvement in light absorption for both the short and long wavelength regions.

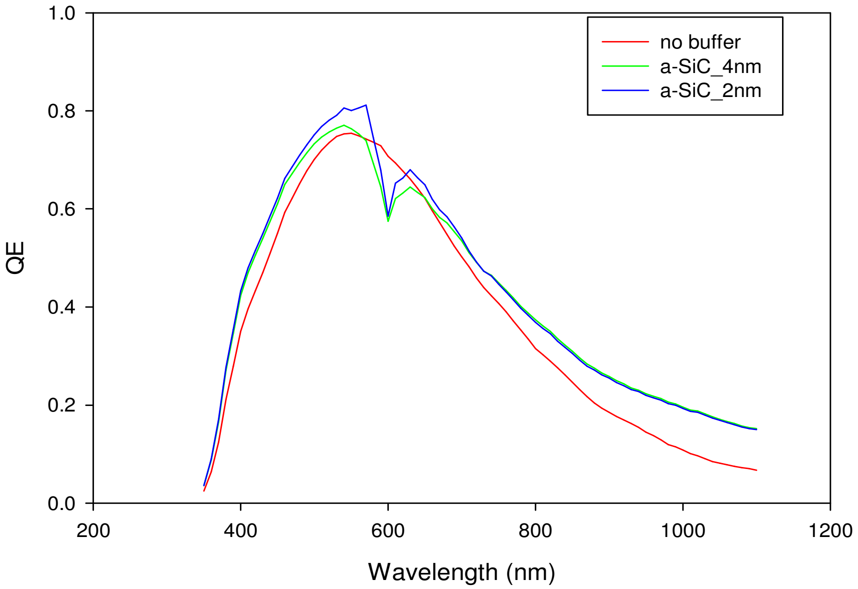

Figure 4-25QE plot for amorphous silicon carbide buffer layer

Table 6. Amorphous silicon carbide buffer

PARAMETER	REFERENCE	a-SiC_4nm	a-SiC_2nm
J_{sc} (A/m$^{2)}$	-172.7	-184.9	-188.0
Voc (V)	0.4774	0.6045	0.5359
FF	0.6095	0.4108	0.5233
Efficiency (%)	5.026	4.591	5.272

The results of the simulations carried out are shown in table 6 above. These results shown an improvement in certain parameters of the solar cell and we advice that this be tried out experimentally.

4.6 Graded i-layer

The i-layer of the solar cell was further investigated by simulating a graded intrinsic layer structure. We implemented this in ASA by making multiple i-layers in the input file and varying their mobility gaps incrementally or in decreasing order as we go deeper into the i-layer. We implemented about 5 successive i-layers of 220nm to achieve the grading. Each layer had a different value of mobility gap, while all other parameters remained the unchanged. Two cases were studied, the first was decreasing the mobility gap of each successive graded layer as we go deeper into the material, that is reducing the mobility gap in the i-layer by 0.01eV after every 200nm. The second case was exactly the same, but rather than decreasing the mobility gap, we increased it after every 200nm. The purpose of this study was to improve the Voc and other external parameters of the solar cell.

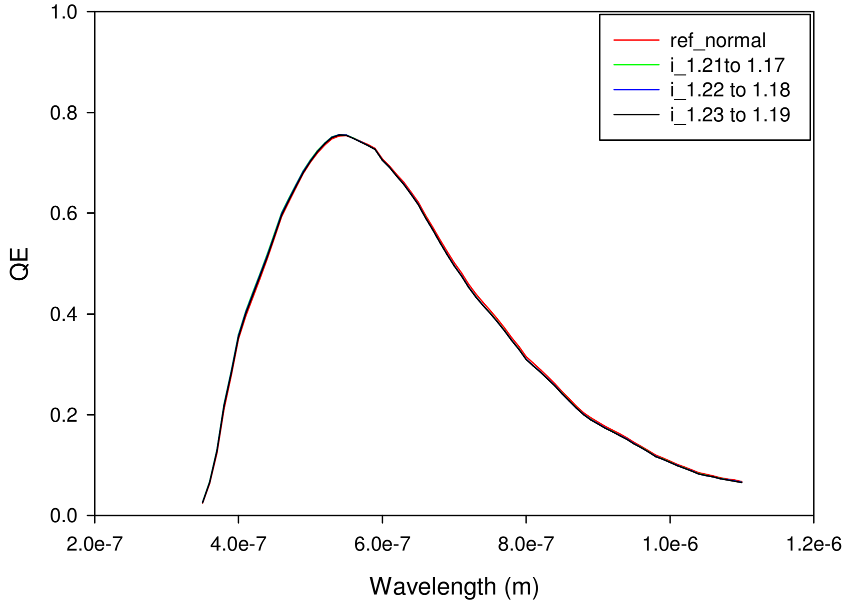

Figure 4-26Graded i-layer with mobility gap decreasing downwards

Table 7. Graded i-layer with mobility gap decreasing downwards

PARAMETER	REFERENCE	1.21 to 1.17	1.22 to 1.18	1.23 to 1.18
J_{sc} (A/m$^{2)}$	-172.7	-172.1	-172.0	-171.8
Voc (V)	0.4774	0.4887	0.4998	0.5081
FF	0.6095	0.6067	0.6067	0.6088
Efficiency (%)	5.026	5.103	5.214	5.315

The results of the simulations are shown in figure 4-26 and 4-27 as well as in table 7 and 8. Interesting results were obtained from the simulations. In the first case of mobility gap decreasing as thickness increased, the short circuit current density experienced little changes whereas the open circuit voltage was affected more. Different cases were taken into account as seen in the tables, we obtained higher values of Voc and lower values of Jsc for cases with higher mobility gaps. The overall efficiencies of the solar cell increased.

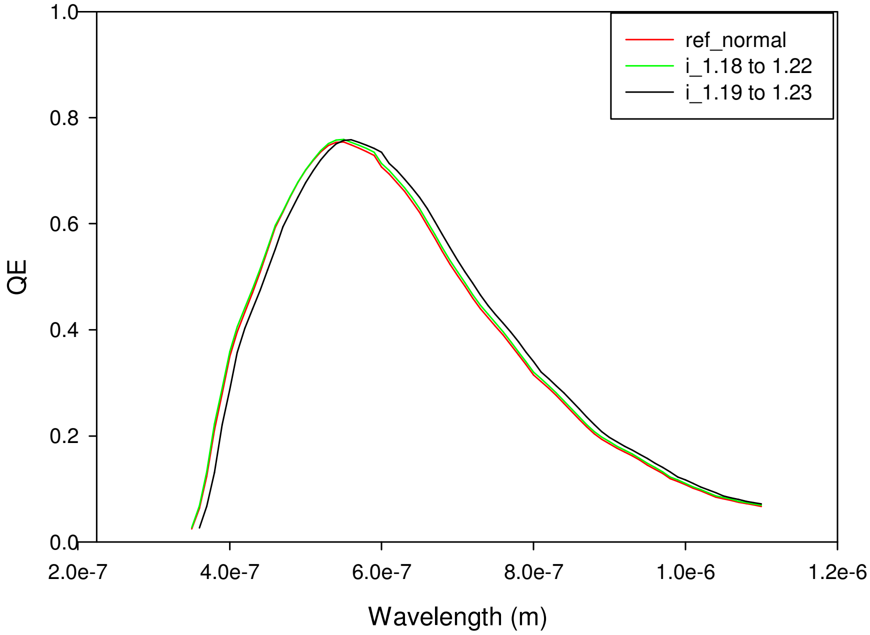

Figure 4-27Graded i-layer with mobility gap increasing downwards

For the second case where mobility gap increases as we go deeper into the material, we notice a slight shift in the QE curve towards the long wavelength region, this effect can be said to be good for a microcrystalline bottom cell in tandem configuration. For this case, both the short circuit current density and the Voc were improved.

Table 8. Graded i-layer with mobility gap increasing downwards

PARAMETER	REFERENCE	1.18 TO 1.22	1.18 TO 1.22
J_{sc} (A/m$^{2)}$	-172.7	-175.1	-174.9
Voc (V)	0.4774	0.4925	0.5027
FF	0.6095	0.6193	0.6206
Efficiency (%)	5.026	5.339	5.458

4.7 Anti reflective coating (TiO_2)

A TiO_2 anti reflective coating layer was simulated between the TCO and p-layer. This was in a bid to optimize light trapping. Unfortunately, we were not able to optimize the solar cell in this set of simulations. The QE was decreased in the long wavelength region. Even though there was improvement in absorption in the short wavelength region, the losses in the long wavelength region led to a decline in the performance of the solar cell. All solar cell external parameters except the FF were affected negatively.

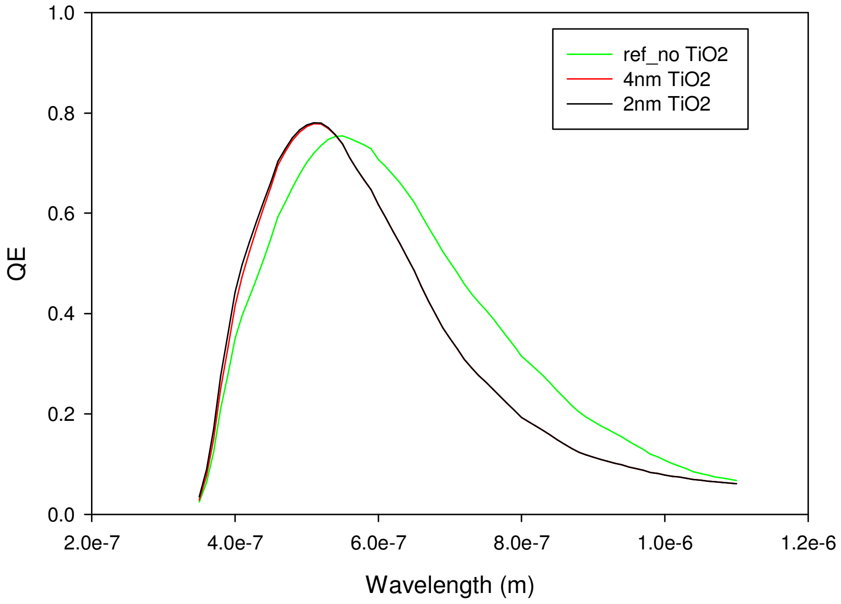

Figure 4-28 TiO2 anti reflective coating

Table 9. TiO2 anti reflective coating

PARAMETER	REFERENCE	4nm_TiO2	2nm_TiO2
J_{sc} (A/m^{2})	-172.7	-148.7	-149.5
Voc (V)	0.4774	0.4704	0.4707
FF	0.6095	0.6098	0.6098
Efficiency (%)	5.026	4.264	4.292

4.8 Conclusion

Sensitivity studies were carried out for some optical and electrical properties of the solar cell. This study showed how different parameters that were varied affected the efficiency as well as other external parameters of the solar cell. The study of the optical properties of the cell was first performed, parameters like absorption coefficient of different layers, Rms roughness, and thicknesses of different layers were investigated. A sensitivity study for the electrical parameters of the solar cell was also carried out, parameters such as mobility gap, activation energy, defect density and thicknesses of different layers were investigated. Results of these studies show that decreasing the p and the n layer thicknesses by about 2 or 3 nanometers could increase the efficiency of the solar cell. Increasing the p-layer mobility gap and the n-layer activation energy both improved the performance of the solar cell.

The inclusion of either a p-layer microcrystalline silicon buffer layer with a higher mobility gap than the i-layer but lower than the p-layer and the inclusion of an amorphous silicon carbide buffer layer at the p-i interface proved to optimize the solar cell. The solar cell was also seen to be improved when grading of the i-layer was implemented. We performed simulations in order to improve light trapping making use of a titanium dioxide layer at the TCO-p interface, this had a negative effect on the performance of the solar cell, but we believe it can be optimized to give an improvement in the cells performance.

5 Conclusion and Recommendations

The µc-Si:H solar cells are used in a tandem combination with a top a-Si:H cell in order to maximize the efficiency of the solar cell as the µc-Si:H solar cells have a higher light absorbing property in the long wavelength region (infrared region) than the a-Si:H. The combination of these two cells (an amorphous cell performing better in the short wavelength region and a microcrystalline cell performing better in the long wavelength region in tandem) give rise to a higher performing solar cell. Therefore understanding µc-Si:H solar cells in view of optimizing them is necessary in the bid to achieving better thin-film silicon solar cells in tandem or micromorph configuration.

In this thesis, the optical and electrical calibrations of a hydrogenated microcrystalline thin-film silicon solar cell was successfully carried out, obtaining results that closely matched experimental cells. A sensitivity study was carried out for both the optical and electrical characteristics of the cell, exploring ways to further optimize the performance of the solar cell. Optically, parameters such as the absorption coefficient, rms roughness, ADF function and thickness of layers were studied. The study showed that decreasing the absorption coefficient of the p and n-layers yielded higher external QE and short circuit current density of the solar cell. Also increasing the rms roughness of the TCO led to higher performance of the solar cell.

Electrically, it is shown that quite a portion of the electrical losses in the solar cell are losses due to recombination. The effect of the mobility gap, activation energy, defect density and thickness of different layers were investigated. Our simulations showed that a decrease in the i-layer thickness by up to 500nm decreased the Jsc but increased other external parameters of the solar cell including its efficiency. Decreasing thickness of the TCO, p and n-layers also led to an increase in all the external parameters of the solar cell. Increasing the mobility gap of the p-layer also increases solar cell external parameters. The inclusion of either a p-layer microcrystalline silicon buffer layer with a higher mobility gap than the i-layer but lower than the p-layer and the inclusion of an amorphous silicon carbide buffer layer at the p-i interface proved to optimize the solar cell. The solar cell was also seen to be improved when grading of the i-layer was implemented. We performed simulations in order to improve light trapping making use of a Titanium dioxide layer at the TCO-p interface, this had a negative effect on the performance of the solar cell, but it can be optimized to give an improvement in the cells performance.

The ASA simulator proved to be a very helpful tool in this study, there is a wide range of possibilities of what can be investigated by simulations.

Appendix A

Input files

A.1 Electrical calibrated input file

```
C Name Layer-f.1 Glass;
C Name Layer-f.2 TCO;
C Name Layer-1 p;
C Name Layer-2 i;
C Name Layer-3 n;
C Name Layer-b.1 ag;
C Name Layer-b.2 Al;

c options        suppress.warnings ignore.bounds;

layers           front=2 electrical=3 back=2;

grid[f.1]        d=1.5e-3;
grid[f.2]        d=800e-09;

grid[1]          d=24e-09 spaces=50;
grid[2]          d=1100e-09 spaces=110;
grid[3]          d=20e-09 spaces=20;

grid[b.1]        d=100e-09;
grid[b.2]        d=200e-09;

optical[f.1]     ref.index=1.5 ext.coeff=0 incoherent;
optical[f.2]     lnk.file=TCO_ZnO_d_sputtered_TUD_2008_fitted_3.nk;

optical[1]       lnk.file=p_ucSi_Prague_JAP.nk;
optical[2]       lnk.file=i_ucSi_Prague_JAP.nk;
c optical[3]     lnk.file=n_a_SiH_Prague[1].nk;
optical[3]       lnk.file=n_ucSi_Prague2_JAP.nk;

c optical[b.1]   lnk.file=TCO_ZnO_d_sputtered_TUD_2008_fitted_3.nk;
optical[b.1]     lnk.file=Ag_Prague.nk;
optical[b.2]     lnk.file=tud_al.nk;


bands[1]         e.mob=1.18 chi=4.05 nc=1.25E+25 nv=0.62E+25 epsilon=11.9;
bands[2]         e.mob=1.18 chi=4.05 nc=1.25E+25 nv=0.62E+25 epsilon=11.9;
bands[3]         e.mob=1.75 chi=3.90 nc=4.0E+26 nv=4.0E+26 epsilon=11.9;

doping[1]        e.act.acc=0.01;
doping[3]        e.act.don=0.05;
```

```
mobility[1]      mu.e=5.0e-3 mu.h=1.5e-3;
mobility[2]      mu.e=5.0e-3 mu.h=1.5e-3;
mobility[3]      mu.e=2.0e-3 mu.h=0.5e-3;

cbtail[1]        e.char=0.031 n.emob=2.8E+26 c.neut=5.0e-15 c.neg=50.0e-15
e.range=0.9 levels=30;
cbtail[2]        e.char=0.031 n.emob=2.8E+26 c.neut=5.0e-15 c.neg=50.0e-15
e.range=0.9 levels=30;
cbtail[3]        e.char=0.070 n.emob=7.0E+27 c.neut=0.70e-15 c.neg=7.0e-15
e.range=0.9 levels=30;

vbtail[1]        e.char=0.031 n.emob=1.04e26 c.neut=5.0e-15 c.pos=50.0e-15
e.range=0.9 levels=30;
vbtail[2]        e.char=0.031 n.emob=1.04e26 c.neut=5.0e-15 c.pos=50.0e-15
e.range=0.9 levels=30;
vbtail[3]        e.char=0.080 n.emob=5.00e27 c.neut=0.7e-15 c.pos=07.0e-15
e.range=0.9 levels=30;

dbond[1]         e.corr=0.2 ce.neut=3.0e-15 ce.pos=30.0e-15 ch.neut=3.0e-
15 ch.neg=30.0e-15 d.e=0.15 e.range=5.0 levels=40 n=3e22 e.rel.mg=0.0;
dbond[2]         e.corr=0.2 ce.neut=3.0e-15 ce.pos=30.0e-15 ch.neut=3.0e-
15 ch.neg=30.0e-15 d.e=0.15 e.range=5.0 levels=40 n=2e22 e.rel.mg=0.0;
dbond[3]         e.corr=0.2 ce.neut=0.7e-15 ce.pos=7.0e-15 ch.neut=0.7e-15
ch.neg=7e-15 d.e=0.15 e.range=5.0 levels=40 n=2e22 ep.def.pool=1.22;

# ######### i put;
recom[1]   tau.e=10e-11 tau.h=10e-07;
recom[3]         tau.e=10e-07 tau.h=10e-11;

interface[i.3]   adf.s.rf=user adf.s.rb=user adf.s.tf=user adf.s.tb=user
adf.s.file="ADF_input_external_correct.dat";
interface[i.3]   adf.h.rf=user adf.h.rb=user adf.h.tf=user adf.h.tb=user
adf.h.file="tco_p.dat";
interface[i.4]   adf.s.rf=user adf.s.rb=user adf.s.tf=user adf.s.tb=user
adf.s.file="ADF_input_external_correct.dat";
interface[i.4]   adf.h.rf=user adf.h.rb=user adf.h.tf=user adf.h.tb=user
adf.h.file="p_i.dat";
c interface[i.5] adf.s.rf=user adf.s.rb=user adf.s.tf=user adf.s.tb=user
adf.s.file="ADF_input_external_correct.dat";
c interface[i.5] adf.h.rf=user adf.h.rb=user adf.h.tf=user adf.h.tb=user
adf.h.file="i_n.dat";
c interface[i.7] adf.s.rf=user adf.s.rb=user adf.s.tf=user adf.s.tb=user
adf.s.file="ADF_input_external_correct.dat";
c interface[i.7] adf.h.rf=user adf.h.rb=user adf.h.tf=user adf.h.tb=user
adf.h.file="buffer_Ag.dat";

model[1]         vbtail cbtail dbond srh;
model[2]         vbtail cbtail dbond srh;
model[3]         vbtail cbtail dbond powell.deane.1996.mod;
```

```
model               external;

c frontcon  schottky;

settings            temp=300 max.iter=25 damp=3 dv.max=10 gummel.starts=2 ;
settings            t.freeze.in=500 newton Rs=4.5e-5 Rp=1e10 D0=1e-10;
settings            update.rec;


# #################### Generation profile;
opticgen    spectrum=AM1[1].5.dat genpro3;
print       opticgen file="gen2.dat";

# #####################;

title              Spectral response simulation;


solve               equil;
solve               jv illum n.step=20 v.start=0 v.end=1;
solve               sr wl.start=350nm wl.step=10nm wl.end=1100nm;
print               sr file="qe2";



title               Dark iv simulation;

variable            v_start=-1 v_end=1;

solve               equil;
print               bands file="Bands2.asp";

solve               n.step=20 v.start=-1 v.end=1 jv;
print               jv file="div2.dat";


# ###################;
title AM1.5 simulation;

solve               equil;
solve               v.start=0 v.end=1 n.step=40 illum;
print               jv file="liv2.dat";
print               sol.par file="par2";
print               efield file="efield.dat";
print               rec file="rec.dat";
```

A.2 Input file for buffer layer inserted in-between the p&i layers.

```
C Name Layer-f.1 Glass;
C Name Layer-f.2 TCO;
C Name Layer-1 p;
C Name Layer-2 ibuffer;
C Name Layer-3 i;
C Name Layer-4 n;
C Name Layer-b.1 ag;
C Name Layer-b.2 Al;

c options   suppress.warnings ignore.bounds;

layers           front=2 electrical=4 back=2;

grid[f.1]        d=1.5e-3;
grid[f.2]        d=800e-09;

grid[1]          d=24e-09 spaces=50;
grid[2]          d=4e-09 spaces=50;
grid[3]          d=1100e-09 spaces=110;
grid[4]          d=20e-09 spaces=20;

grid[b.1]        d=100e-09;
grid[b.2]        d=200e-09;

optical[f.1]     ref.index=1.5 ext.coeff=0 incoherent;
optical[f.2]     lnk.file=TCO_ZnO_d_sputtered_TUD_2008_fitted_3.nk;

optical[1]       lnk.file=p_ucSi_Prague_JAP.nk;
optical[2]       lnk.file=p_ucSi_Prague_JAP.nk;
optical[3]       lnk.file=i_ucSi_Prague_JAP.nk;
c optical[3]     lnk.file=n_a_SiH_Prague[1].nk;
optical[4]       lnk.file=n_ucSi_Prague2_JAP.nk;

c optical[b.1]   lnk.file=TCO_ZnO_d_sputtered_TUD_2008_fitted_3.nk;
optical[b.1]     lnk.file=Ag_Prague.nk;
optical[b.2]     lnk.file=tud_al.nk;


bands[1]         e.mob=1.25 chi=4.05 nc=1.25E+25 nv=0.62E+25 epsilon=11.9;
bands[2]         e.mob=1.21 chi=4.05 nc=1.25E+25 nv=0.62E+25 epsilon=11.9;
bands[3]         e.mob=1.18 chi=4.05 nc=1.25E+25 nv=0.62E+25 epsilon=11.9;
bands[4]         e.mob=1.75 chi=3.90 nc=4.0E+26 nv=4.0E+26 epsilon=11.9;

doping[1]        e.act.acc=0.01;
doping[2]        e.act.acc=0.01;
doping[4]        e.act.don=0.05;

mobility[1]      mu.e=5.0e-3 mu.h=1.5e-3;
```

```
mobility[2]      mu.e=5.0e-3 mu.h=1.5e-3;
mobility[3]      mu.e=5.0e-3 mu.h=1.5e-3;
mobility[4]      mu.e=2.0e-3 mu.h=0.5e-3;

cbtail[1]        e.char=0.031 n.emob=2.8E+26 c.neut=5.0e-15 c.neg=50.0e-15
e.range=0.9 levels=30;
cbtail[2]        e.char=0.031 n.emob=2.8E+26 c.neut=5.0e-15 c.neg=50.0e-15
e.range=0.9 levels=30;
cbtail[3]        e.char=0.031 n.emob=2.8E+26 c.neut=5.0e-15 c.neg=50.0e-15
e.range=0.9 levels=30;
cbtail[4]        e.char=0.070 n.emob=7.0E+27 c.neut=0.70e-15 c.neg=7.0e-15
e.range=0.9 levels=30;

vbtail[1]        e.char=0.031 n.emob=1.04e26 c.neut=5.0e-15 c.pos=50.0e-15
e.range=0.9 levels=30;
vbtail[2]        e.char=0.031 n.emob=1.04e26 c.neut=5.0e-15 c.pos=50.0e-15
e.range=0.9 levels=30;
vbtail[3]        e.char=0.031 n.emob=1.04e26 c.neut=5.0e-15 c.pos=50.0e-15
e.range=0.9 levels=30;
vbtail[4]        e.char=0.080 n.emob=5.00e27 c.neut=0.7e-15 c.pos=07.0e-15
e.range=0.9 levels=30;

dbond[1]         e.corr=0.2 ce.neut=3.0e-15 ce.pos=30.0e-15 ch.neut=3.0e-
15 ch.neg=30.0e-15 d.e=0.15 e.range=5.0 levels=40 n=3e22 e.rel.mg=0.0;
dbond[2]         e.corr=0.2 ce.neut=3.0e-15 ce.pos=30.0e-15 ch.neut=3.0e-
15 ch.neg=30.0e-15 d.e=0.15 e.range=5.0 levels=40 n=1e21 e.rel.mg=0.0;
dbond[3]         e.corr=0.2 ce.neut=3.0e-15 ce.pos=30.0e-15 ch.neut=3.0e-
15 ch.neg=30.0e-15 d.e=0.15 e.range=5.0 levels=40 n=2e22 e.rel.mg=0.0;
dbond[4]         e.corr=0.2 ce.neut=0.7e-15 ce.pos=7.0e-15 ch.neut=0.7e-15
ch.neg=7e-15 d.e=0.15 e.range=5.0 levels=40 n=2e22 ep.def.pool=1.22;

interface[i.3]   adf.s.rf=user adf.s.rb=user adf.s.tf=user adf.s.tb=user
adf.s.file="ADF_input_external_correct.dat";
interface[i.3]   adf.h.rf=user adf.h.rb=user adf.h.tf=user adf.h.tb=user
adf.h.file="tco_p.dat";
interface[i.5]   adf.s.rf=user adf.s.rb=user adf.s.tf=user adf.s.tb=user
adf.s.file="ADF_input_external_correct.dat";
interface[i.5]   adf.h.rf=user adf.h.rb=user adf.h.tf=user adf.h.tb=user
adf.h.file="p_i.dat";
c interface[i.5] adf.s.rf=user adf.s.rb=user adf.s.tf=user adf.s.tb=user
adf.s.file="ADF_input_external_correct.dat";
c interface[i.5] adf.h.rf=user adf.h.rb=user adf.h.tf=user adf.h.tb=user
adf.h.file="i_n.dat";
c interface[i.7] adf.s.rf=user adf.s.rb=user adf.s.tf=user adf.s.tb=user
adf.s.file="ADF_input_external_correct.dat";
c interface[i.7] adf.h.rf=user adf.h.rb=user adf.h.tf=user adf.h.tb=user
adf.h.file="buffer_Ag.dat";

model[1]         vbtail cbtail dbond;
model[2]         vbtail cbtail dbond;
```

```
model[3]          vbtail cbtail dbond;
model[4]          vbtail cbtail dbond powell.deane.1996.mod;


model             external;

c frontcon  schottky;

settings          temp=300 max.iter=25 damp=3 dv.max=10 gummel.starts=2 ;
settings          t.freeze.in=500 newton Rs=4.5e-5 Rp=1e10 D0=1e-10;


# #################### Generation profile;
opticgen   spectrum=AM1[1].5.dat genpro3;
print      opticgen file="gen2.dat";

# #####################;

title            Spectral response simulation;


solve             equil;
solve             jv illum n.step=20 v.start=0 v.end=1;
solve             sr wl.start=350nm wl.step=10nm wl.end=1100nm;
print             sr file="qe2";



title             Dark iv simulation;

variable          v_start=-1 v_end=1;

solve             equil;
print             bands file="Bands2.asp";

solve             n.step=20 v.start=-1 v.end=1 jv;
print             jv file="div2.dat";


# ###################;
title AM1.5 simulation;

solve             equil;
solve             v.start=0 v.end=1 n.step=40 illum;
print             jv file="liv2.dat";
print             sol.par file="par2";
print             efield file="efield.dat";
print             rec file="rec.dat";
```

A.3 Input file for optical simulation

```
c microcrystalline silicon solar cell: Optical simulations


C Name Layer-1 Glass;
C Name Layer-2 TCO;
C Name Layer-3 p;
C Name Layer-4 i;
C Name Layer-5 n;
C Name Layer-6 buffer;
C Name Layer-7 Ag;

c options        ignore.bounds;
layers           electrical=7;

grid[1]          d=700000e-9 spaces=200;
grid[2]          d=800e-09 spaces=200;
grid[3]          d=25e-09 spaces=50;
grid[4]          d=1230e-09 spaces=123;
grid[5]          d=20e-09 spaces=20;
grid[6]          d=1e-09 spaces=10;
grid[7]          d=300e-09 spaces=100;


optical[1]       lnk.file=glass.nk incoherent;
optical[2]       lnk.file=TCO_ZnO_d_sputtered_TUD_2008_fitted_3.nk;
optical[3]       lnk.file=p_ucSi_Prague_JAP2.nk;
optical[4]       lnk.file=i_ucSi_Prague_JAP.nk;
optical[5]       lnk.file=n_ucSi_Prague_JAP.nk;
optical[6]       lnk.file=n_Ag_08_Prague.nk;
optical[7]       lnk.file=Ag_Prague.nk;

interface[i.3]   adf.s.rf=user adf.s.rb=user adf.s.tf=user adf.s.tb=user
adf.s.file="ADF_input_external_correct.dat";
interface[i.3]   adf.h.rf=user adf.h.rb=user adf.h.tf=user adf.h.tb=user
adf.h.file="tco_p.dat";
interface[i.4]   adf.s.rf=user adf.s.rb=user adf.s.tf=user adf.s.tb=user
adf.s.file="ADF_input_external_correct.dat";
interface[i.4]   adf.h.rf=user adf.h.rb=user adf.h.tf=user adf.h.tb=user
adf.h.file="P_i.dat";
interface[i.5]   adf.s.rf=user adf.s.rb=user adf.s.tf=user adf.s.tb=user
adf.s.file="ADF_input_external_correct.dat";
interface[i.5]   adf.h.rf=user adf.h.rb=user adf.h.tf=user adf.h.tb=user
adf.h.file="i_n.dat";
interface[i.7]   adf.s.rf=user adf.s.rb=user adf.s.tf=user adf.s.tb=user
adf.s.file="ADF_input_external_correct.dat";
interface[i.7]   adf.h.rf=user adf.h.rb=user adf.h.tf=user adf.h.tb=user
adf.h.file="buffer_Ag.dat";
```

```
settings          temp=300 eps.pois=1e-5 eps.cone=1e-5 eps.conh=1e-5
max.iter=50 damp=0 dv.max=10 gummel.starts=3 newton max.step.reduc=4;


# #################### Generation profile;
opticgen          spectrum=AM1[1].5.dat genpro3;
print             opticgen file="genrough_mine.dat";

solve rt          wl.start=350e-9 wl.step=10e-9 wl.end=1090e-9;
print rt          file="RT_rough_mine.dat";
```

Appendix B

Tables and charts from electrical sensitivity study

Table 10: P-Layer mobility gap series

PARAMETER	REFERENCE: 1.18	-0.10	-0.05	+0.05	+0.10
Jsc	17.27	17.06	17.18	17.33	17.73
Voc	0.4774	0.4763	0.4770	0.4776	0.4778
FF	0.6095	0.6069	0.6086	0.6100	0.6103
Pmax	50.26 W/m^2	49.31 W/m^2	49.89 W/m^2	50.50 W/m^2	50.65 W/m^2
Efficiency	5.026	4.931	4.987	5.048	5.170

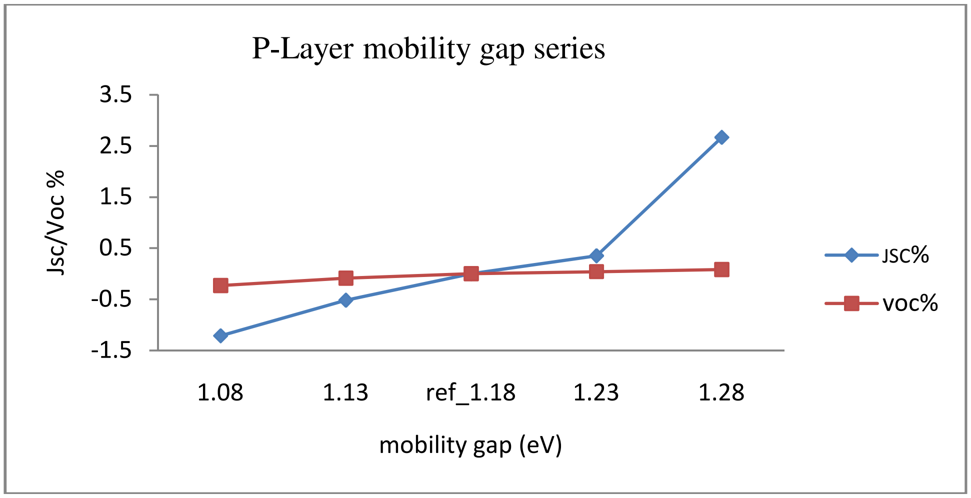

Figure A-1 Percentage plot of p-layer mobility gap series

Table 11: i-Layer mobility gap series

PARAMETER	REFERENCE: 1.18	-0.10	-0.05	+0.05	+0.10
Jsc	17.27	17.27	17.28	17.23	17.16
Voc	0.4774	0.3805	0.4288	0.5261	0.5744
FF	0.6095	0.5839	0.5992	0.6222	0.6316
pmax	50.26 W/m^2	38.38W/m^2	44.42W/m^2	56.40W/m^2	62.25W/m^2
Efficiency	5.026	3.837	4.442	5.64	6.225

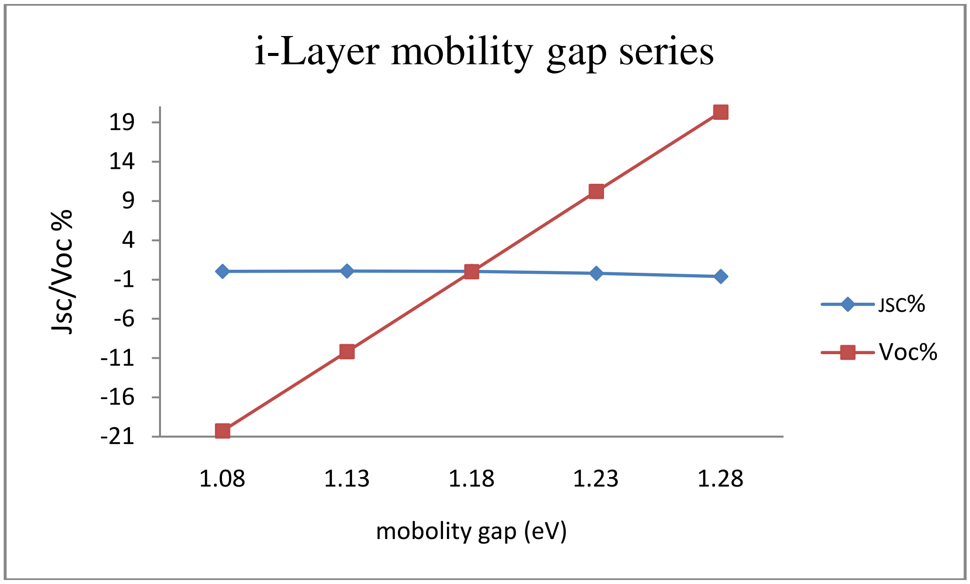

Figure A-2 Percentage plot of i-layer mobility gap series

Table 12: n-Layer mobility gap series

PARAMETER	REFERENCE: 1.75	-0.20	-0.10	+0.10	+0.20
Jsc	17.27	17.27	17.27	17.26	17.24
Voc	0.4774	0.4774	0.4774	0.4774	0.4774
FF	0.6095	0.6095	0.6095	0.6095	0.6095
pmax	50.26 W/m^2	50.25W/m^2	50.27W/m^2	50.23W/m^2	50.18W/m^2
Efficiency	5.026	5.025	5.025	5.022	5.016

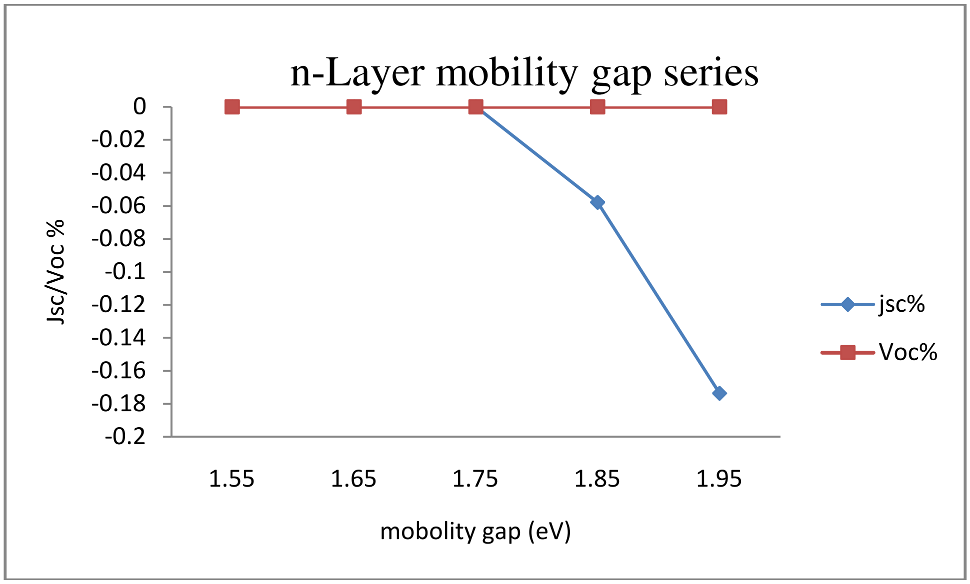

Figure A-3 Percentage plot of n-layer mobility gap series

Table 13: P-Layer activation energy series

PARAMETER	REFERENCE: 0.01	0.001	0.05	0.11	0.20	0.30
Jsc	17.27	17.26	17.32	17.46	17.68	17.31
Voc	0.4774	0.4774	0.4774	0.4769	0.4625	0.4124
FF	0.6095	0.6096	0.6089	0.6061	0.6005	0.5613
pmax	50.26W/m^2	50.25W/m^2	50.35W/m^2	50.47W/m^2	49.10W/m^2	40.07W/m^2
Efficiency	5.026	5.023	5.035	5.047	4.91	4.007

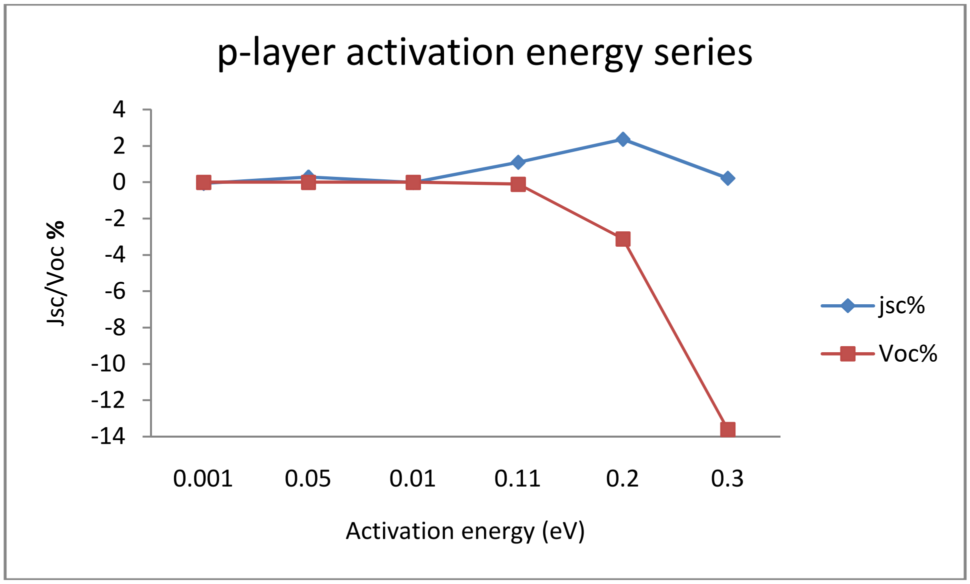

Figure A-4 Percentage plot of p-layer activation energy series

Table 14 n-Layer activation energy series

PARAMETER	0.01	0.10	REFERENCE: 0.05	0.15	0.20
Jsc	17.07	17.66	17.27	18.18	18.76
Voc	0.4770	0.4782	0.4774	0.4792	0.4804
FF	0.6094	0.6099	0.6095	0.6105	0.6112
pmax	49.62W/m^2	51.51W/m^2	50.26 W/m^2	53.20W/m^2	55.09W/m^2
Efficiency	4.962	5.151	5.026	5.320	5.509

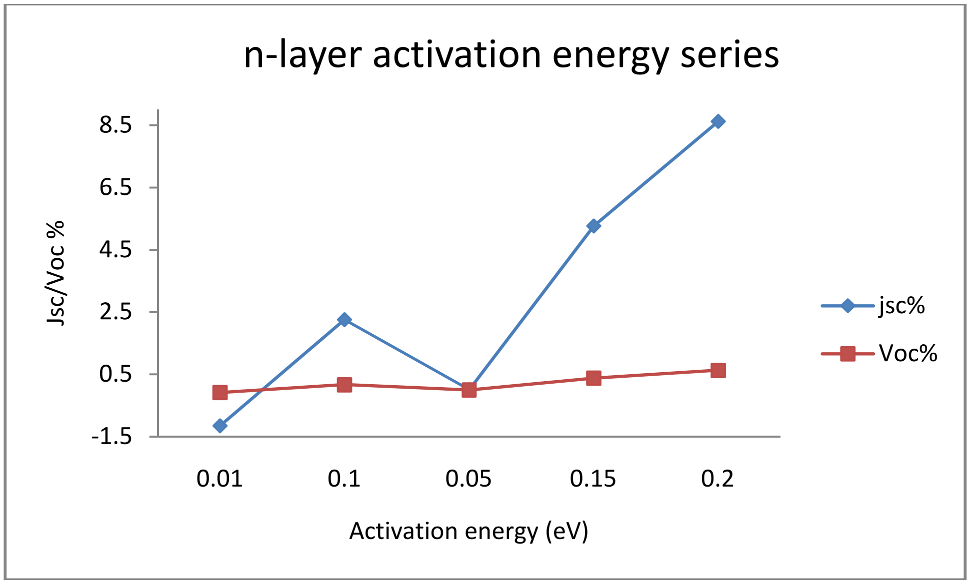

Figure A-5 Percentage plot of n-layer activation energy series

Table 15: DOS in valance band in p-layer series

PARAMETER	0.62E24	REFERENCE: 0.62E25	0.62E26	0.62E27
Jsc	17.39	17.27	17.23	17.23
Voc	0.4777	0.4774	0.4773	0.4773
FF	0.6095	0.6095	0.6095	0.6095
pmax	50.65W/m^2	50.26 W/m^2	50.14W/m^2	50.12W/m^2
Efficiency	5.065	5.026	5.014	5.012

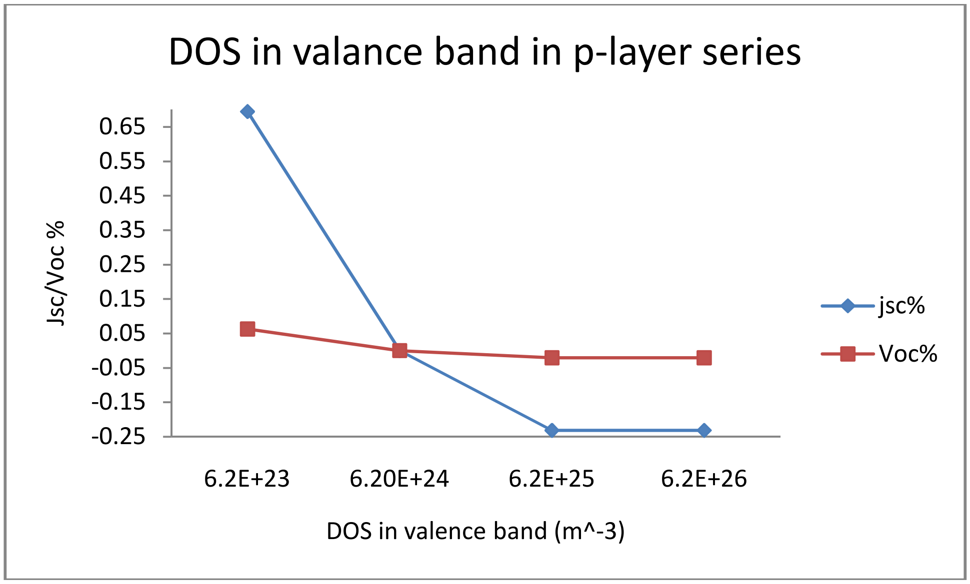

Figure A-6 percentage plot of DOS in valence band in p-layer series

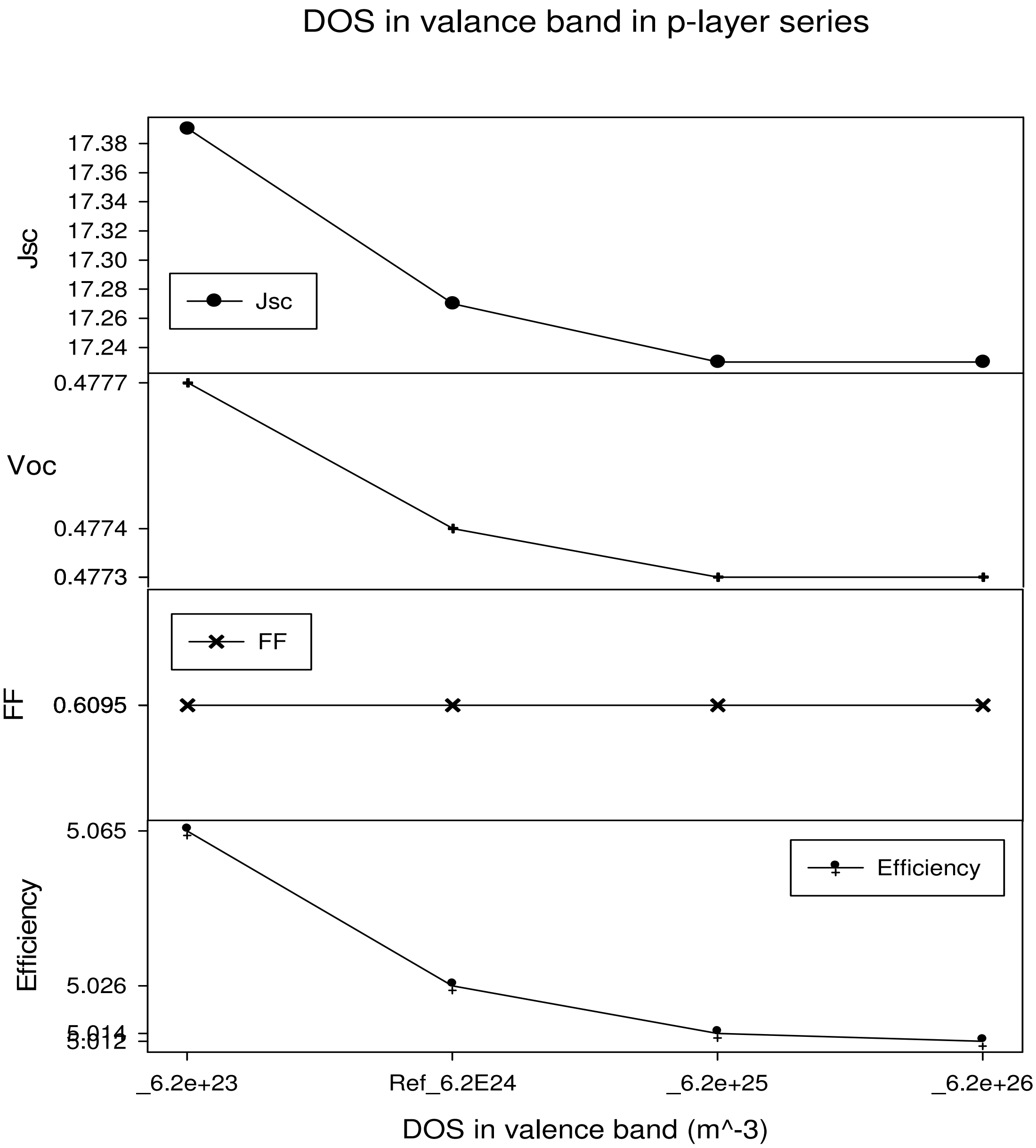

Figure A-7 solar cell external parameters for DOS in valence band in p-layer series

Table 16: DOS in conduction band in p-layer series

PARAMETER	1.25E24	REFERENCE: 1.25E25	1.25E26	1.25E27
Jsc	17.34	17.27	17.07	16.41
Voc	0.4776	0.4774	0.4769	0.4750
FF	0.6097	0.6095	0.6088	0.6076
pmax	50.49W/m^2	50.26 W/m^2	49.56W/m^2	47.36W/m^2
Efficiency	5.049	5.026	4.956	4.736

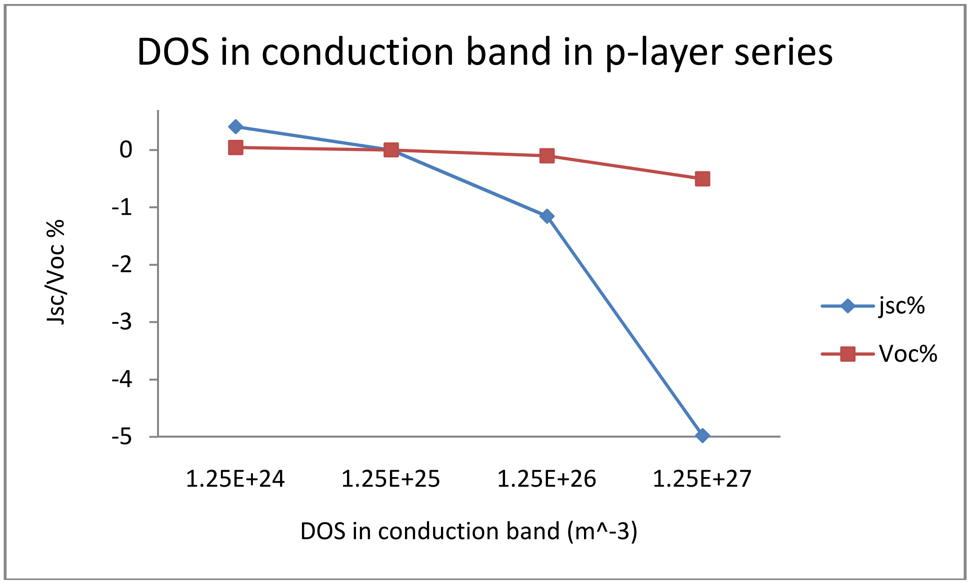

Figure A-8 percentage plot of DOS in conduction band in p-layer series

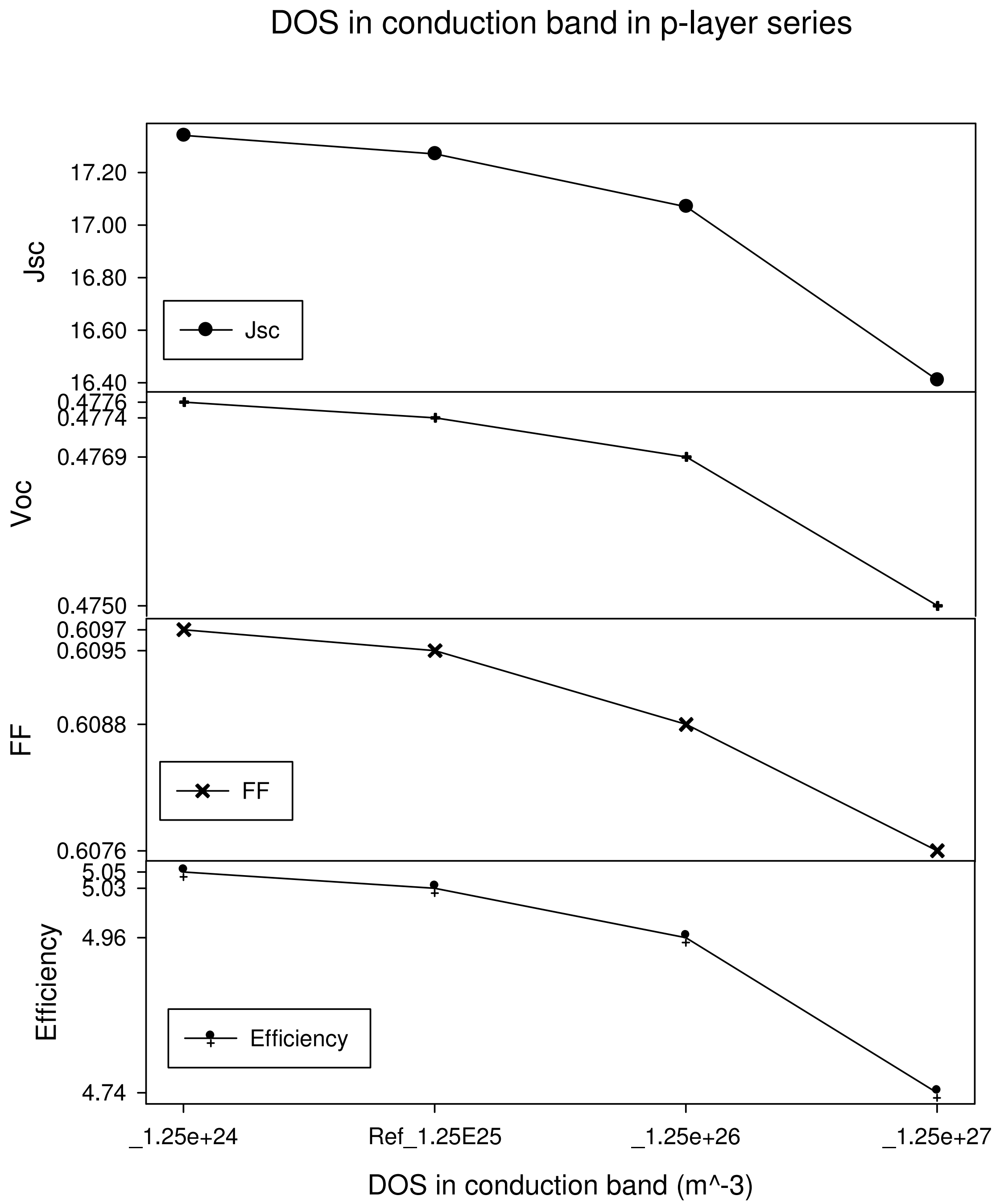

Figure A-9 solar cell external parameters for DOS in conduction band band in p-layer series

Table 17: concentration of dangling bonds in p-layer series

PARAMETER	3E23	3E24	REFERENCE: 3E22	3E25	1E26
Jsc	17.27	17.21	17.27	16.82	16.40
Voc	0.4774	0.4773	0.4774	0.4764	0.4755
FF	0.6095	0.6095	0.6095	0.6089	0.6094
pmax	50.24W/m^2	50.06W/m^2	50.26 W/m^2	48.80W/m^2	47.51W/m^2
Efficiency	5.024	5.006	5.026	4.880	4.751

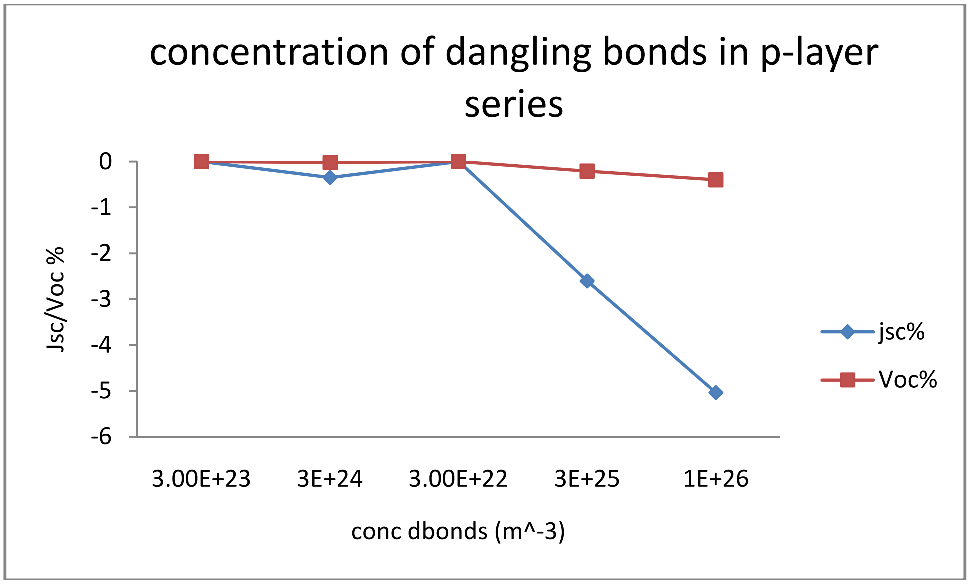

Figure A-10 percentage plot of concentration of dangling bonds in p-layer series

Table 18: concentration of dangling bonds in i-layer series

PARAMETER	2E18	2E20	REFERENCE: 2E22	3E22	2E23
Jsc	17.83	17.83	17.27	16.76	11.87
Voc	0.5216	0.5209	0.4774	0.4627	0.3897
FF	0.7527	0.7506	0.6095	0.5842	0.4286
pmax	69.98W/m^2	69.72W/m^2	50.26 W/m^2	45.29W/m^2	19.83W/m^2
Efficiency	6.998	6.972	5.026	4.529	1.983

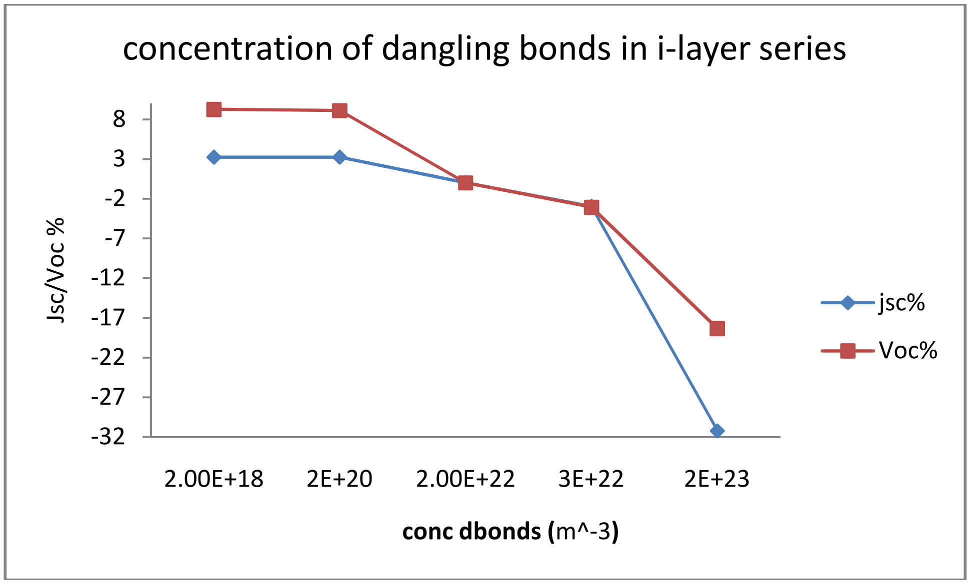

Figure A-11 percentage plot of concentration of dangling bonds in i-layer series

Table 19: p-layer thickness series

PARAMETER	15	10	REFERENCE: 24	30	50
Jsc	17.75	18.03	17.27	16.96	15.96
Voc	0.4784	0.4790	0.4774	0.4768	0.4744
FF	0.6100	0.6103	0.6095	0.6092	0.6095
pmax	51.81W/m^2	52.70W/m^2	50.26 W/m^2	49.27W/m^2	46.13W/m^2
Efficiency	5.181	5.270	5.026	4.927	4.613

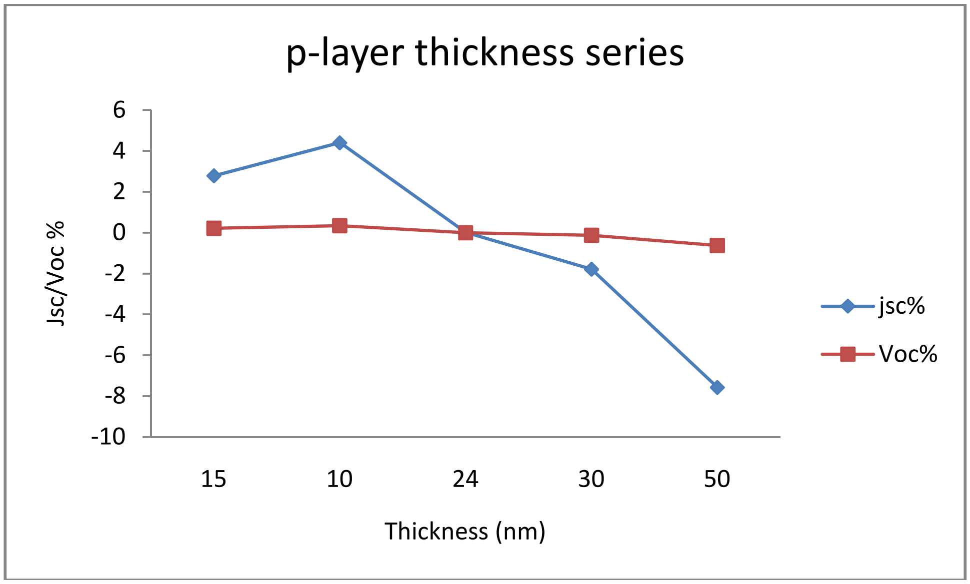

Figure A-12 percentage plot of p-layer thickness series

Table 20: i-layer thickness series

PARAMETER	500	REFERENCE: 1100	1230	1500
Jsc	15.04	17.27	17.43	17.56
Voc	0.5044	0.4774	0.4748	0.4686
FF	0.7035	0.6095	0.5941	0.5648
pmax	53.38W/m^2	50.26 W/m^2	49.15W/m^2	46.48W/m^2
Efficiency	5.338	5.026	4.915	4.648

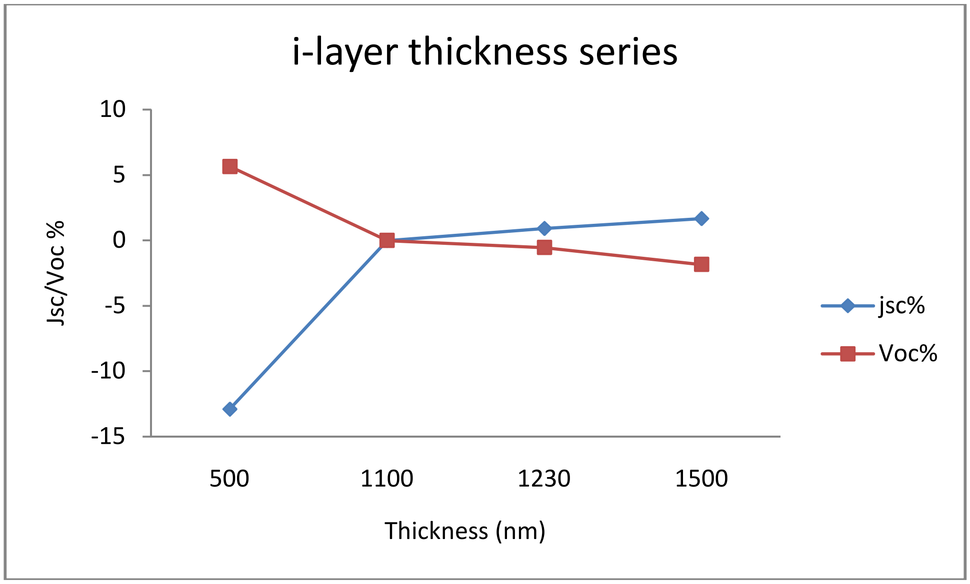

Figure A-13 percentage plot of i-layer thickness series

Table 21: n-layer thickness series

PARAMETER	10	15	REFERENCE: 20	25	30
Jsc	17.72	17.45	17.27	17.17	17.12
Voc	0.4783	0.4778	0.4774	0.4772	0.4771
FF	0.6100	0.6097	0.6095	0.6094	0.6093
pmax	51.70W/m^2	50.83W/m^2	50.26 W/m^2	49.94W/m^2	49.77W/m^2
Efficiency	5.170	5.083	5.026	4.994	4.977

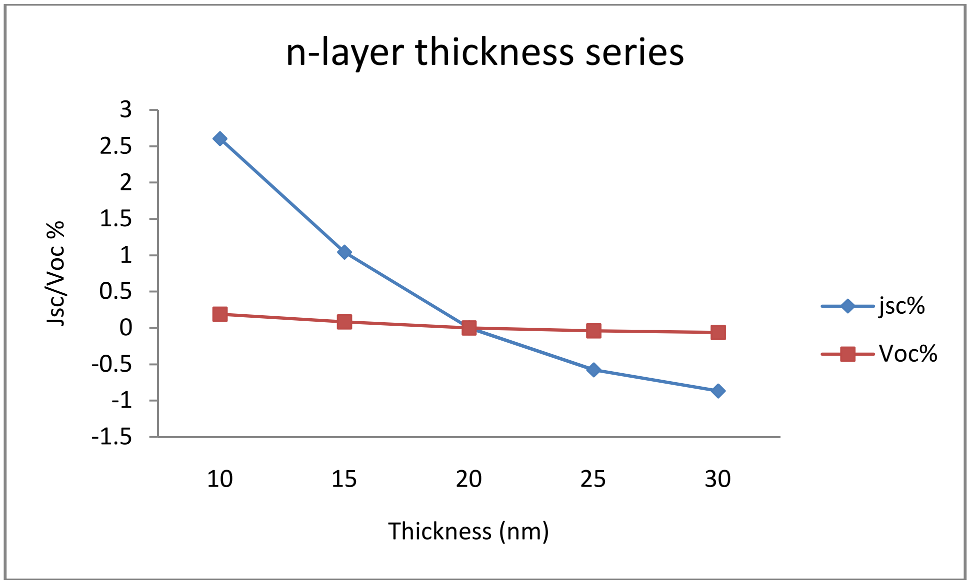

Figure A-14 percentage plot of n-layer thickness series

Table 22: TCO-layer thickness series

PARAMETER	600	REFERENCE: 800	1000
Jsc	17.64	17.27	16.93
Voc	0.4782	0.4774	0.4767
FF	0.6099	0.6095	0.6092
pmax	51.45W/m^2	50.26 W/m^2	49.18W/m^2
Efficiency	5.145	5.026	4.918

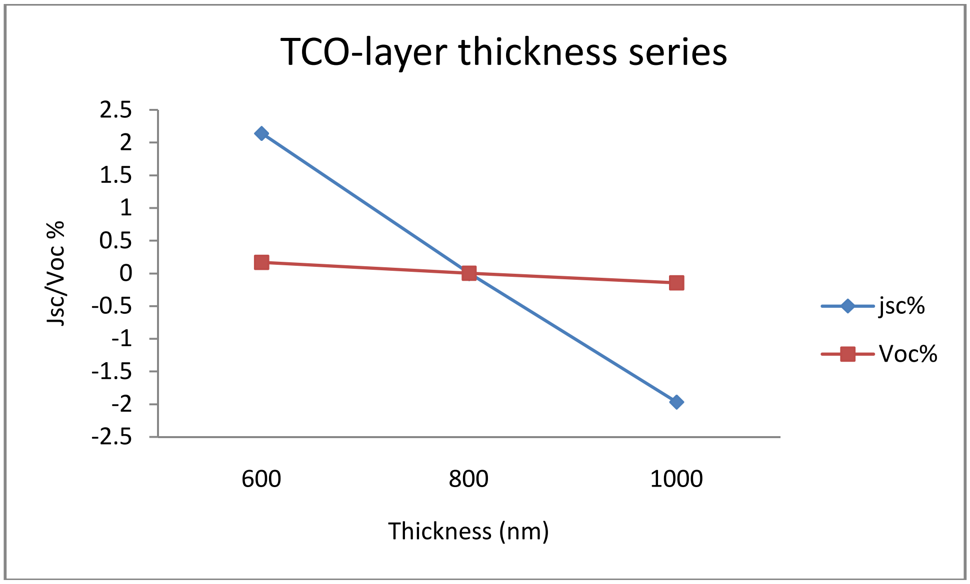

Figure A-15 percentage plot of TCO-layer thickness series

References

[1] M. Zeman, solar cells lecture notes, Delft University of Technology, Delft, The Netherlands, 2008

[2] Wikipedia, Renewable energy, http://en.wikipedia.org/wiki/Renewable_energy

[3] Wikipedia Solar cells http://en.wikipedia.org/wiki/Solar_cell

[4] http://org.ntnu.no/solarcells/pages/introduction.php

[5] Wikimedia, solar Cell-Equivalent Circuit, Wikimedia commons, 2006

[6] http://org.ntnu.no/solarcells/pages/Chap.2.php

[7] A.V. Shah, H. Schade, M. Vanecek, J. Meier, E. Vallat-Sauvain, N. Wyrsch, U. Kroll, C. Droz and J. Bailat, Thin-film Silicon Solar Cell Technology, Progress in Photovoltaics 12, 2004, p. 113

[8] A. Shah et al. Microcrystalline silicon and micromorph tandem solar cells, Thin solid films 403-404 (2002) 179-187

[9] A. Shah, J. Meier, P. Torres, U. Kroll, D. Fischer, N. Beck, N. Wyrsch, and H. Keppner, Recent progress on microcrystalline solar cells, 26th PVSC; Sept:30-Oct. 3, 1997; Anaheim, CA.

[10] A. V. Shah et al. Materials and solar cells research in microcrystalline silicon, Solar Energy Materials and Solar Cells 78 (2003) 469-491

[11] Janez Krc, Presentation on Light management in thin-film silicon solar cells, Delft University of Technology, 2008

[12] Janez Krc and Marco Topic, Optical modeling and simulations of thin-film solar cells, NUMOS Workshop Gent, Belgium, March 28, 2008.

[13] Janez Krc, Franc Smole, Marko Topic, Improving thin-film solar cells through optical modeling, 31 August 2006, SPIE Newsroom. DOI: 10.1117/2.1200606.0286

[14] J. Krc, F. Smole, M. Topic, Optical simulation of the role of reflecting interlayers in tandem micromorph silicon solar cells, University of Ljubljana, Faculty of Electrical Engineering, Ljubljana, Slovenia. Solar Energy Materials & Sola r Cells 86 (2005) 537-550

[15] H. Takakura, Y. Hamakawa, Device simulation and modeling of microcrystalline silicon solar cells, Department of photonics, Faculty of science and Engineering, Ritsumeikan University, Japan. Solar Energy Materials & Solar Cells 74 (2002) 479-487

[16] T. Brammer, H. Stiebig, Applying analytical and numerical methods for the analysis of microcrystalline silicon solar cells, Institute of Photovoltaics, forschungszentrum Julich, Germany, Solar Energy Materials &solar Cells 90 (2006) 3021-3030

[17] Joost A. Willemen. Modelling of Amorphous Silicon Single and Multi-Junction Solar Cells. 1998

[18] Bart Pieters. Characterization of thin-Film Silicon Materials and Solar Cells through Numerical Modelling. 2008

[19] P. Campbell and M Keevers, Light trapping and reflection control for silicon thin-films deposited on glass substrates textured by embossing. photovoltaic specialists conference, 2000

[20] J. Krc, M. Zeman, A. Campa, F. Smole and M. Topic, Novel approaches of light management in thin-film silicon solar cells. MRS Conference, 2006

[21] Olindo Isabella, Miro Zeman, State of the art in light management, ECTM\DIMES, 2008

[22] Miro Zeman, Joost van den Heuvel, Martin Kroon, Joost Willemen, Bart Pieters and Janez Krc, ASA User's manual, version 5.0, DIMES, 2005

[23] J. Krc, M. Zeman, O. Kluth, F. Smole, M. Topic, Effect of Surface Roughness of ZnO:Al films on Light cattering in Hydrogenated Amorphous Silicon Solar Cells, 1-2, February 2003, Pages 296-304, Thin Solid Films, 2003, Vol. 426

[24] Ruud E. I. Schropp and Miro Zeman, Amorphous and Microcrystalline Silicon Solar Cells: Modeling, Materials and Device Technology, Kluwer Academic Publishers, 1998

[25] B. Vet, M. Zeman, Relation between the open –circuit voltage and the band gap of the absorber and buffer layers in a-Si:H solar cell. Thin Solid Films (2008) 6873-6876

List of Figures

List of tables

Acknowledgements

I thank God for giving me life, health and the grace to get this far.
I first want to express my gratitude to Prof. Dr. Miro Zeman, for giving me the opportunity of carrying out my thesis in the Photo-Voltaic Materials and Devices group. I thank him also for accepting to be my supervisor and for all the time he made to come by my table and ask after my work and how life was in general, I found it really encouraging.

I want to thank Dr. Rene van Swaaij and Dr. M. Bartek for accepting to be members of my examination committee and for taking the time to read my thesis. I would also like to show my appreciation to Dr. Rene van Swaaij in his capacity as my Msc coordinator, for the concern he showed and for asking me to feel free to fix an appointment to meet him to discuss semiconductor device physics even in my first year before I joined the PVMD group.

Special thanks to my daily supervisor Solomon Agbo, for all the discussions we had together, for the guidance he gave me during the period of this thesis, for making himself available for questions at all times that I could even call his phone when he was at home with family. Special thanks to all the members of the PVMD group, especially to Dr. Renrong Liang and Dr. Janez Krc for the discussions we had which proved helpful.

Great thanks to my family, for all their encouragement and prayers, my parents Chinedu and Ify Nebo, my sisters Chidinma and Chinenye, my brother Chinedu, and my smallie Nneka. I would not have stayed a day extra in delft after my first lecture if not for your encouragements.

I also want to thank all my friends who made my stay here in Delft feel as if I had family with me. Much thanks to my main buddies Adewale and Jerry, the two Paul's, David, Innocent, Noela, Sandra, Dayo, Tope, Yang, Chi Liu, Li and Deolah who were there for me all the way.

I also want to thank my coaches and team mates at the Delft Dragons, for giving me the opportunity to play American football with them. I really had fun, the trainings, the games, the outings, travelling with you guys. Even though I ended up in the hospital twice, I would do it all over again if given the opportunity.

Finally I want to thank my officemates, David, Sten, Folkert, Aster, Arash, Liang, Kehinde and Lijing. You guys came to mean so much to me, not just officemates but real friends. All the help I got from you, our outings together, the pies we shared on birthdays, trips to the coffee machine and all the interesting discussions. It was only as the end drew near that I started to realize how much I will miss you all.